(12)

AD A113383

RADC-TR-81-352
Final Technical Report
February 1982

APPLICATION OF PHASE RETRIEVAL

EIKONIX Corporation

Sponsored by
Defense Advanced Research Projects Agency (DoD)
ARPA Order No. 3655

APPROVED FOR PUBLIC RELEASE; DISTRIBUTION UNLIMITED

ROME AIR DEVELOPMENT CENTER
Air Force Systems Command
Griffiss Air Force Base, New York 13441

This report has been reviewed by the RADC Public Affairs Office (PA) and is releasable to the National Technical Information Service (NTIS). At NTIS it will be releasable to the general public, including foreign nations.

RADC-TR-81-352 has been reviewed and is approved for publication.

APPROVED: Doris Hamill

DORIS HAMILL, Capt, USAF
Project Engineer

APPROVED: Frank J. Rehm

FRANK J. REHM
Technical Director
Surveillance Division

FOR THE COMMANDER: John P. Huss

JOHN P. HUSS
Acting Chief, Plans Office

APPLICATION OF PHASE RETRIEVAL

Dr. Robert Gonsalves

Contractor: EIKONIX Corporation
Contract Number: F30602-80-C-0186
Effective Date of Contract: 23 June 1980
Contract Expiration Date: 31 July 1981
Short Title of Work: Application of Phase Retrieval
Program Code Number: 0E20
Period of Work Covered: 23 June 80 - 31 July 81

Principal Investigator: Dr. Robert Gonsalves
Phone: 617-275-5070

Project Engineer: Capt Doris Hamill
Phone: 315-330-3148

Approved for public release; distribution unlimited

This research was supported by the Defense Advanced Research Projects Agency of the Department of Defense and was monitored by Doris Hamill, Capt, USAF (OCSE), Griffiss AFB NY 13441 under Contract F30602-80-C-0186.

UNCLASSIFIED

SECURITY CLASSIFICATION OF THIS PAGE (When Data Entered)

REPORT DOCUMENTATION PAGE — READ INSTRUCTIONS BEFORE COMPLETING FORM

1. REPORT NUMBER RADC-TR-81-352	2. GOVT ACCESSION NO. AD-A113 352	3. RECIPIENT'S CATALOG NUMBER
4. TITLE (and Subtitle) APPLICATION OF PHASE RETRIEVAL		5. TYPE OF REPORT & PERIOD COVERED Final Technical Report 23 Jun 80 - 31 Jul 81 6. PERFORMING ORG. REPORT NUMBER EC/2112901
7. AUTHOR(s) Dr. Robert Gonsalves		8. CONTRACT OR GRANT NUMBER(s) F30602-80-C-0186
9. PERFORMING ORGANIZATION NAME AND ADDRESS EIKONIX Corporation 23 Crosby Drive Bedford MA 01730		10. PROGRAM ELEMENT, PROJECT, TASK AREA & WORK UNIT NUMBERS 62301E C6550102
11. CONTROLLING OFFICE NAME AND ADDRESS Defense Advanced Research Projects Agency 1400 Wilson Blvd Arlington VA 22209		12. REPORT DATE February 1982 13. NUMBER OF PAGES 122
14. MONITORING AGENCY NAME & ADDRESS (if different from Controlling Office) Rome Air Development Center (OCSE) Griffiss AFB NY 13441		15. SECURITY CLASS. (of this report) UNCLASSIFIED 15a. DECLASSIFICATION/DOWNGRADING SCHEDULE N/A

16. DISTRIBUTION STATEMENT (of this Report)

Approved for public release; distribution unlimited

17. DISTRIBUTION STATEMENT (of the abstract entered in Block 20, if different from Report)

Same

18. SUPPLEMENTARY NOTES

RADC Project Engineer: Doris Hamill, Capt, USAF

19. KEY WORDS (Continue on reverse side if necessary and identify by block number)

phase estimation
phase sensing
wavefront sensing
phase retrieval
active mirrors

20. ABSTRACT (Continue on reverse side if necessary and identify by block number)

The purpose of this study was to determine how the phase retrieval algorithm developed under previous contract, worked in the face of real world constraints. The problems of finite detector size, noise in the measurements, and non-point objects were handled analytically, experimentally, and by blind testing. No significant problems were uncovered.

DD FORM 1 JAN 73 1473 EDITION OF 1 NOV 65 IS OBSOLETE

UNCLASSIFIED

SECURITY CLASSIFICATION OF THIS PAGE (When Data Entered)

UNCLASSIFIED

SECURITY CLASSIFICATION OF THIS PAGE(When Data Entered)

UNCLASSIFIED

SECURITY CLASSIFICATION OF THIS PAGE(When Data Entered)

1 INTRODUCTION

The objective of this study is to demonstrate the utility of the phase retrieval concept for determining the wavefront aberrations of an optical system from image intensity data. Phase retrieval techniques use only the focal plane detector array to estimate the wave aberration function θ of an active optical system. The estimate would then be used to derive control signals to align or maintain alignment of the optical system. See Figure 1.

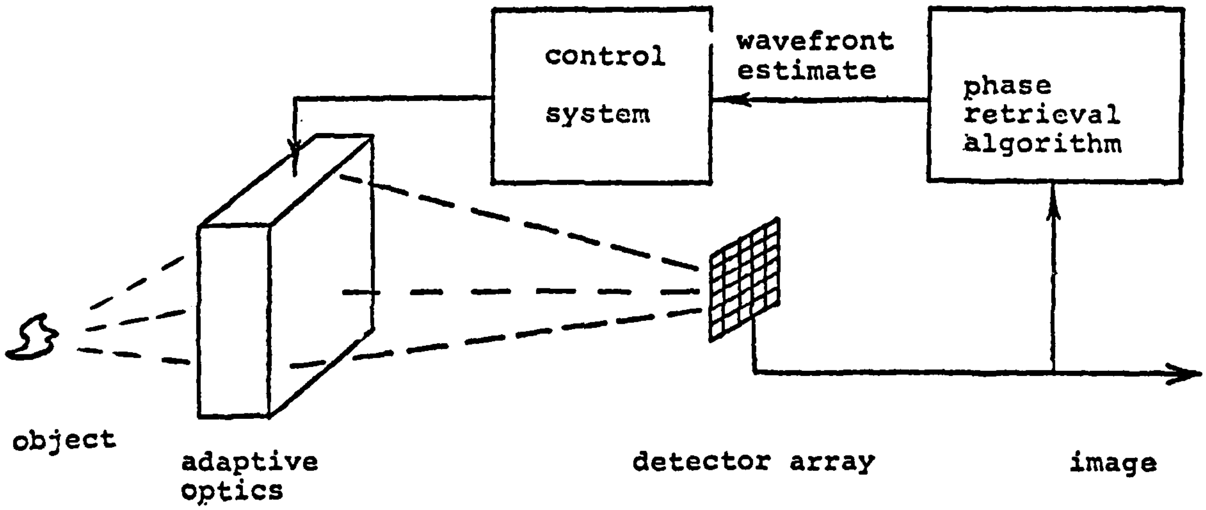

Figure 1. Phase retrieval in an adaptive imaging system

In a previous study (F30602-77-C-0176) we showed that phase retrieval is a promising technique to maintain alignment of an active optical system. However, most of the study was theoretical in nature and the best results were obtained with point sources, little or no noise on the detector output, and adequately sampled data (at or higher than the Nyquist sampling rate). In this follow-on effort we are charged to thoroughly simulate the algorithm's performance, particularly with respect to noise, undersampling (because of the finite detector size), and extended objects. We are also charged to show how phase retrieval can be developed into a system level proof-of-concept demonstration, where the system is to be specified by the government.

In this report we review the phase retrieval concept, show the effects of undersampling and noise, present algorithms for extended objects, show several ways in which the algorithm can be speeded up, introduce the concept of phase diversity imaging (as a research by-product of our extended object algorithm), give results of an experiment that attempts to verify the extended object concept, and present the results of a series of blind tests of the phase retrieval algorithm when the data is noisy and undersampled.

2 REVIEW OF THE PHASE RETRIEVAL CONCEPT

When a monochromatic point object is imaged through an optical system, the observable is the point spread function (PSF) $p(x)$. The PSF is the modulus squared of the coherent system function $h(x)$,

$$p(x) = |h(x)|^2.$$

The Fourier transform of $h(x)$,

$$H(f) = \int_{-\infty}^{\infty} h(x)\exp(-i2\pi fx)\,dx,$$

is the coherent system function of the optical system. Its modulus, $A(f)$, is a zero-one function, corresponding to the pupil function, and its phase $\theta(f)$ is proportional to the aberrated wavefront across the aperture. Thus,

$$H(f) = A(f)\,\exp(i\theta(f)).$$

Although we use a one-dimensional representation in this discussion, the results are valid for the physical, two-dimensional problem, except as noted.

Concisely stated, the phase retrieval concept is to estimate $\theta(f)$ based on observation of $p(x)$.

The basic algorithm uses a polynomial expansion for $\theta(f)$,

$$\theta(f) = \sum_{k=1}^{\infty} c_k\,\theta_k(f)$$

where $\{\theta_k(f)\}$ is a suitable set of f-polynomials. A phase estimate $\hat{\theta}(f)$ with a finite number of c_k's is formed and an estimated OTF, $P_c(f)$, is calculated. This is compared to the measured OTF, $P(f)$, and an error metric drives a C-vector search to minimize the error. When the error reaches a stable minimum we declare $\hat{\theta}(f)$ to be the estimate of $\theta(f)$. See Figure 2.

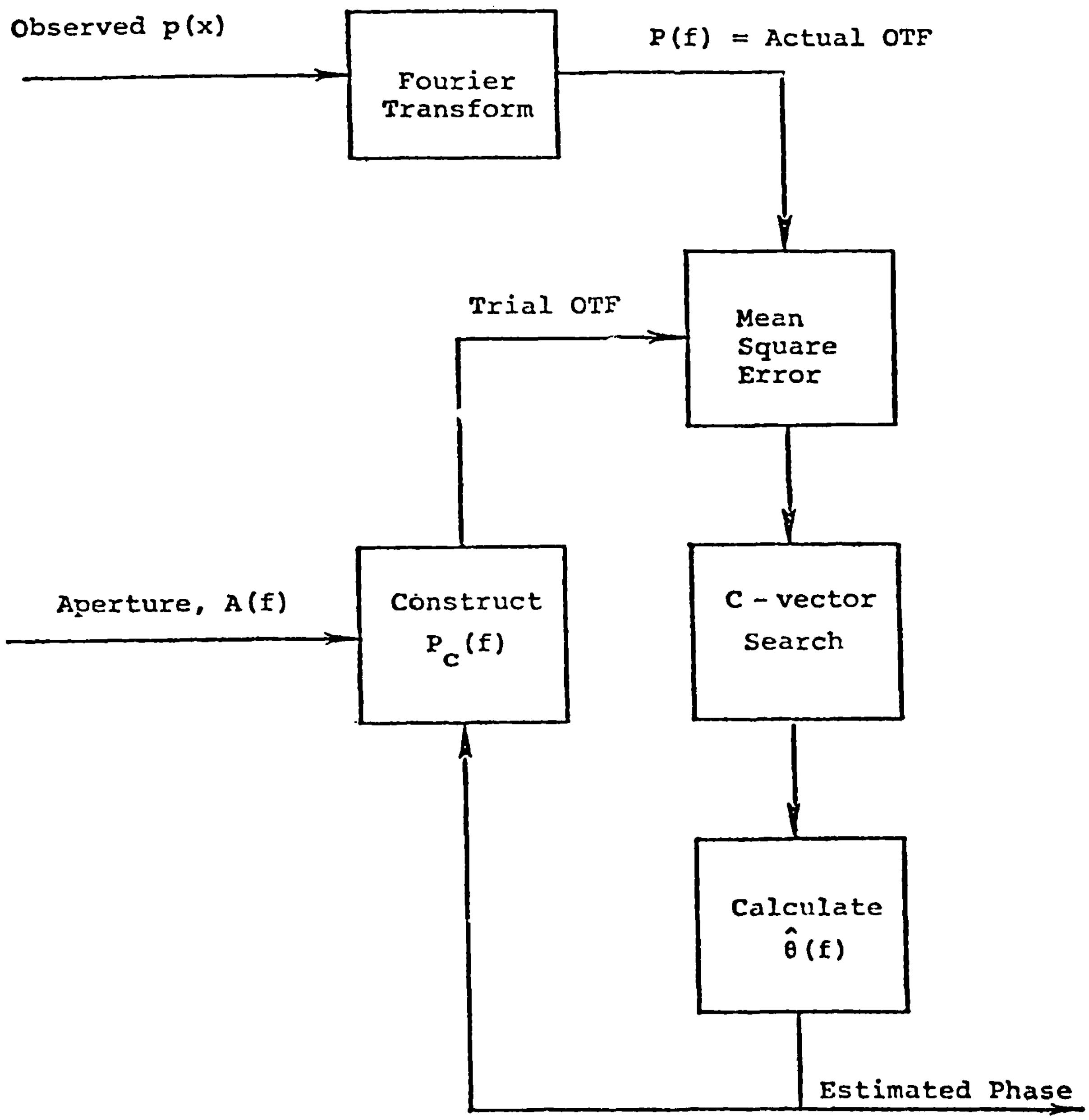

Figure 2 Parameter Search Algorithm

An example of phase retrieval which uses the basic algorithm is shown in Figures 3, 4, and 5. Figure 3 is a contour plot of the phase aberration (about 2 waves, peak-to-valley) across a circular, unobscurated aperture. This yields the PSF shown in Figure 4. When we estimate the phase from Figure 4 and subtract this estimate from the actual phase in Figure 3, the resulting PSF is nearly diffraction limited, as shown in Figure 5.

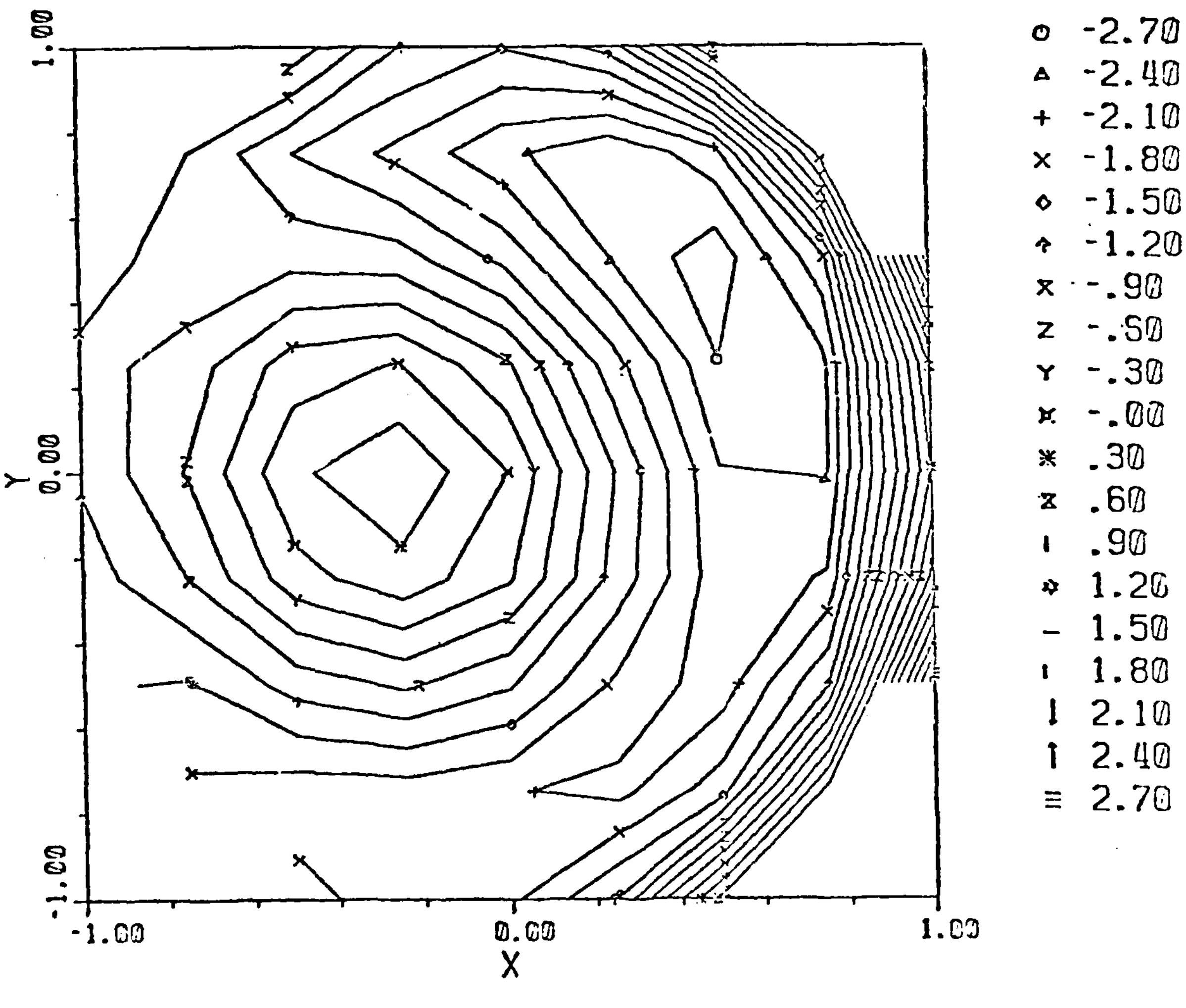

Figure 3 Initial phase aberration across exit pupil. Contour values in waves.

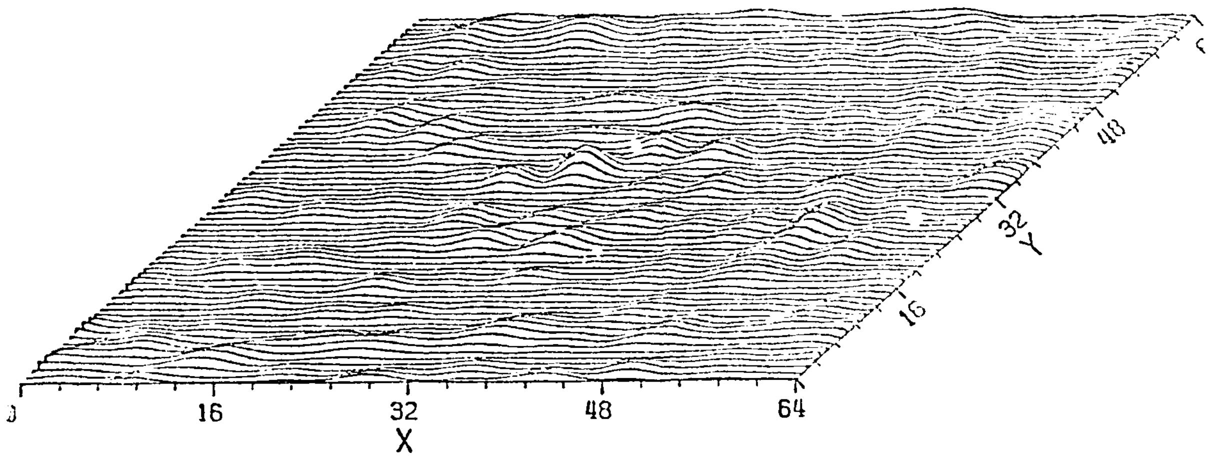

Figure 4 PSF of original aberrated system. Point detectors.

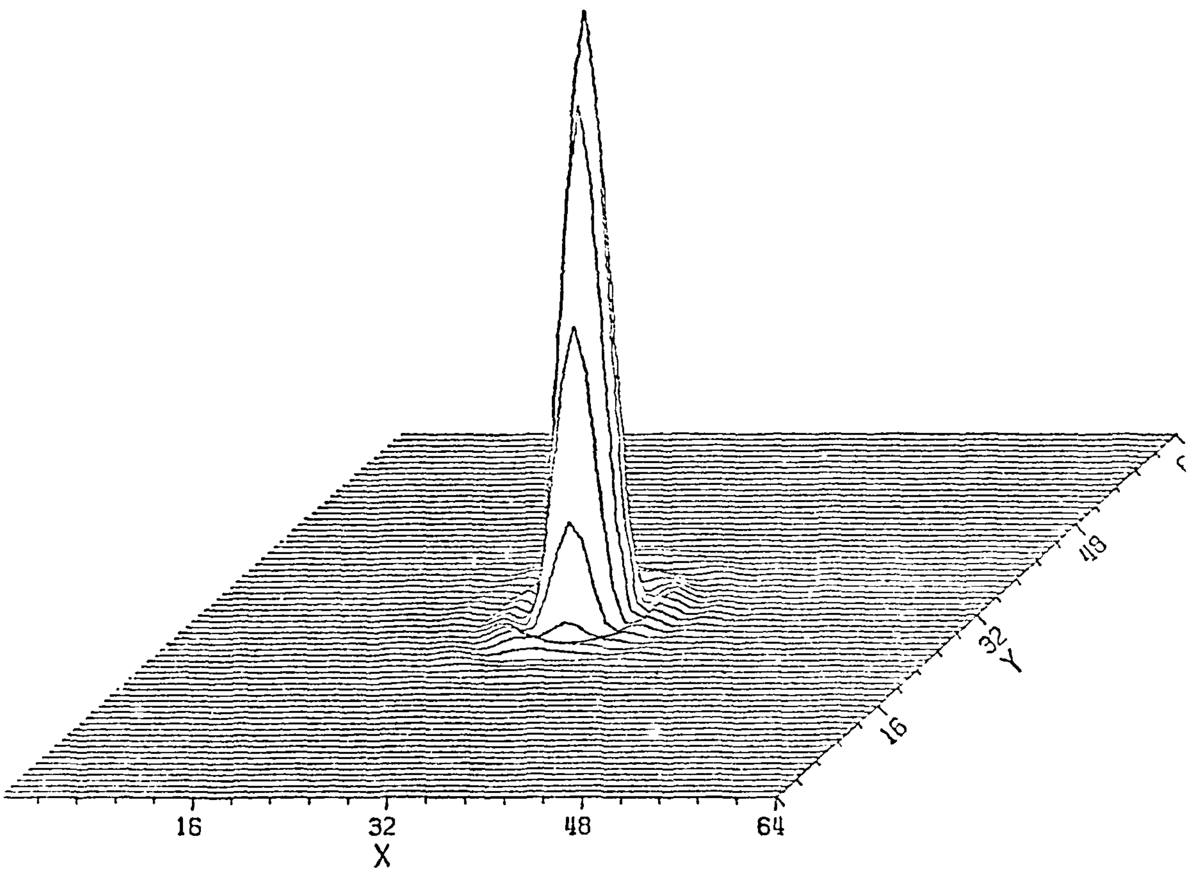

Figure 5 PSF after correction. Point detectors.

Details on the algorithm that implements the phase retrieval concept are given in the final report on the previous contract. These details include discussions of the search technique (a grid search followed by a modified, steepest descent algorithm of the Fletcher-Powell type), the numerical procedures for calculating the PSF, the polynomials (Zernicke polynomials, to order 24), and the computer code itself. The final report also describes successful blind tests of the algorithm that were conducted with Draper Labs and with Hughes Aircraft Company; it describes a simple experimental verification of the theory (point source, aberrated by a phase-distorted imaging system); and it gives some preliminary results on extended objects.

3 ALIASING

An array of detectors in the focal plane spatially averages the image over the detector profile of each individual detector and produces an array of numbers that describes a sampled image. The sampling interval is the spacing between detectors, measured from center-to-center. If the image a(x) is band-limited to a spatial frequency f_{max} (cycles per unit distance), then a(x) is completely determined if spatial samples are taken at intervals smaller than $1/(2\ f_{max})$, the Nyquist sampling interval. In what follows we will set f_{max} equal to $1/(\lambda F\#)$, as is the case for a diffraction-limited optical system.

For the purposes of this study we assume that the diode spacing will be up to five times larger than the Nyquist sampling interval. Thus, the image will be undersampled and there will be a severe amount of "aliasing". This aliasing effect is described as follows. If the image is a(x) with Fourier transform A(f), the sampling procedure produces a spectrum G(f),

$$G(f) = \sum_{k=-\infty}^{\infty} A(f - kf_o),$$

where

$$x_o = 1/f_o$$

is the spatial sampling interval. If f_o is less than twice the highest frequency in A(f), the aliases in G(f) overlap and the spectrum A(f) (and, therefore, a(x)) cannot be recovered. See Figure 6.

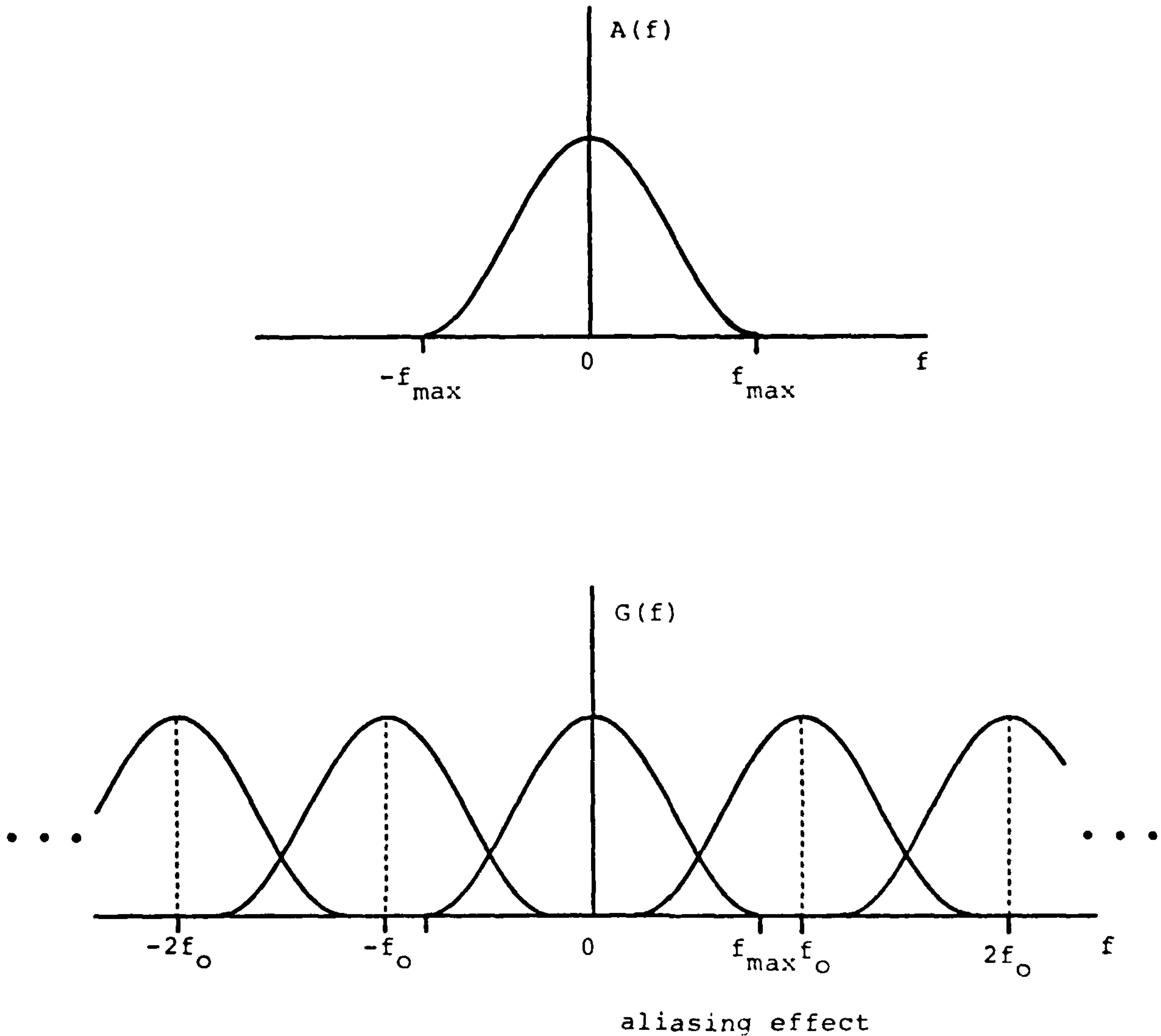

Figure 6. The aliases overlap if $f_o < 2f_{max}$.

The effects of undersampling are more graphic when shown in the spatial domain. Thus, Figure 7 shows a digital image of a point spread function sampled at the Nyquist sampling rate. This PSF is the result of about one wave (peak-to-peak) of wavefront distortion in the aperture. In Figure 8 we show another PSF with approximately the same amount of wavefront distortion. But this has been sampled by detectors that are four times larger than the Nyquist sampling rate. Note the loss of detail.

0	0	1	0	1	1	1	0	1	1	1	2	1	1	1	1	2	1	0	0	0	0	1	0	0
0	0	0	0	0	0	1	1	1	1	0	0	0	1	1	0	0	0	0	1	1	0	0	0	0
0	1	1	1	0	2	1	0	1	2	2	2	3	2	2	2	2	2	1	0	1	1	0	0	0
0	0	0	0	0	1	0	1	2	1	1	1	1	1	1	1	1	1	1	1	1	0	1	1	0
0	0	0	0	0	1	2	1	2	3	4	4	4	4	5	4	3	2	1	0	2	1	0	1	0
0	0	1	0	1	2	0	1	3	3	3	3	3	2	2	2	2	3	4	2	1	1	1	0	0
0	0	0	1	1	1	2	4	3	3	6	9	8	7	7	8	5	2	1	1	2	1	0	1	0
0	0	1	1	0	3	2	3	5	8	8	6	5	5	5	4	5	5	4	7	1	3	1	1	1
1	0	1	0	1	1	1	5	6	6	8	11	11	14	12	9	5	2	4	6	2	1	2	1	1
0	0	0	0	1	1	4	5	4	12	17	15	12	9	9	11	13	11	3	2	4	1	1	1	0
0	0	0	1	1	2	3	4	10	14	11	14	17	17	14	9	4	8	10	3	1	3	0	1	0
1	0	0	1	1	2	1	7	10	11	23	32	25	19	22	26	20	5	4	8	1	3	2	0	2
1	0	0	0	1	1	3	7	6	21	31	19	11	8	5	7	18	23	4	5	6	1	3	0	2
0	0	1	0	1	0	3	3	10	23	19	30	40	30	31	31	3	18	18	1	8	1	2	0	1
0	0	1	0	1	0	3	1	13	13	31	63	31	4	23	80	39	2	20	3	5	2	1	1	1
0	0	0	0	1	0	2	1	10	7	57	63	10	37	6	44	61	7	13	4	3	1	1	1	1
1	0	0	0	1	0	2	0	6	5	41	47	54	159	60	5	34	15	10	3	3	1	1	0	1
1	0	1	0	1	0	1	0	2	3	18	42	140	393	272	48	16	17	8	2	3	1	2	0	0
1	1	1	0	0	0	0	0	0	2	4	30	139	280	228	73	18	13	5	3	2	0	1	0	0
0	0	1	0	0	1	0	0	0	0	1	12	64	133	121	54	19	8	3	3	1	0	0	1	1
1	0	0	0	0	0	0	0	0	1	1	5	22	46	47	26	9	2	2	1	1	1	0	1	0
0	0	0	0	0	0	0	0	0	1	1	2	4	8	7	3	1	1	1	0	1	0	0	0	0
0	0	0	0	0	1	0	0	0	0	0	0	0	0	0	1	1	0	0	0	0	0	0	0	1
1	1	0	0	0	0	0	0	0	0	0	1	0	0	0	0	0	1	0	0	1	1	0	0	0
0	0	1	0	0	0	0	0	0	0	0	1	1	1	1	1	1	0	0	0	0	0	0	0	0
0	0	0	0	0	0	1	0	0	1	0	0	0	0	0	0	0	0	0	0	0	1	0	0	0
0	0	0	0	0	0	0	0	0	0	0	0	1	1	0	1	1	1	0	0	0	0	0	0	0
0	0	0	0	0	0	0	0	0	1	0	0	0	0	0	0	0	0	0	0	0	0	0	0	0
0	0	0	0	0	0	0	0	0	1	1	1	0	1	1	1	1	1	1	0	0	1	0	0	1
1	0	0	0	1	0	0	1	0	0	0	1	0	0	0	0	0	0	0	0	0	0	0	0	0
0	0	0	0	1	0	0	0	0	1	1	1	0	1	1	1	1	1	0	0	0	1	1	0	0
0	0	1	0	0	0	1	0	0	0	0	0	0	0	0	0	0	0	0	0	0	0	0	0	0

Figure 7. Part of a 32 by 32 point spread function sampled at the Nyquist sampling rate

1	1	3	5	5	3	2	1
1	2	9	20	17	8	3	2
1	2	16	61	53	18	5	1
1	2	16	116	106	35	4	2
1	1	3	151	448	25	3	1
1	1	1	10	38	3	1	1
1	1	1	1	2	1	1	1
0	1	1	2	2	1	1	1

Figure 8. 8 by 8 detected point spread function undersampled by a factor of 4 in both X and Y directions

This example illustrates the concern for the utility of a phase retrieval algorithm when the detectors are large. The image data is grossly washed out. It turns out, however, that the phase associated with the PSF of Figure 8 was accurately captured by the algorithm, even when a small amount of noise is added to the observed PSF.

In order to study the effects of aliasing on phase retrieval, a new computer program was written which works on PSF's instead of OTF's. Square blocks of pixels may be summed into one output pixel, simulating the effect of using square detectors that are an integral number of samples wide. The initial, unaliased PSF is sampled at the Nyquist interval of $\lambda F\#/2$. The pupil is a circular aperture in a 16 by 16 array, as shown in Figure 9. A phase aberration is constructed over the aperture and the generalized pupil function computed. It is buffered out to 32 by 32 and a Fast Fourier Transform taken, resulting in a 32 by 32 coherent spread function. The magnitude squared gives the PSF.

4	4	4	4	4	0	0	0	0	0	0	4	4	4	4	4
4	4	4	0	0	0	0	0	0	0	0	0	0	4	4	4
4	4	0	0	0	0	0	0	0	0	0	0	0	0	4	4
4	0	0	0	0	0	0	0	0	0	0	0	0	0	0	4
4	0	0	0	0	0	0	0	0	0	0	0	0	0	0	4
0	0	0	0	0	0	0	0	0	0	0	0	0	0	0	0
0	0	0	0	0	0	0	0	0	0	0	0	0	0	0	0
0	0	0	0	0	0	0	0	0	0	0	0	0	0	0	0
0	0	0	0	0	0	0	0	0	0	0	0	0	0	0	0
0	0	0	0	0	0	0	0	0	0	0	0	0	0	0	0
0	0	0	0	0	0	0	0	0	0	0	0	0	0	0	0
4	0	0	0	0	0	0	0	0	0	0	0	0	0	0	4
4	0	0	0	0	0	0	0	0	0	0	0	0	0	0	4
4	4	0	0	0	0	0	0	0	0	0	0	0	0	4	4
4	4	4	0	0	0	0	0	0	0	0	0	0	4	4	4
4	4	4	4	4	0	0	0	0	0	0	4	4	4	4	4

Figure 9. Pupil function used in simulations. 0 indicates inside aperture, 4 indicates outside aperture.

Simulations were run by reading in an aberration (in terms of Zernicke polynomials) and constructing a PSF. The detector model was applied and noise added. This is the simulated measured PSF. The program attempts to deduce the aberrations by searching over the parameters which are the coefficients of the Zernicke polynomials to find a PSF which yields the best possible fit to the measured PSF. The error metric is

$$E(\vec{p}) = \sum_{i,j} (P_{ij}(\vec{p}) - D_{ij})^2,$$

where D is the measured PSF data and P the trial PSF, which is a function of the parameters $\vec{p}$.

The Zernicke polynomials used are shown in Table 1. The results for various noise levels and amounts of aliasing are presented in Table 2. The row labelled "initial" is the aberration corresponding to the simulated measured PSF. This aberration across the aperture is shown in Figure 10. Cases 1 through 7 all used detectors which were averages of a 4 by 4 array of the original Nyquist sampled pixels. Figure 7 shows the Nyquist sampled 32 by 32 PSF from the initial aberration. Figure 8 shows the 8 by 8 detected PSF. In Figure 11 is the noisy PSF from case 2.

Table 1

Zernicke Polynomials

Number	Form	Name
2	x	x tilt
3	y	y tilt
4	x^2+y^2	focus
5	x^2-y^2	0° astigmatism
6	$2xy$	45° astigmatism
7	$x(r^2-3)$	x coma
8	$y(r^2-3)$	y coma

Case	Zernicke Polynomial Coefficient							Noise Standard Deviation		RMS Phase	Strehl Ratio
	2	3	4	5	6	7	8	DL Peak	Aberrated Peak		
Initial	0.	0.	.3	.15	.1	-.3	.05			.224	.30
1	.099	-.006	.293	.156	.104	-.313	.051	0.	0.	.051	.90
2	-.017	-.023	.290	.169	.096	-.312	.035	.46%	1.03%	.019	.99
3	-.030	-.043	.280	.182	.097	-.316	.015	.91%	2.06%	.036	.95
4	-.055	-.025	.309	.145	.120	-.292	.017	.91%	2.06%	.035	.95
5	-.033	-.085	.247	.198	.127	-.321	-.034	1.82%	4.12%	.070	.83
6	.097	-.050	.310	.140	.143	-.290	-.008	1.82%	4.12%	.063	.85
7	.148	-.110	.267	.234	.224	-.325	-.140	3.65%	8.25%	.119	.54

Table 2 Results of Phase Retrieval when the PSF is undersampled by a factor of 4 in both X and Y directions

0.000	0.000	0.000	0.000	0.000	1.009	0.912	0.853	0.834	0.856	0.921	0.000	0.000	0.000	0.000	0.000
0.000	0.000	0.000	0.929	0.775	0.652	0.562	0.505	0.485	0.502	0.559	0.657	0.799	0.000	0.000	0.000
0.000	0.000	0.805	0.640	0.499	0.386	0.302	0.249	0.228	0.242	0.291	0.379	0.506	0.674	0.000	0.000
0.000	0.745	0.577	0.429	0.303	0.200	0.124	0.074	0.053	0.064	0.106	0.183	0.296	0.447	0.638	0.000
0.000	0.562	0.416	0.286	0.175	0.084	0.015	-0.030	-0.050	-0.043	-0.006	0.061	0.161	0.295	0.465	0.000
0.571	0.436	0.312	0.201	0.105	0.026	-0.034	-0.075	-0.093	-0.088	-0.057	0.001	0.088	0.206	0.356	0.541
0.464	0.355	0.254	0.163	0.084	0.017	-0.035	-0.070	-0.086	-0.082	-0.057	-0.007	0.068	0.170	0.301	0.463
0.392	0.310	0.233	0.162	0.099	0.045	0.003	-0.025	-0.039	-0.037	-0.015	0.026	0.090	0.177	0.289	0.429
0.344	0.290	0.237	0.187	0.141	0.101	0.069	0.047	0.036	0.039	0.056	0.090	0.143	0.215	0.310	0.428
0.310	0.285	0.256	0.227	0.199	0.174	0.153	0.138	0.130	0.133	0.147	0.174	0.216	0.275	0.353	0.450
0.279	0.283	0.280	0.273	0.263	0.252	0.243	0.235	0.233	0.236	0.247	0.268	0.301	0.346	0.407	0.484
0.000	0.274	0.297	0.313	0.322	0.327	0.329	0.330	0.332	0.337	0.346	0.361	0.384	0.417	0.461	0.000
0.000	0.248	0.298	0.336	0.365	0.386	0.400	0.411	0.418	0.425	0.432	0.443	0.457	0.478	0.507	0.000
0.000	0.000	0.272	0.333	0.382	0.420	0.447	0.467	0.481	0.490	0.497	0.502	0.509	0.518	0.000	0.000
0.000	0.000	0.000	0.293	0.363	0.417	0.459	0.489	0.509	0.521	0.527	0.529	0.528	0.000	0.000	0.000
0.000	0.000	0.000	0.000	0.000	0.369	0.424	0.465	0.492	0.508	0.515	0.000	0.000	0.000	0.000	0.000

Figure 10 Phase aberrations used in simulations, evaluated across the aperture, in units of waves.

10	10	10	0	2	0	8	9
2	-2	12	15	21	12	1	0
2	2	20	61	50	22	6	0
11	5	8	116	104	32	1	13
1	10	6	159	448	9	12	3
4	5	-3	3	30	5	0	-2
-7	5	5	0	7	0	3	5
5	3	6	-3	0	2	-5	2

Figure 11 Noisy Detected Point Spread Function from Case 2.

The noise is added to each pixel of the detected PSF, and is independent and Gaussian distributed. The standard deviation of the noise is expressed in two ways in Table 2; as a percentage of the peak value of a diffraction-limited PSF as detected, and of the peak of the aberrated detected PSF. Cases 3 and 4, and 5 and 6, have the same noise levels but have different random realizations.

The parameter values listed in each row are the values at which the search terminated, and is the final estimate. When the initial parameters are corrected by the estimate, the residual phase aberration has an RMS value across the aperture as listed in the column labelled "RMS Phase". The Strehl ratio of the corrected, Nyquist sampled PSF is in the column labelled "Strehl Ratio". Not surprisingly, the quality of the final corrected PSF deteriorates as the noise level increases, until case 7 which results in only slight improvement.

From the results in Table 2 we see that a PSF, undersampled by a factor of 4, can provide a good estimate of the wavefront. The PSF has additive noise to a level of about 2% of the diffraction-limited peak.

Table 3 shows, for the same initial aberration the results of increasing the detector size. Even with 10 by 10 detectors, phase retrieval is still successful. Figure 12 shows the detected and noisy detected PSF's for case 13, with the 10 by 10 detectors. Table 3 lists, in the rows labelled "G" and "D", where the grid search terminated and the final result where the Davidon search finished.

Table 4 shows two different aberrations. Cases 14, 15, and 16 are for a detector size of 10 by 10. The noise-free case worked, and the noisest case resulted in significant improvement, while the less noisy one essentially failed in the grid search to find a good starting point for the Davidon search. Cases 17 and 18 show another aberration failing with 5 by 5 detectors, both for noise-free and noisy data. With 2 by 2 or 4 by 4 detectors, phase retrieval was successful.

These results show that aliasing is not a major problem to phase retrieval. There are still problems with regard to doing a fine enough mesh on the grid search to insure detection of the global minimum, but aliasing does not seem to create any new difficulties.

INITIAL PSF (DETECTED)

5	42	11	1	0
5	366	33	1	0
2	21	3	0	0
0	1	1	0	0
0	0	0	0	0

INITIAL PSF (DETECTED WITH NOISE)

7	44	22	13	10
14	363	47	25	13
5	25	3	23	-17
-6	4	23	-1	14
8	16	12	-12	11

Figure 12 Case 13 Point spread functions (10 by 10 detector size)

Case	Detector size		Zernicke Polynomial Coefficient							Noise Standard Deviation		RMS Phase	Strch Ratio
			2	3	4	5	6	7	8	DL Peak	Aberrated Peak		
Initial			0.	0.	.3	.15	.1	-.3	.05			.224	.30
8	5	G			.250	.125	.125	-.375	.0				
		D	.035	.014	.264	.094	.097	-.365	.027	.45%	.79%	.044	.93
9	6	G			.250	.125	.01	-.375	.0				
		D	.070	-.052	.263	.151	.110	-.344	.068	.43%	.72%	.051	.90
10	7	G			.250	.250	.125	-.250	.125				
		D	.025	.035	.263	.162	.159	-.346	.051	.41%	.69%	.043	.93
11	8	G			.375	.125	.125	-.250	.0				
		D	-.024	.030	.339	.120	.086	-.271	.031	.41%	.90%	.035	.95
12	8	G			.375	.125	.125	-.125	-.125				
		D	.0	.063	.366	.076	.102	-.268	.042	1.65%	3.6%	.060	.87
13	10	G			.250	.125	.0	-.375	.125				
		D	.037	-.015	.259	.043	-.022	-.393	.063	2.5%	3.16%	.082	.76

Table 3 Results of Phase Retrieval for Various Detector Sizes

Case	Detector Size		Zernicke Polynomial Coefficient 2	3	4	5	6	7	8	Noise Standard Deviation DL Peak	Noise Standard Deviation Aberrated Peak	RMS Phase	Strehl Ratio
Initial			0.	0.	.17	.08	.34	.11	.23			.202	.38
14	10	G			.250	.0	.375	.125	.125	1.62%	4.26%	.098	.78
		D	.148	.064	.043	.032	.359	.126	.196				
15	10	G			.125	.125	.375	.125	.250	0.	0.	.040	.94
		D	-.011	.022	.132	.130	.390	.105	.221				
16	10	G			.125	.0	.625	.0	.125	.81%	2.13%	.160	.38
		D	-.087	.071	.177	.032	.626	.065	-.004				
Initial			0.	0.	.43	.02	.19	.20	.29			.298	.20
17	5	G			.250	.0	.625	.375	.375	.9%	4.4%	.227	.21
		D	.031	-.015	.225	.085	.582	.414	.406				
18	5	G			.250	.0	.625	.375	.375	0.	0.	.235	.20
		D	-.031	-.064	.178	.076	.558	.406	.393				
19	2	G			.375	.125	.250	.125	.375	0.	0.	.010	.996
		D	-.013	-.010	.424	.020	.179	.199	.291				
20	1	G			.375	.0	.250	.125	.375	0.	0.	.004	.999
		D	-.006	-.002	.429	.019	.186	.200	.291				

Table 4 Results of Phase Retrieval

4 NOTES ON EFFICIENT SEARCH TECHNIQUES

Previously proposed phase retrieval search methods have involved comparing a measured PSF (or, equivalently, an OTF) with a large number of PSF's from a grid of parameter values covering the region of parameter space which is expected to include the actual aberration. These PSF's have always been recomputed for each search, even though they do not change. A faster method, which actually uses less computational hardware, is to compute the PSF's once and store them on disk, and retrieve them as needed during the search.

To work out the speed of this operation, suppose that we wish to examine, in the grid search, three values for each of thirteen parameters. This yields 1.6×10^6 PSF's. (Five values for nine parameters gives a slightly larger number.) Storing an eight by eight PSF, quantized to 256 levels (so that each pixel will fit in a single byte) for each grid point would take 102 megabytes, which is within the capacity of a single large disk drive. If the data is read off the disk in an optimum manner so as not to waste disk head movements, three minutes are taken to transfer all the data to the CPU. To compute the error metric on a 64 pixel PSF takes 128 additions and 64 multiplications. The total for all 1.5×10^6 PSF's is $192 \cdot 10^6$ additions and $96 \cdot 10^6$ multiplications. To perform the computation in three minutes of disk read time requires a speed of 500 nsec per addition and 1000 nsec per multiplication. This is within the capability of a PDP 11/70 doing integer arithmetic. (Floating point is not needed for these calculations.) Since the CPU would be active at the same time as the disk transfer were taking place, the computation time and I/O time could be totally overlapped so that only three minutes are required for the entire search.

There remains the problem of the second grid search. This is performed at half the grid spacing of the first search in the region immediately around the best points of the first search. It has proven necessary only occasionally to actually do the second grid search in the simulations that have been run previously, but for higher dimensions of parameter space the distance from a point in the center of any hypercube formed by the grid points grows as the square root of the dimensionality. Prestoring PSF's calculated for parameter values on a finer grid mesh would take far too much storage. Calculating them as needed for a second grid search would dwarf the time of the first search. If the first grid spacing is small enough, then the second search can be avoided. Alternatively, a downhill search can be started from each of the best survivors of the first search. The downhill search time rises only linearly with the dimensionality.

A faster method for the first grid search involves the use of moments, or some other characterization of distinctive properties of the PSF. Five moments, as we use in Section 5, seem a good number. The PSF's used for the first grid search are sorted on their moments, into 15 bins adjusted for each moment to span the range of moment values, and perhaps so that approximately equal numbers of PSF's fall into each bin. The PSF's are placed on the disk in an order beginning with the PSF's where moments all fall into the first bins, stepping through all bins on the fifth moment, then moving onto the second bin of the fourth moment and stepping through all fifth moment bins, and continuing until the PSF's in the fifteenth bin for all moments are written. This order is listed in Table 5.

TABLE 5

Order of PSF's Sorted in Moments

M_1	M_2	M_3	M_4	M_5
1	1	1	1	1
1	1	1	1	2
	.	...		.
1	1	1	1	15
1	1	1	2	1
		...		
1	1	1	2	15
		...		
1	1	1	15	15
1	1	2	1	1
		...		
15	15	15	15	15

This is a total of 15^5, or 759,375 possible slots for a PSF to be assigned to. If we have 3^{13} grid points, or 1,594,323, there will be an average of two PSF's in each slot, although considerable variation may be expected. Given a measured PSF, its five moments may be calculated and a decision made as to which bin each moment falls in, in negligible time. A way of pointing to the area on disk which holds the PSF's corresponding to the five moments is needed. Such a table, with 759,375 entries may be constructed. Its size is such that it too must be on disk. Each table entry holds an address on the disk for where PSF data begins for that particular slot. Data continues on the disk until the next address in the table is reached. Access into table is easily computable; if the bin values for each moment are i, j, k, ℓ, and m, then element number $(i-1)*15^4 + (j-1)*15^3 + (k-1)*15^2 + (\ell-1)*15 + m$ is the proper table address. Generating the sorted PSF file and the address table will require a great deal of computer time, but it only needs to be done once.

Examining only the bins into which the moments of measured PSF fall is unwise, since noise and the presence of other aberrations will perturb the moments. A safer course is to examine three bins for each moment, the one into which the measured moment falls and the ones on either side. This corresponds to 20% of the range of moment values for each moment. For five moments, only .00032 of the full set of grid points survive. Taking three bins for each moment results in making 3^5, or 243, references in the address table, which will point to, on the average, a total of 486 PSF's. Each of these PSF's may be compared with the measured PSF and a metric computed. This should take less than 30 seconds to do. Downhill searches can be started from the parameter sets associated with the PSF's with the lowest metrics. The parameters from the search that terminates at the smallest metric are the final estimate.

5 THE USE OF MOMENTS TO SPEED UP THE ALGORITHM

The search method which has been used for phase retrieval applications consists of an initial search over a rectangular grid of points in parameter space, a second search around the best (lowest metric) grid points at half the first grid spacing, and a downhill Davidon search from the best point of the second grid search. The initial grid search is the most crucial to obtaining a good phase estimate, and is quite time-consuming to compute the metric of the sum of the squares of the differences between the measured and trial PSF's point by point.

A method was sought that would allow, by means of a quick comparison of only a very few numbers associated with each PSF, whether or not a trial PSF is worthy of further consideration. A natural approach is to use moments of the PSF distribution. The most fundamental moment is the center of gravity, defined by

$$E = \int P(x,y)\,dxdy$$

$$x_{c.g.} = \int x\ P(x,y)\,dxdy/E$$

$$y_{c.g.} = \int y\ P(x,y)\,dxdy/E.$$

Given that the ideal position of the point object is known, the location of the c.g. (in the absence of noise) exactly determines the tilt parameters of the aberration. A slightly modified set of Zernicke polynomials may be constructed such that only the tilt terms move the c.g.

Previous work has shown the c.g. to be rather sensitive to quantization noise (and presumably any other sort of noise) on the PSF. In the work reported here, we have assumed that the tilt problem will be dealt with in some appropriate fashion. The aberrations tested had no tilt errors.

Five more moments around the c.g. were defined; the weighting factors were taken to be the aberration polynomials themselves. They are:

$$M_1 = \int (x'^2 + y'^2)\ P\ dxdy/E$$

$$M_2 = \int x'y'\ P\ dxdy/E$$

$$M_3 = \int (x'^2 - y'^2)\ P\ dxdy/E$$

$$M_4 = \int x'r^2\ P\ dxdy/E$$

$$M_5 = \int y'r^2\ P\ dxdy/E\ ,$$

where $x' = x - x_{cg}$

$y' = y - y_{cg}$

Some intuitive meanings may be assigned to these moments. M_1 is an indication of the overall width of the PSF. M_2 is large and positive for a PSF of an elliptical sort of shape, with the long axis oriented at 45° to the X axis. It is negative for the long axis along 135°. The greater the asymmetry between the long and short axes, the larger the magnitude of M_2. M_3 is similar to M_2 except that the orientations for maximum magnitude are 0° and 90°. Orientations of the long axis at other angles give contributions to both M_2 and M_3. M_4 and M_5 measure the asymmetry along either the X or Y directions relative to the c.g. A PSF like Figure 13 would have a positive M_4 value.

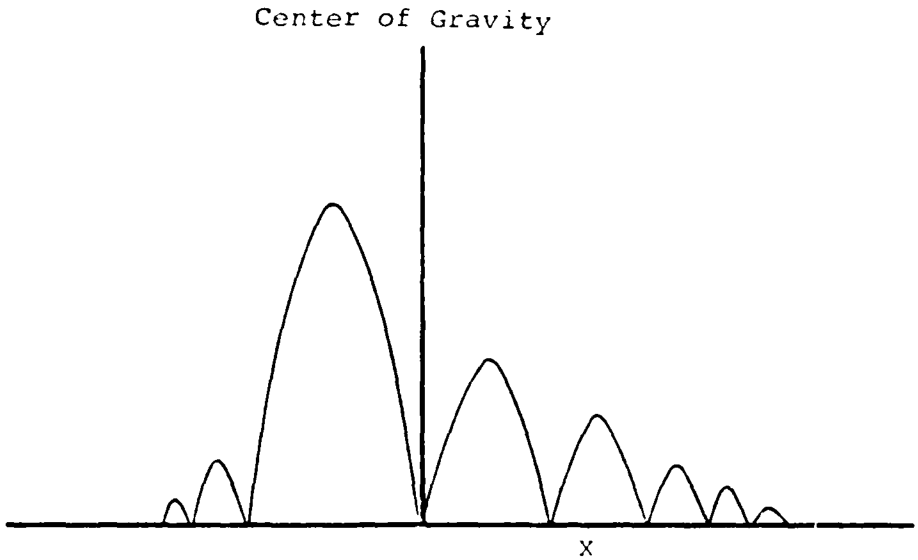

Figure 13 PSF with large positive M_4

Sofware was written to calculate these moments from simulated PSF's. An investigation was made of the sensitivity of the moments to noise on the PSF. Table 6a shows the five moments and the c.g. for the PSF from an aberration consisting of 1/4 wave of 45° astigmatism and 1/4 wave of x-coma. The sample spacing of the PSF is $\lambda F\#/2$. The first line shows results with no noise. The next two lines show the averages and standard deviations of the moments for 100 realizations of signal-independent white noise on the PSF. The noise variance was 1.85% of the maximum value of the diffraction-limited PSF. Since this aberration has a Strehl ratio of .468, the variance was 3.95% of the peak value of the aberrated PSF. The variation of the moments is too large for them to be useful. Figures 14 and 15 show this PSF noise-free and with noise.

Table 6

Moments and Centers of Gravity

6a No Window

	M_1	M_2	M_3	M_4	M_5	$X_{c.g.}$	$Y_{c.g.}$
Noise-free	18.43915	-0.02660	2.54868	17.68840	-9.06288	17.83975	16.97017
Average	11.16394	0.70817	0.34411	40.25219	-17.61442	17.80108	16.84488
Standard Deviation	26.04207	12.31852	12.84923	359.42038	307.76523	1.17613	1.18405

6b Gaussian Window on Moment Calculations

	M_1	M_2	M_3	M_4	M_5	$X_{c.g.}$	$Y_{c.g.}$
Noise-free	5.56922	-0.01721	1.23211	1.58887	0.21246	17.83975	16.97017
Average	7.39776	0.13930	0.96507	-0.63317	0.46233	17.80108	16.84488
Standard Deviation	2.42691	1.27252	1.68210	13.25964	12.05371	1.17613	1.18405

6c Gaussian Window on Moments and Center of Gravity

	M_1	M_2	M_3	M_4	M_5	$X_{c.g.}$	$Y_{c.g.}$
Noise-free	5.18473	-0.00154	1.03292	4.87469	0.3419	17.41641	16.99483
Average	5.32479	0.05235	1.00183	4.45818	-0.28306	17.44165	16.96510
Standard Deviation	0.62237	0.29024	0.39897	2.71539	2.02424	0.32990	0.29117

0	0	0	0	0	0	0	0	0	0	0	0	0	0	1	1	0	1	1	0	0	0	0	0	0	0	0	0	0	0	0	0
0	0	0	0	0	1	1	0	0	1	0	0	0	0	0	0	0	0	0	0	0	0	0	1	0	0	1	1	0	0	0	0
0	0	0	0	0	0	0	0	0	0	0	0	0	1	1	1	0	1	1	1	0	0	0	0	0	0	0	0	0	0	0	0
0	0	0	0	0	0	0	0	0	0	1	0	0	0	0	0	0	0	0	0	0	0	1	0	0	0	0	0	0	0	0	0
0	0	0	1	0	0	0	0	0	0	0	0	0	0	0	0	1	0	0	0	0	0	0	0	0	0	0	0	0	1	0	0
0	0	0	0	0	0	0	0	0	0	1	1	0	0	0	0	0	0	0	0	0	1	1	0	0	0	0	0	0	0	0	0
0	0	0	0	0	0	0	0	0	0	0	0	0	0	0	0	0	0	0	0	0	0	0	0	0	0	0	0	0	0	0	0
1	0	0	0	0	0	0	0	0	0	0	0	0	0	0	0	0	0	0	0	0	0	0	0	0	0	0	0	0	0	0	0
0	0	0	0	0	0	0	1	0	0	1	0	0	0	1	0	0	0	1	0	0	0	1	0	0	1	0	0	0	0	0	0
0	0	0	0	0	0	0	0	0	0	0	0	0	0	0	0	0	0	0	0	0	0	0	0	0	0	0	0	0	0	0	0
1	0	0	0	0	0	0	1	0	0	0	0	0	0	1	1	0	1	1	0	0	0	0	0	0	1	0	0	0	0	0	0
0	0	0	0	1	0	0	1	0	0	0	0	1	0	1	1	2	1	1	0	1	0	0	0	0	1	0	0	1	0	0	0
0	0	0	0	1	0	0	0	0	0	1	1	0	0	2	11	17	11	2	0	0	1	1	0	0	0	0	0	1	0	0	0
0	0	0	0	0	0	0	0	1	0	1	0	2	1	5	33	52	33	5	1	2	0	1	0	1	0	0	0	0	0	0	0
0	0	0	0	0	1	0	1	0	1	1	2	4	3	28	99	145	99	28	3	4	2	1	1	0	1	0	1	0	0	0	0
0	0	0	0	0	0	0	1	0	1	0	3	4	4	47	218	353	218	47	4	4	3	0	1	0	1	0	0	0	0	0	0
0	1	0	0	0	1	0	1	0	1	0	2	3	4	19	247	468	247	19	4	3	2	0	1	0	1	0	1	0	0	0	1
0	0	0	1	0	1	0	1	0	2	0	2	3	35	42	113	216	113	42	35	3	2	0	2	0	1	0	1	0	1	0	0
0	0	0	1	0	1	0	1	0	2	0	6	3	54	125	66	4	66	125	54	3	6	0	2	0	1	0	1	0	1	0	0
0	1	0	0	0	1	0	1	0	2	0	10	18	24	80	73	27	73	80	24	18	10	0	2	0	1	0	1	0	0	0	1
0	0	0	0	0	1	0	1	0	2	3	5	27	26	10	7	5	7	10	26	27	5	3	2	0	1	0	1	0	0	0	0
0	0	0	0	0	0	0	0	2	1	6	6	8	24	22	13	11	13	22	24	8	6	6	1	2	0	0	0	0	0	0	0
0	0	0	0	1	0	1	0	2	2	3	10	7	3	6	9	9	9	6	3	7	10	3	2	2	0	1	0	1	0	0	0
0	0	1	0	1	1	1	1	0	3	1	2	7	7	4	2	1	2	4	7	7	2	1	3	0	1	1	1	1	0	1	0
1	0	0	0	0	0	0	1	0	1	3	3	1	2	4	6	6	6	4	2	1	3	3	1	0	1	0	0	0	0	0	0
0	0	0	0	0	0	0	0	1	1	1	2	3	2	1	0	0	0	1	2	3	2	1	1	1	0	0	0	0	0	0	0
0	0	0	0	0	0	1	1	0	2	2	0	0	2	3	3	2	3	3	2	0	0	2	2	0	1	1	0	0	0	0	0
1	0	1	0	0	0	0	1	0	0	1	1	1	1	0	0	0	0	0	1	1	1	1	0	0	1	0	0	0	0	1	0
1	0	1	1	0	1	0	0	0	0	1	0	1	2	1	1	1	1	1	2	1	0	1	0	0	0	0	1	0	1	1	0
0	0	0	0	0	0	0	0	0	0	1	1	0	0	0	0	0	0	0	0	0	1	1	0	0	0	0	0	0	0	0	0
0	0	0	0	0	0	0	0	1	0	0	0	0	1	1	1	1	1	1	1	0	0	0	0	1	0	0	0	0	0	0	0
0	0	0	0	0	1	1	0	0	0	1	1	0	0	0	0	0	0	0	0	0	1	1	0	0	0	1	1	0	0	0	0

Figure 14 Aberrated PSF, Nyquist sampling

-6	46	-13	0	12	16	16	12	18	3	6	9	9	12	29	20	-19	-5	-1	-13	1	-26	-24	25	60	-1	-4	7	12	-11	0	4
-34	7	-9	15	-20	-2	-1	10	21	12	-4	-5	-4	7	-17	16	2	0	6	-9	-21	3	8	0	16	-34	-24	7	30	11	-1	-13
-4	1	8	-2	-20	-5	14	15	13	-16	-13	-8	-21	-24	23	8	22	-14	-13	-3	-3	-37	5	0	-11	4	1	16	4	1	20	-3
-44	34	2	-19	-12	-4	-7	13	-27	-13	-1	17	18	-29	-3	1	5	-10	-10	14	22	-7	1	12	-29	-4	3	26	-4	-30	12	3
-10	29	27	7	-10	1	-8	2	-32	11	3	10	-15	-6	16	22	-3	12	4	-22	-11	-5	14	-14	11	3	-5	8	-18	0	-6	12
5	-42	-4	-25	-4	-2	-29	11	53	14	5	4	24	-29	12	22	2	-44	-25	-8	0	18	23	-14	0	-11	-11	19	-3	-3	24	11
24	13	5	-34	-12	18	-25	-7	-27	-9	-6	-14	7	-4	-3	18	-37	-11	-16	1	36	29	8	-21	-1	15	-24	1	7	-15	13	-6
24	-23	-11	1	-20	-1	2	26	-20	-11	1	-6	9	-19	28	16	0	-8	24	-14	34	3	-40	34	0	16	3	35	22	32	-18	21
-4	-3	-6	35	13	-40	4	42	-7	5	10	-17	-40	17	3	32	-56	24	2	18	19	16	-54	-22	-14	-9	39	8	6	-37	-56	9
-1	11	4	-36	-14	-16	2	0	17	11	-19	-4	-5	-18	-14	-8	19	12	-20	7	0	28	-9	-1	9	-15	1	8	6	-38	-12	-20
19	3	-6	17	0	1	0	-4	5	-3	0	-16	-10	-21	14	-30	3	4	-42	-42	-6	15	29	41	-8	1	-19	-2	19	-17	1	9
0	-11	10	-9	-4	10	12	-3	5	-9	-10	-10	23	9	56	19	-8	16	21	2	15	-28	16	-21	10	-18	11	4	-11	-14	9	19
8	22	23	2	-27	-8	0	3	-36	14	14	-8	27	41	11	45	33	-2	-13	-23	-12	-16	10	-2	10	-7	-16	-5	0	0	7	27
-1	23	-14	-2	29	-6	26	6	19	28	-9	-29	-15	1	-2	54	41	7	-15	-4	4	-21	10	9	12	15	6	20	8	-1	39	-8
13	-30	-12	-19	-16	-31	28	33	-3	0	47	0	11	-15	35	117	121	92	27	-10	-13	14	-26	0	5	-29	-1	7	-31	3	-23	-30
-5	-33	-9	-21	-11	-7	-16	28	5	4	-5	1	-3	25	48	248	347	232	92	3	2	-10	-31	-1	-7	26	45	5	-28	-3	12	0
8	-34	7	16	-27	-23	-3	-8	-6	24	4	0	6	32	-1	259	488	237	15	15	-11	-34	-3	-4	31	8	10	-4	-14	-22	28	18
-16	13	16	24	-3	27	-12	-17	22	19	1	-7	23	21	47	114	218	121	33	35	5	0	-22	-24	12	24	31	18	12	8	-25	-14
-6	-7	32	5	12	7	-9	12	-7	9	12	-19	-10	37	152	69	-2	56	124	47	4	-28	22	2	-9	-20	-13	-7	-4	3	15	-9
14	13	-4	15	-4	21	14	37	4	12	6	-8	10	50	104	79	10	40	88	25	26	13	13	3	0	8	4	16	26	0	-18	13
20	0	9	-19	-2	35	-2	19	36	10	11	38	34	33	-7	-9	-13	-14	-9	4	9	21	-26	7	-2	-25	14	25	-39	-10	44	18
6	21	-10	0	12	19	9	-39	18	-36	32	46	39	65	-12	14	42	45	-24	34	17	16	29	-9	-15	0	12	25	-22	-4	24	-8
5	-16	-9	36	-37	10	25	7	-14	9	25	22	8	37	-4	26	28	16	-21	17	-10	16	0	0	14	20	-16	-10	-29	10	20	-27
18	-24	-18	11	-7	-23	12	-10	8	21	-11	24	-4	-8	21	0	5	13	-11	-3	11	-11	3	13	17	-16	30	13	21	-23	0	23
8	-2	16	20	24	40	-20	0	10	-15	-16	0	8	-13	5	2	46	10	-2	7	-9	-7	7	-12	-7	-13	-1	14	-11	-8	22	14
-24	-37	4	11	-7	3	33	1	11	0	-12	-3	7	-10	4	-30	37	-7	0	36	36	26	-5	11	8	-8	-16	12	-38	4	-47	-11
-2	13	-39	6	25	9	13	3	-7	43	-24	-5	29	16	0	-12	0	1	34	13	-27	5	0	9	25	37	4	-21	21	6	7	22
-17	3	31	-4	0	-11	-1	30	23	15	21	35	4	18	-9	-12	27	-5	1	5	17	3	23	33	19	2	-16	-12	-6	6	-4	7
-15	-17	-22	0	0	26	-13	-20	-15	40	-21	-19	11	-20	-13	2	6	-14	-1	24	2	20	14	15	-26	-32	16	4	-4	15	30	-2
-31	-25	-22	3	4	-9	-17	22	24	31	-18	-2	9	26	5	-29	10	-26	10	5	5	-14	-35	11	15	-21	-50	3	-18	-18	0	-10
21	-13	-2	11	15	-7	6	-18	-6	23	-12	22	27	0	-5	21	-12	21	1	0	30	14	-39	18	5	9	19	9	3	-40	-18	-8
7	-4	6	-5	10	-30	2	45	3	12	-6	46	-5	-22	13	-10	-4	-17	-5	4	-4	22	-10	-22	13	-19	-24	-11	8	-6	-29	-12

Figure 15 Aberrated PSF with noise, Nyquist sampling

To reduce the effects of noise, a Gaussian window was applied to the moment calculations, as in

$$E = \int e^{-(x'^2+y'^2)/w^2} P\, dxdy/E$$

$$M_1 = \int (x'^2+y'^2)\, e^{-(x'^2+y'^2)/w^2} P\, dxdy/E$$

The width w was taken to be 5 sample spaces. This eliminates the contribution from small noise fluctuations located at large distances from the c.g., which weight heavily into the moments. This significantly reduced the variations, but they are still too large, as shown in Table 6b.

The successful strategy was to also apply the same Gaussian window to the c.g. calculation. The c.g. was first computed as before, and then recomputed with the Gaussian window centered on the first c.g. estimate. As may be seen in Table 6c. the standard deviation of the c.g., and consequently the five moments, were reduced by factors of four.

The following procedure was used to test the sensitivity of a search on the moments to noise and aliasing. A table of moments was generated for 1575 PSF's on the grid of five values of each aberration coefficient (-.5, -.25, 0., .25, and .5 waves) for five different coefficients (defocus, 0° astigmatism, 45° astigmatism, x coma, and y coma). (The number of such grid points is reduced from 5^5 by a factor of nearly one half due to symmetry.) A particular aberration was chosen (.25 defocus, .5 0° astigmatism, -.25 y-coma), which was exactly one of the grid points. Moments were calculated from the corresponding PSF's for various amounts of noise and aliasing. The table of moments was searched for the best fit to the moments from the noisy PSF's. In the absence of noise, the moments in the table corresponding to the same aberration as the test case would be a perfect match. With enough noise, some other aberrations will have better fits to the trial moments.

At each noise level, one hundred different noise realizations on the PSF were run through the moment calculation and search. Counts were made of the number of cases in which more than a certain number of aberrations had better fits to the noisy trial moments than the moments corresponding to the actual aberration. The worst case (with the largest number better than the actual aberration) was also noted. The worst case indicates how deep in the list of best fits to the moments a search over the PSF itself must go, to insure inclusion of the correct PSF in the PSF's examined. Table 7 presents the results, in terms of the rank of the correct grid point (correct phase).

From Table 7 we see that, for example, with a detector size equal to the Nyquist sampling interval (1 x 1 case) and with 50% dependent noise, there were 13 noisy PSF's (out of 100 tested) where the correct phase was not ranked number 1. The worst rank was number 10.

The noise was added to each point of the PSF by

$$PSF'(X,Y) = PSF(X,Y)\ (1 + N_1 \cdot A_D) + N_2 \cdot A_I$$

where N_1 and N_2 are independent random variables with zero mean and a variance of one. A_D and A_I are the amplitudes of the dependent and independent noise terms. The independent noise amplitude is given as an absolute number and as a percentage of the peak value of a diffraction-limited PSF and of the peak value of the aberrated PSF.

In the case of no aliasing, a remarkable amount of signal dependent noise can be tolerated. Even with A_D equal to 70%, the worst case had only 28 grid points with a better fit to the moments. The permissible dependent noise drops roughly with the linear amount of aliasing. The number of PSF data points drops with the square of the aliasing factor. The permissible signal independent noise expressed as a percentage of the peak value of the aberrated PSF also drops in a linear manner, but a much smaller amount of noise can be tolerated.

Table 7

Cumulative Histogram of the Rank of the Correct Grid Point

For each noise level 100 noisy PSF's are subjected to the grid search.

K = Index of the K^{th} noisy PSF, K = 1,2, . . ., 100,

X_K = Rank of the correct grid point out of all 1575 points tested in the K^{th} search.

Detector Size (units of $\lambda F\#/2$)	Noise Level			Number of times X_K is greater than				Largest X_k
	Independent		Dependent					
	% of D.L. peak	% of signal peak	% of the noise-less signal	1	6	11	101	
1x1	.92	6.6		14	5	1	0	17
	1.39	10.0		42	19	13	1	149
	1.85	13.2		53	26	22	2	672
			10	0	0	0	0	1
			20	0	0	0	0	1
			40	9	0	0	0	3
			50	13	2	0	0	10
			60	30	9	2	0	16
			70	38	14	6	0	29
2x2	.8	4.4		28	14	7	0	15
			30	34	10	7	0	39
			50	59	27	15	4	207
4x4	.45	1.8		8	0	0	0	3
	.90	3.7		31	7	1	0	17
	1.8	7.3		83	55	41	4	226
			5	0	0	0	0	1
			10	13	1	0	0	7
			20	52	19	13	1	116
5x5	.44	1.4		1	0	0	0	2
	.89	2.3		17	7	6	0	67
	1.78	5.5		67	44	30	10	920
			10	6	0	0	0	5
			15	33	10	4	1	132

6 PHASE DIVERSITY IMAGING

In the previous contract we developed several algorithms to perform phase retrieval on distorted images of extended objects. The optical system introduces a phase aberration $\theta(f)$ with its corresponding PSF $p(x)$. The observed image is

$$z(x) = o(x) * p(x) + n(x),$$

where "$*$" means convolution, $o(x)$ is the unknown, extended object and $n(x)$ is noise.

Since $o(x)$ is unknown, we cannot use the algorithm of Section 2 to find $\theta(f)$. However, phase retrieval is still possible if we can acquire two images $z_1(x)$ and $z_2(x)$ of the object. These two images allow us to make a joint estimate of $o(x)$ and $\theta(f)$. The details are in the previous Final Report (Appendix C). Briefly, for an estimated object $\hat{o}(x)$ and estimated PSF's $\hat{p}_1(x)$ and $\hat{p}_2(x)$, we calculate an error metric

$$E = \int [z_1(x) - \hat{o}(x) * \hat{p}_1(x)]^2 \, dx$$
$$\int [z_2(x) - \hat{o}(x) * \hat{p}_2(x)]^2 \, dx.$$

When we use Parseval's theorem to perform this calculation in the spatial frequency domain, we can minimize E by choice of $\hat{O}(f)$: namely

$$\hat{O}(f) = \frac{\hat{P}_1^*(f) Z_1(f) + \hat{P}_2^*(f) Z_2(f)}{|\hat{P}_1(f)|^2 + |\hat{P}_2(f)|^2}$$

We substitute this $\hat{O}(f)$ into the E-metric calculation and find the $\hat{\theta}(f)$ that further minimizes the integrals. The θ-search is now identical to that of Section 2.

To implement this algorithm we have chosen to add a known phase $\phi(f)$ to the already phase-aberrated optical system. With $\phi(f) = 0$ we obtain the first image $z_1(x)$; with $\phi(f) \neq 0$ we get $z_2(x)$. In practice $\phi(f)$ is quadratic so that $z_2(x)$ is an intentionally defocused version of $z_1(x)$. We call $\phi(f)$ a phase diversity and the technique phase diversity imaging.

The algorithm is shown in block diagram form in Figure 16.

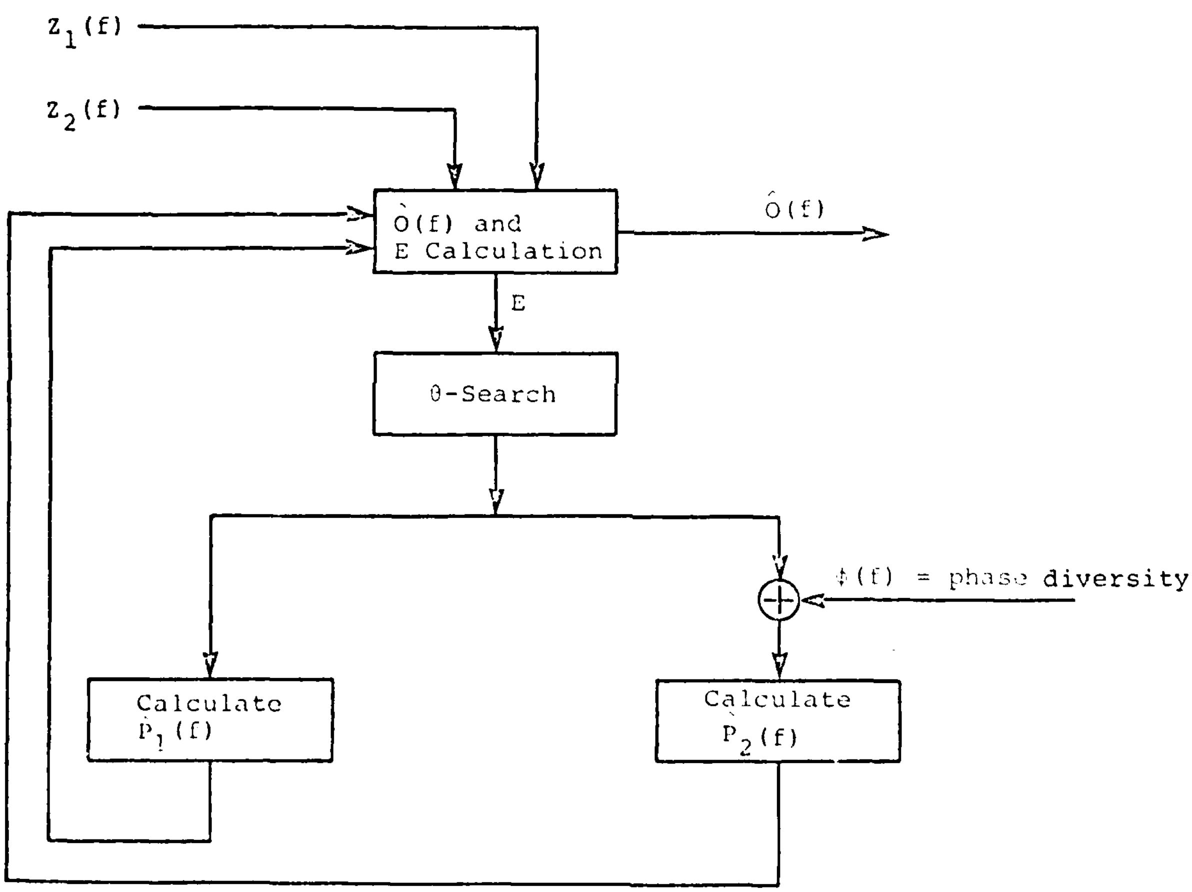

Figure 16 Estimation of θ(f) and the Object Spectrum

Now we show a computer simulation of the technique. A point is imaged through an aberrated optical system, with and without an intentional defocus. The two point spread functions are measured and are used to estimate the object. The estimation procedure, of course, has no knowledge about the object.

In Figure 17 we show a two-dimensional phase aberration θ in a circular, unapodized aperture. The resulting point spread function of the optical system is shown in Figure 18. Next, we intentionally defocus the system (one-half a wave of quadratic phase from the center to the edge of the aperture). The new phase ($\theta + \phi$) is shown in Figure 19 and the corresponding point spread function in 20.

In this example we add no noise so that z_1 and z_2, the observed signals, are those shown in Figures 18 and 20. Their Fourier transforms, Z_1 and Z_2, are the inputs to the block diagram of Figure 16. The outputs are $\hat{\theta}$ (an estimate of θ) and $\hat{O}$ (an estimate of the object's spectrum). The former is shown in Figure 21 and should be compared with Figure 18. The agreement is excellent. The inverse Fourier transform of $\hat{O}$ is the estimated object. This is shown in Figure 22.

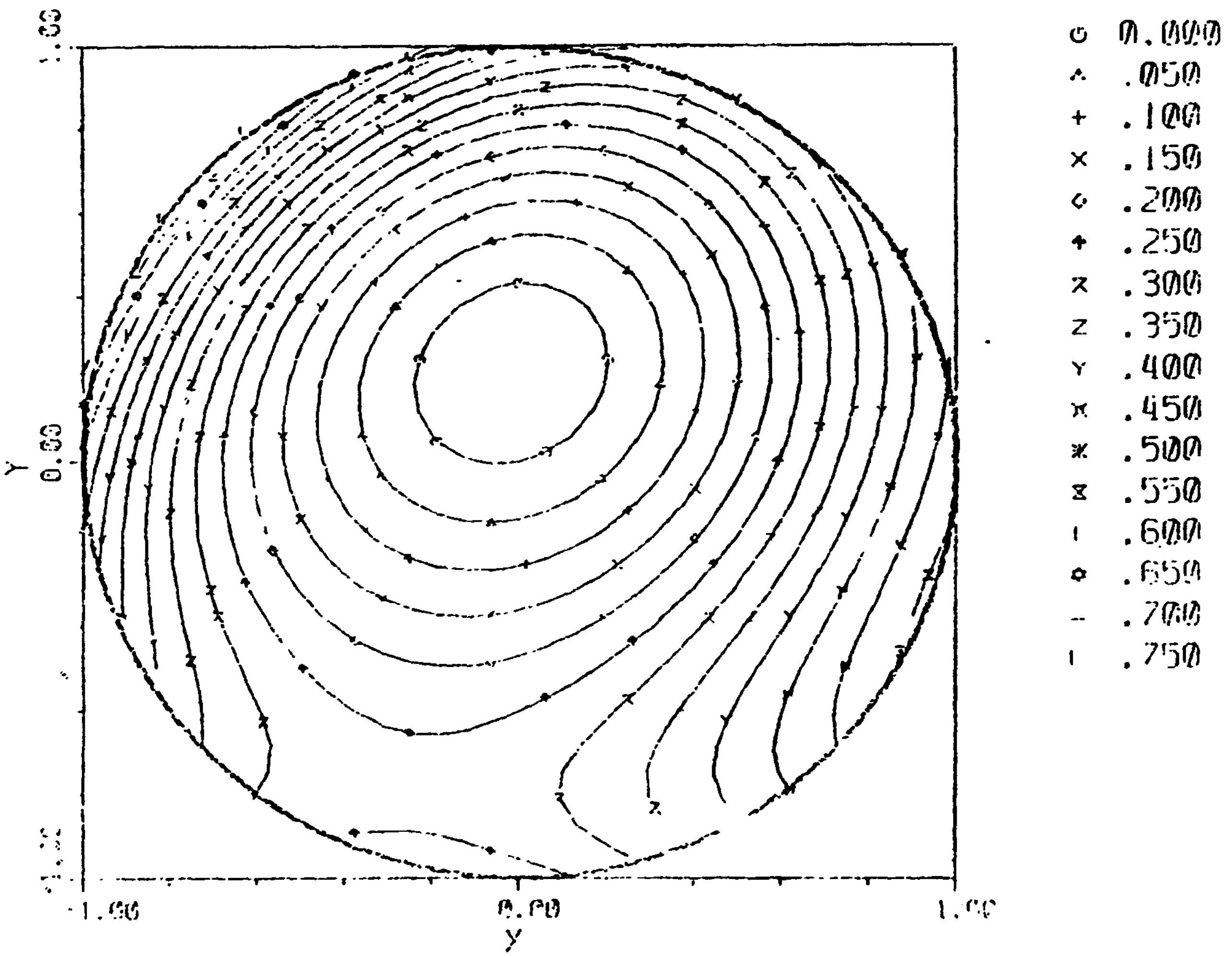

Figure 17. Phase aberration (in waves) across the aperture

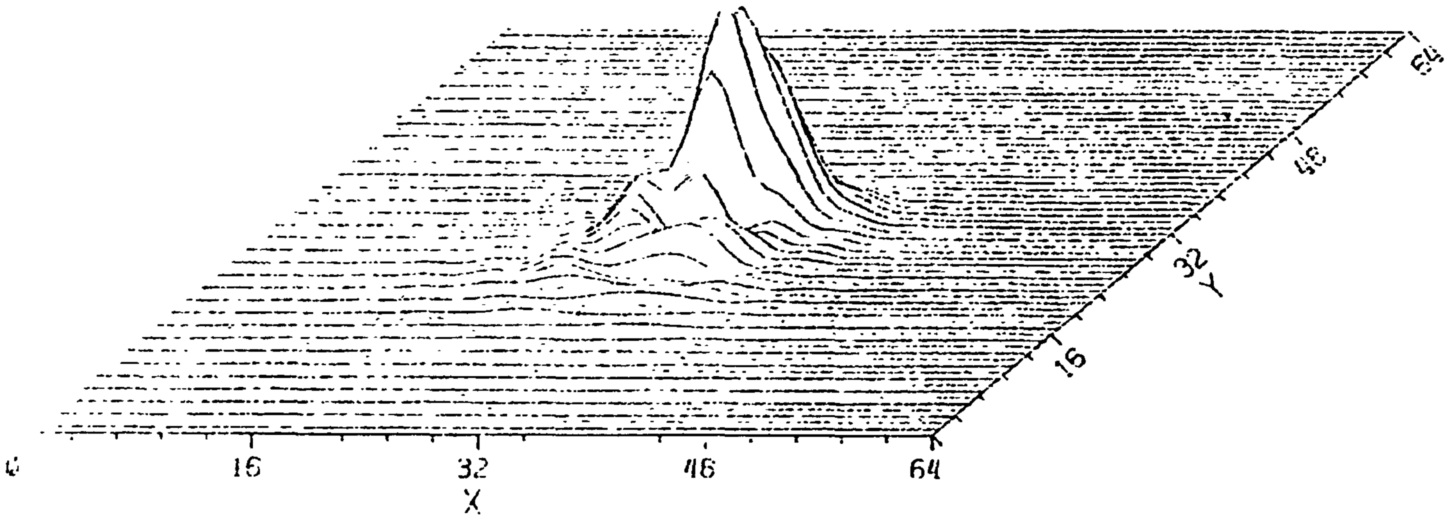

Figure 18. Observed point spread function corresponding to Figure 17

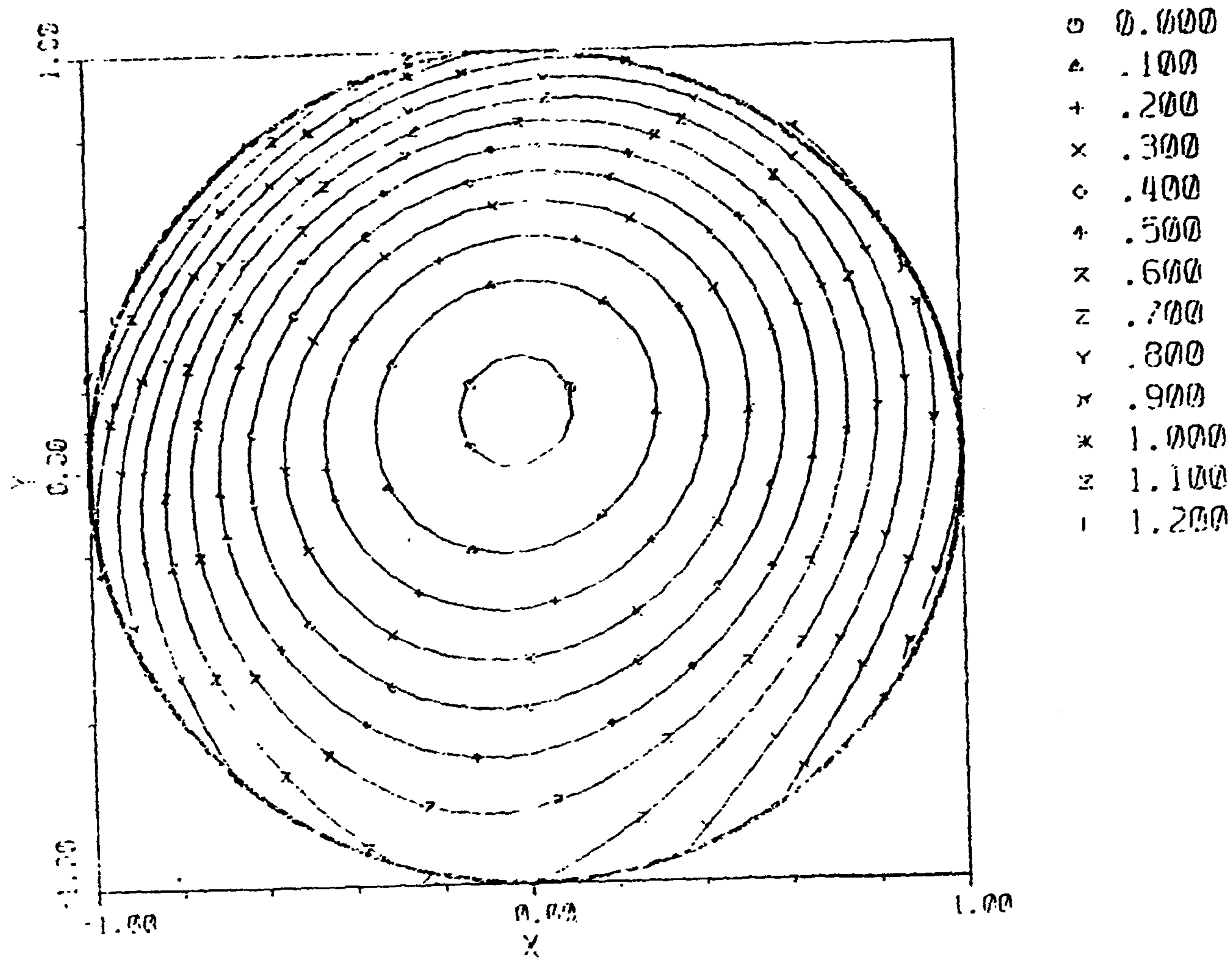

Figure 19. Quadratic phase added to Figure 17

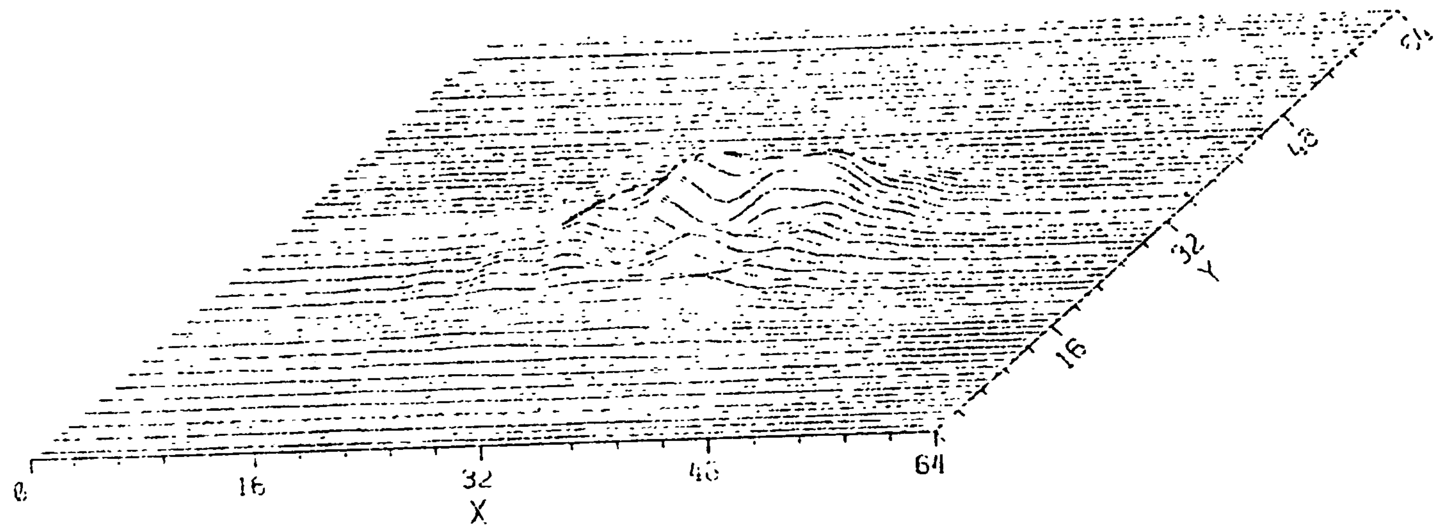

Figure 20. Observed point spread function (defocused version of Figure 18)

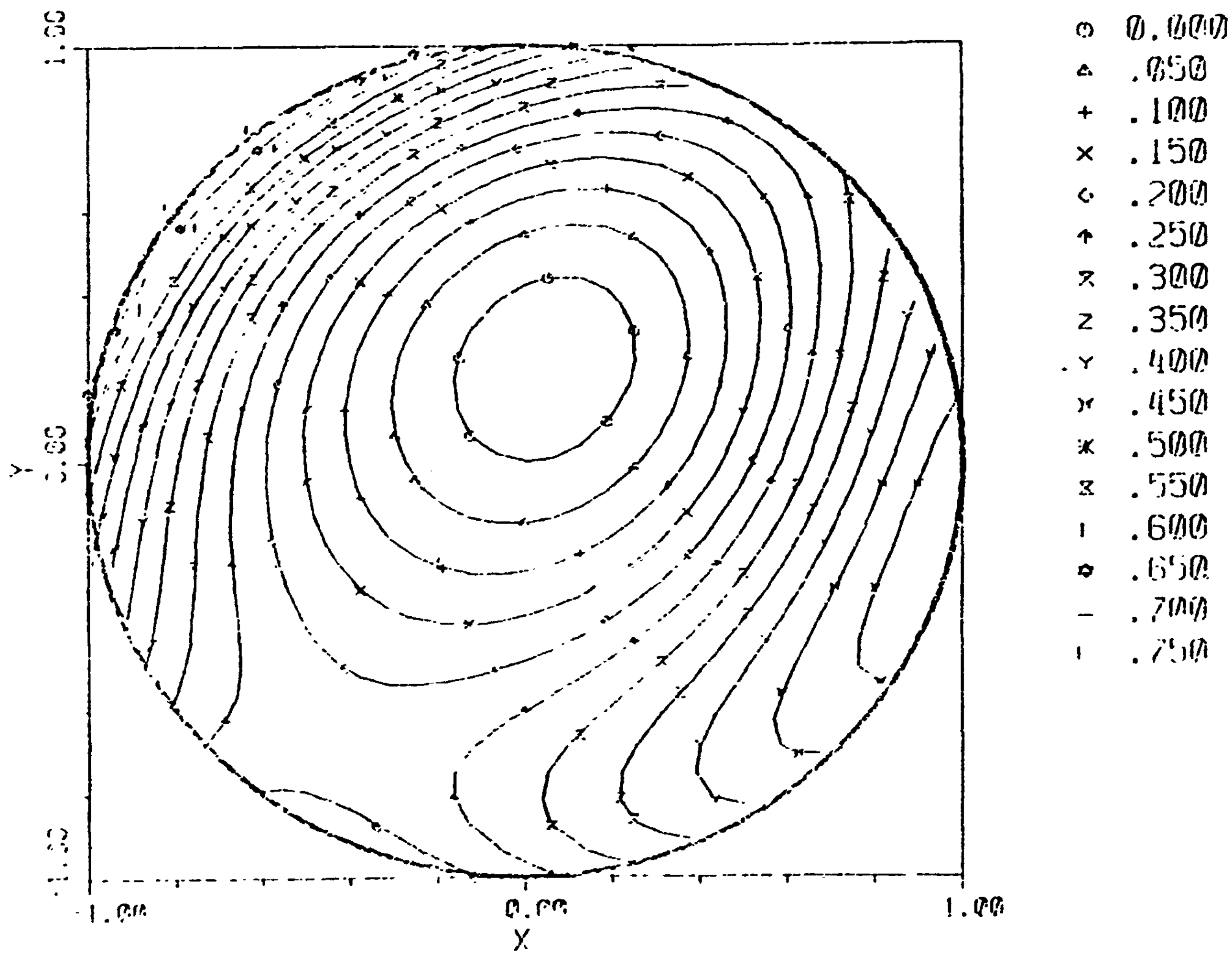

Figure 21. Phase retrieval estimate of Figure 17 based on Figures 18 and 20

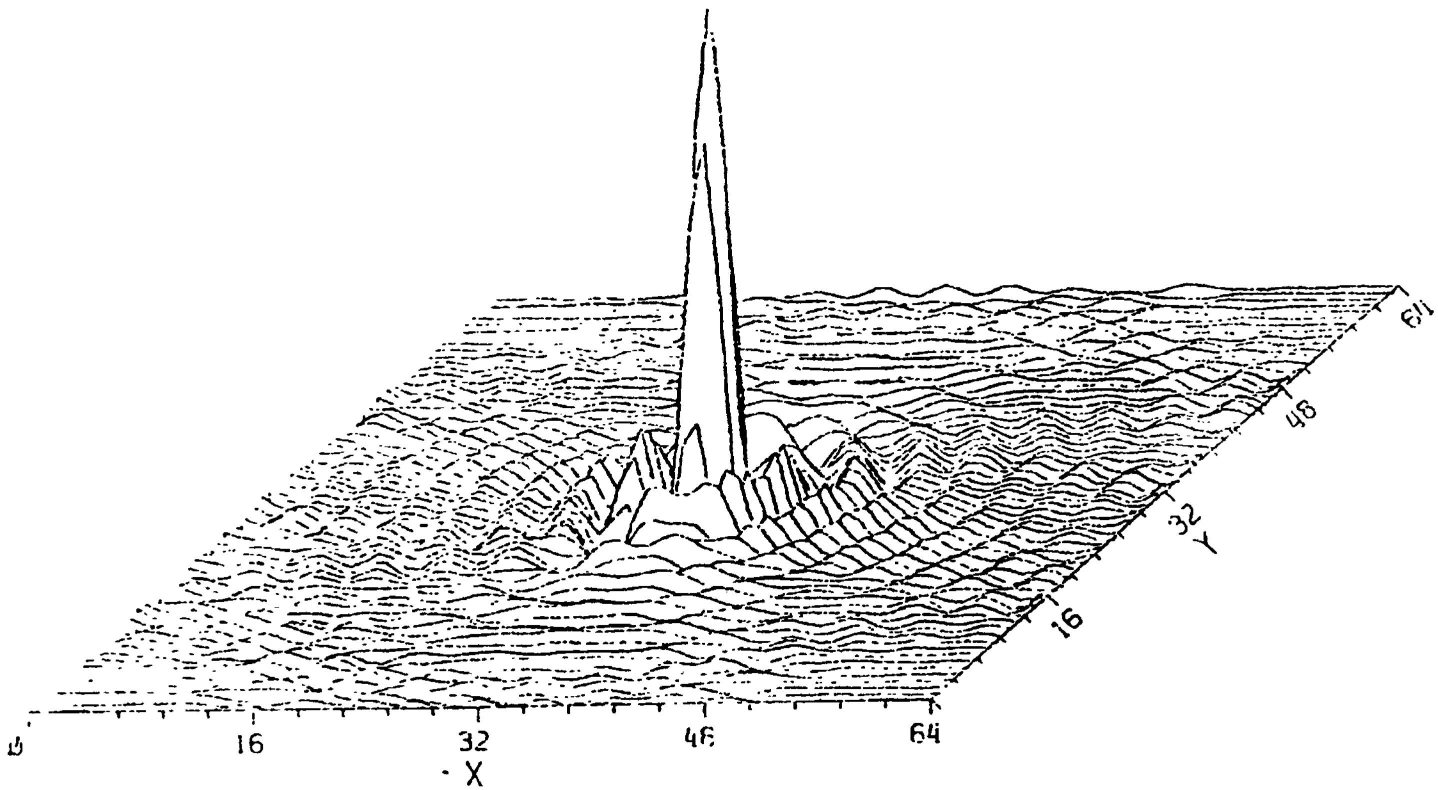

Figure 22. Restored point spread function based on observations in Figures 18 and 20

Next we present a computer simulation where the object is a segment of a water tower as shown in Figure 23(a). The initial system aberration is the same θ as in Figure 17. The resulting image is shown in Figure 23(b) and the defocused image is shown in Figure 23(c). The Fourier transforms of the images in 23(b) and 23(c) are the inputs to the algorithms of Figure 16. The result is shown in Figure 23(d).

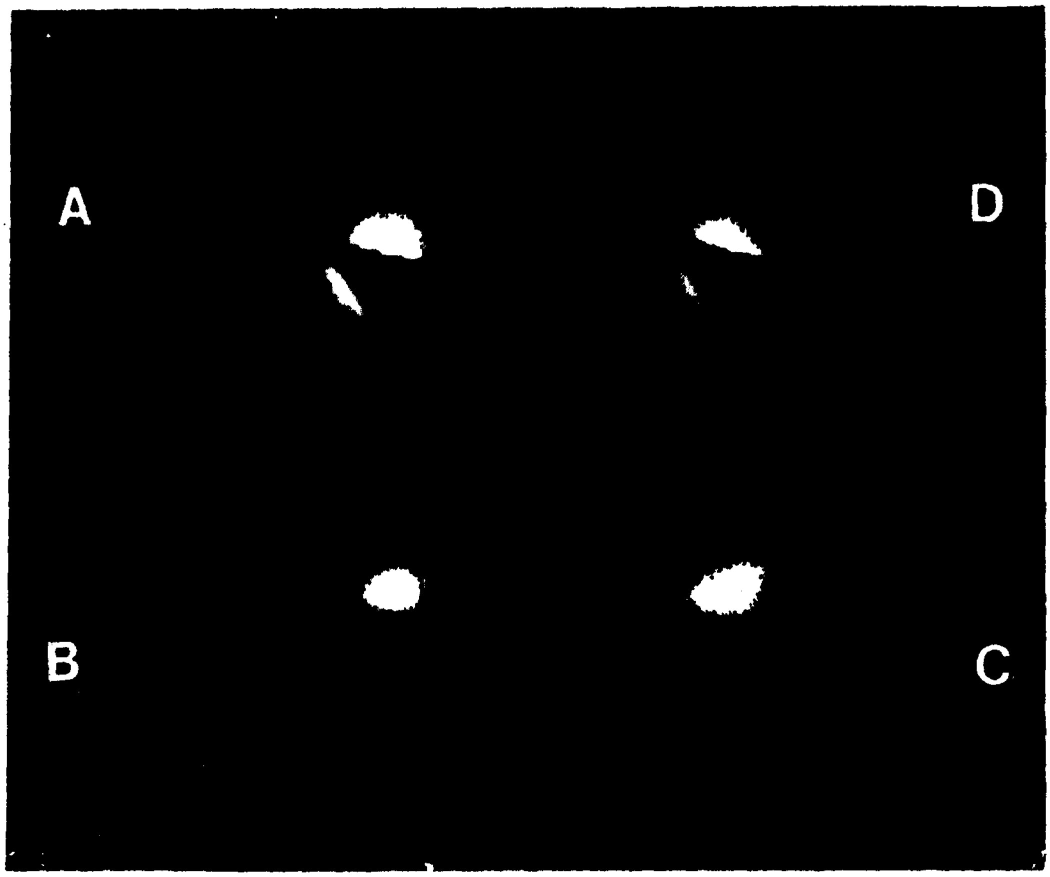

Figure 23. (a) Original, diffraction-limited image
(b) Aberrated image
(c) Aberrated and defocused image
(d) Resulting image after (b) and (c) [illegible] estimate [illegible] the phase aberration [illegible]

When the phase diversity is quadratic, successive images represent the images taken at different values of defocus. This is common practice in electron microscopy for reconstruction of the phase of an object under observation. It seems reasonable to expect that a particular kind of phase diversity, other than quadratic, will allow better object reconstruction for particular kinds of channel distortions.

The main utility of the technique may be the fact that the adaptation is <u>not</u> done in closed loop fashion. Thus, the adaptive optics does not have to track the temporal variation in the channel. The phase diversity allows the images to be unscrambled in post-processing. On the other hand, it would probably be advantageous to include a closed loop with a long time constant to remove gross distortions in the channel. This concept could greatly reduce the burden on the adaptive control mechanism while increasing the burden on post-processing hardware.

7 LABORATORY EXPERIMENT

7.1 Laboratory Set-Up

A procedure has been developed to experimentally test the phase retrieval concept for extended objects. This procedure is similar to earlier experiments in which image data from an optical system is recorded. The optical system contains a known phase aberration function. This function is contained on a clear substrate and is separable from the rest of the optical system. Analysis of the aberration alone is possible by interferometric techniques. This result provides the knowledge of the function against which the retrieved phase is to be compared. To supply sufficient data for phase retrieval of the aberration function in this experiment, the image is recorded at two positions of known focus difference.

The imaging system is sketched in Figure 24. It is a 1:1 projector with condenser illumination. The lamp illuminates a ground glass diffuser. The diffused lamp image is relayed by the condenser to the system aperture stop. At the condenser are filters to limit the spectral transmittance of the system to red light. The aperture stop is located midway between two acromats. Each acromat is 260mm in focal length. A 1:1 objective is made by placing the object and image conjugate at the focus of each lens. The region between lenses contains collimated rays. It is in this region that the phase aberration is inserted. The effect of the aberration on the optical system is therefore the same as its effect in the collimated beam of an interferometer. This maximizes the agreement between the interferometric measure of the aberration and that found by phase retrieval.

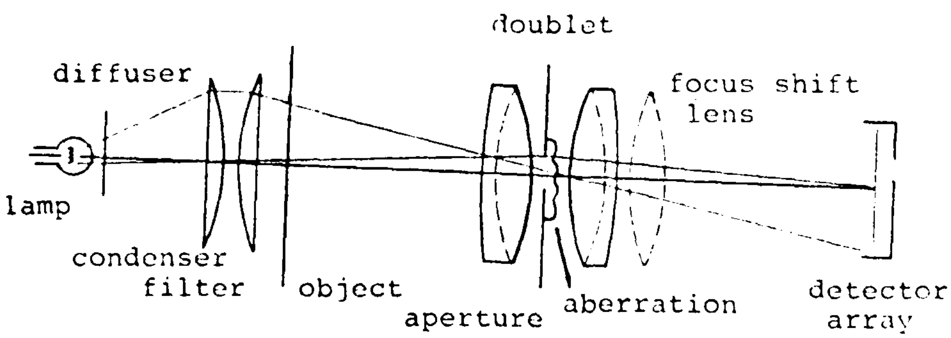

Figure 24. Imaging system

The second doublet focuses the image onto a plane which is scanned by a photodiode array. The array has 1024 elements with 15μm center to center spacing. The array is stopped 15μm at a time to produce a sampled image of 1024x1024 pixels.

The phase aberration can be inserted or removed repeatably between the doublets. A singlet of 1000mm focal length can also be inserted behind the second lens. This lens controllably defocuses the image.

The spectral distribution of the illumination was chosen to be primarily red, the region of peak diode sensitivity. It was desired to be a broad bandwidth for incoherent imaging yet narrow enough to use its central wavelength for calculations which are wavelength dependent. The relative spectral response of the system is centered at 640nm with a spread, roughly, of 100nm. It is the combination of the lamp distribution at 2850K, an infrared sharp cutoff filter, a red broadband interference filter and the spectral response of the photodiodes.

The aperture size of 2.2mm and focal distance of 260mm gives an F# of 118. This was selected to give a diffraction limited spread function width of 10 diodes (150μm), a suitable sampling density for the phase retrieval algorithm.

A two beam interferometer was constructed to provide a direct measure of the aberrations used. The setup was standard. One beam of parallel wavefronts is the reference and the other is the signal beam. The aberration is placed in the signal beam and the two beams, when recombined, display an interference pattern. This pattern is recorded on film as an interferogram. An example is shown in Figure 25. This aberration appears to have about two waves of distortion and was used to produce the images shown later.

Figure 25. Phase aberration interferogram

7.2 Data

Figures 26-29 show a series of images. These represent the four imaging conditions which were available in this experiment. Figure 26 shows an image of a section of a tri-bar target produced by the diffraction limited system. Figure 27 shows the same image with +0.9 waves of defocus added by including the defocusing lens in the system. Figure 28 shows the system with the aberration of Figure 25 added at the aperture stop. Figure 29 shows the effect of the same aberration and +0.9 waves of defocus.

In later data processing we used images in Figures 28 and 29 to determine, by our two-focal-plane algorithm, the wavefront distortion.

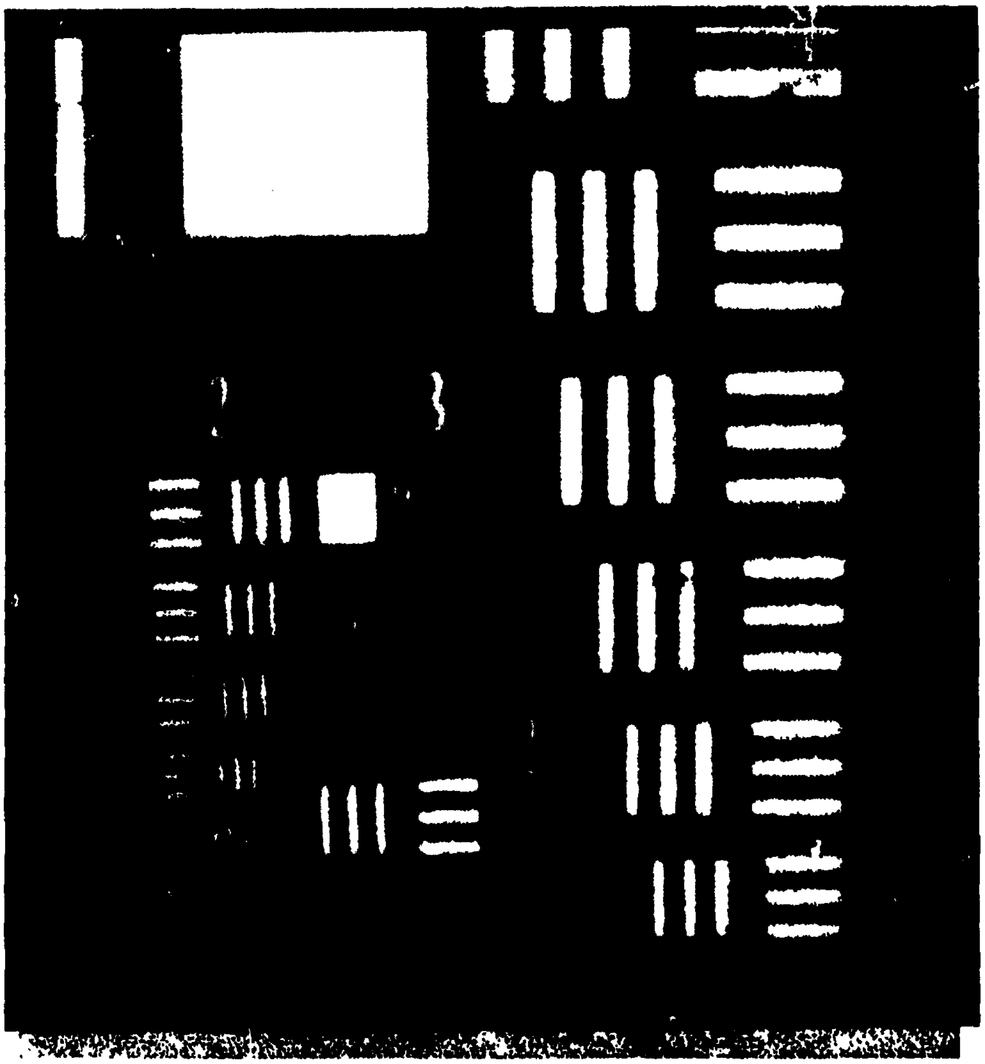

Figure 26. [illegible]

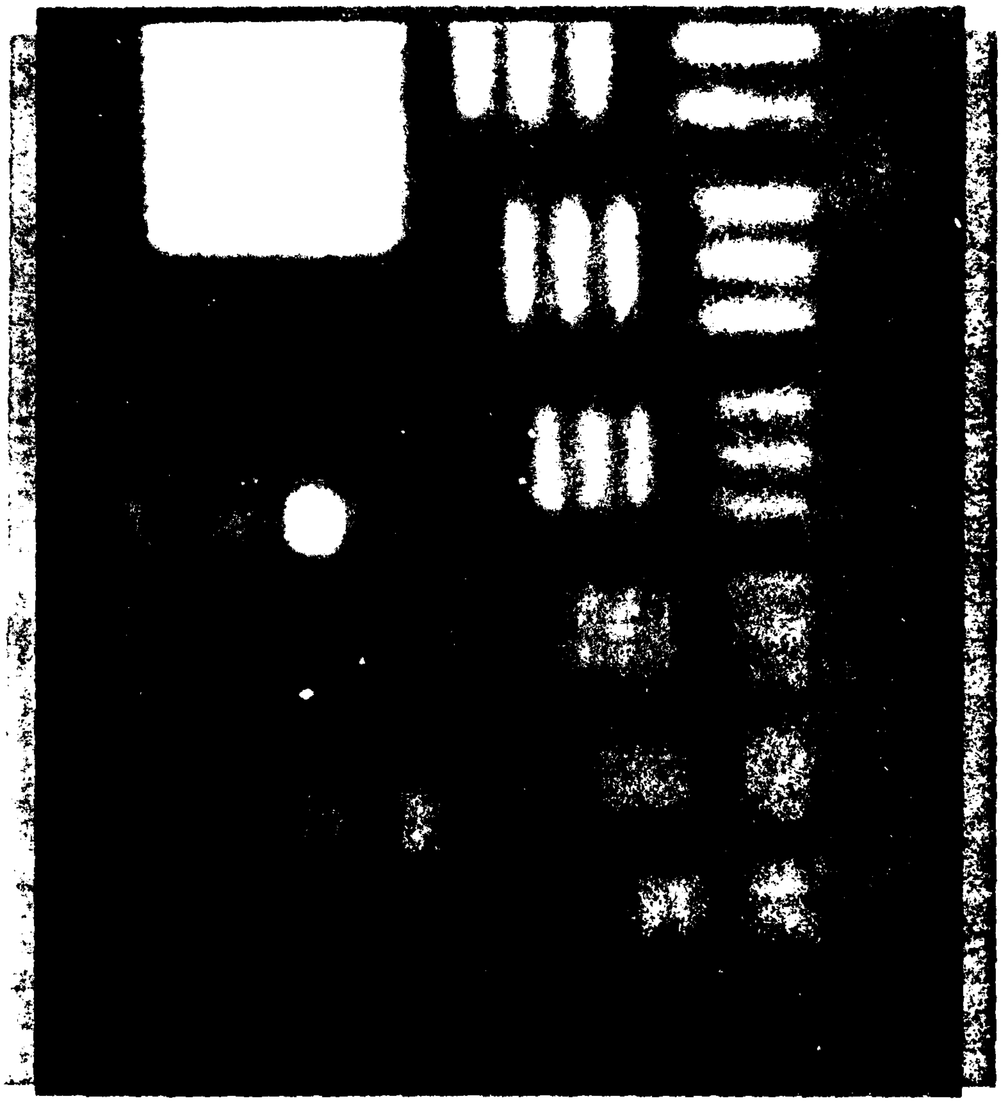

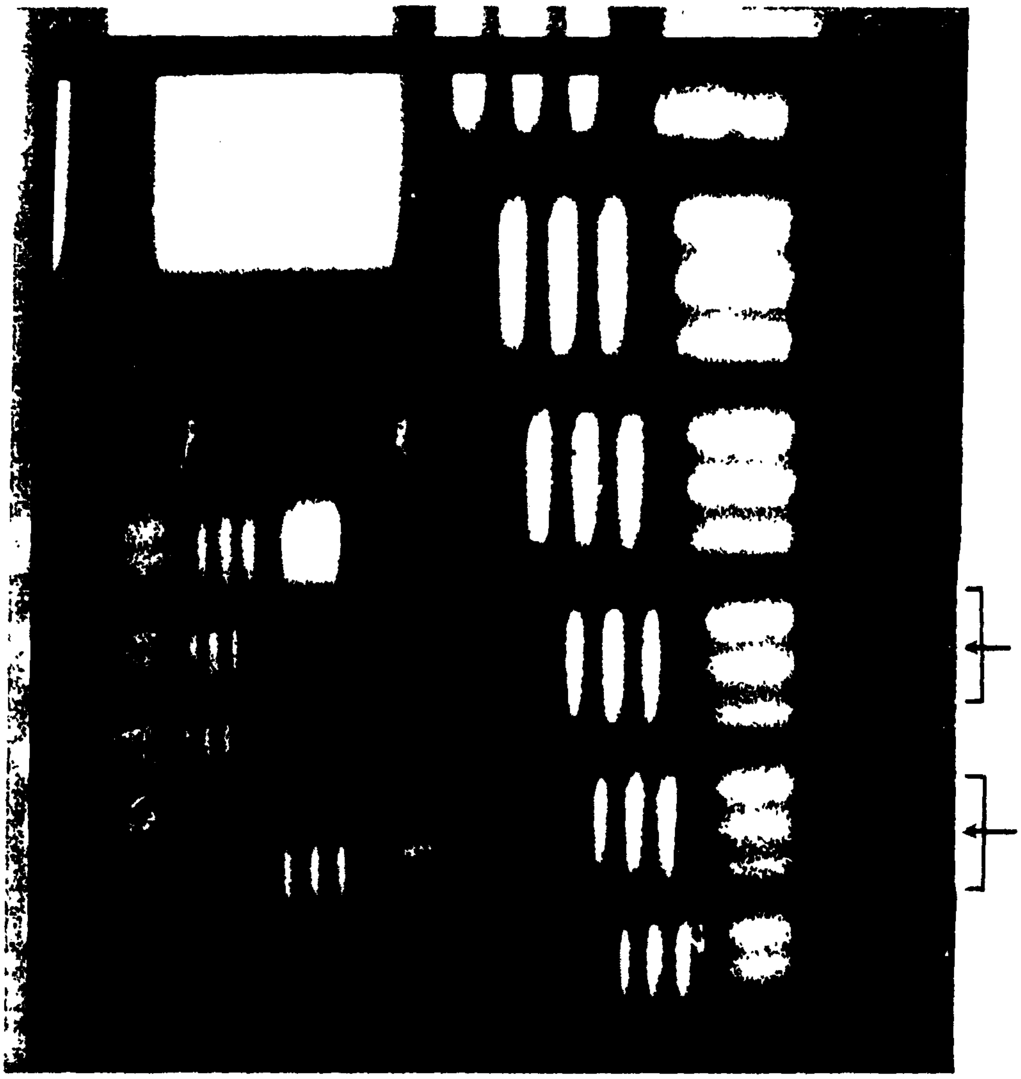

Figure 28. Aberrated image

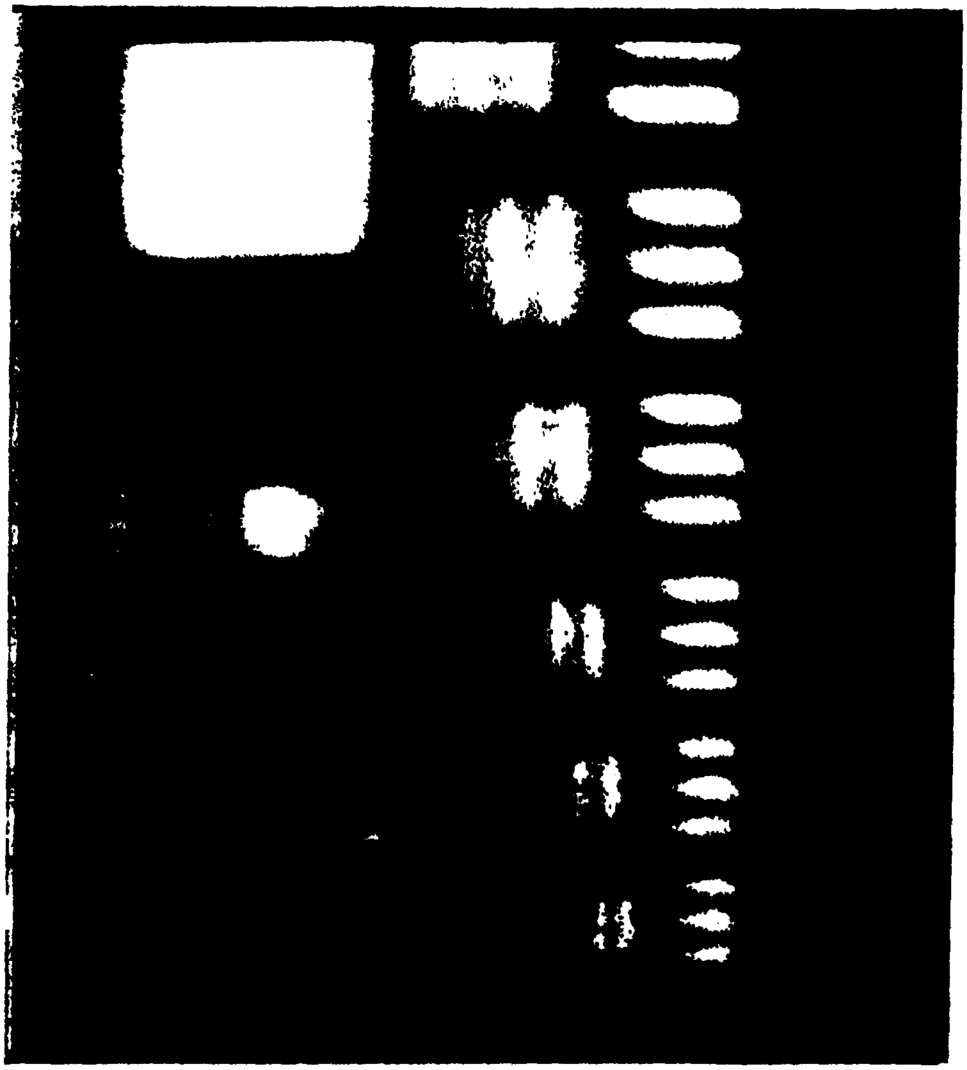

Figure 29. Aberrated and defocused image

7.3 Determination of the Quadratic Phase

Two measured diffraction limited images (one with quadratic phase added to the phase and one without) were input to the phase-retrieval algorithm. The images used are given in the preceding section (Figures 26 and 27). The idea was to determine, from these two images, the estimated phase distortion across the aperture of the system. By imposing the known focus error between the two images, the calculated phase-estimate should be a constant and thus verify that the estimated focus error is correct. The first step in processing the data was to obtain a smaller region of the images to use as input to the algorithm, for the simple reason that the entire image would have been burdensome computationally. Corresponding 80x80 pixel regions of each image were chosen for processing. The actual region corresponds to the area surrounding the number "4" in the right side of the tri-bar target in Figure 26.

The first moment (center of gravity) of each image was calculated so that each image could be aligned to remove major tilts in the phase estimate. The slow Fourier transform was performed on each section, each output transform being a 17x17 sampled OTF. The transform was sampled so that the outer point corresponds to the diffraction-limited cutoff of the system. These two OTF's were then input to the two-focal plane phase-retrieval search algorithm in order to estimate the phase. The input focus error was assumed to be 0.9 waves.

The phase estimate found from the search algorithm is given in Figure 30. The RMS phase was calculated to be .022 waves and is .06 waves peak to peak. The result is consistent with a diffraction-limited phase to within the errors expected in the experimental procedure.

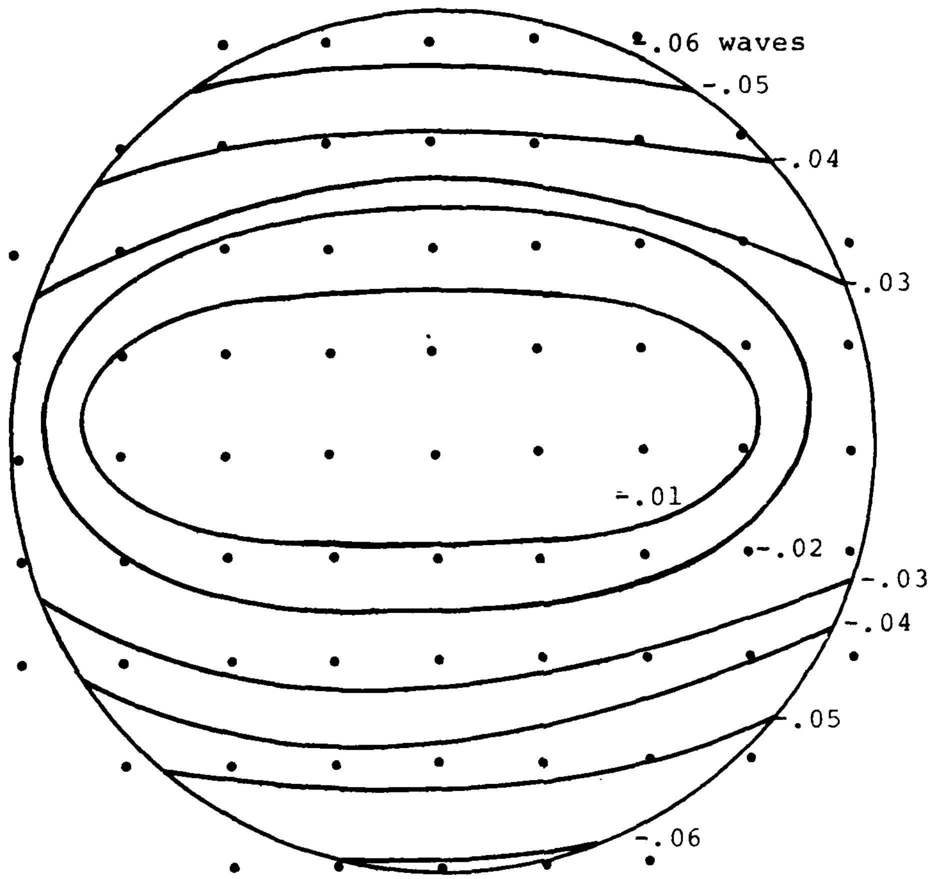

Figure 30. Diffraction limited phase estimate

7.4 Determination of the Unknown Aberration

The two aberrated images (one with focus error added and one without) were input to the phase retrieval algorithm. The same corresponding 80x80 images section used for the diffraction limited (Number "4") was processed using the exact same procedure as the diffraction limited case. The phase retrieval algorithm was allowed to search over 20 Zernike coefficients in order to fit the correct phase. The Zernike coefficients are given in Figure 31 and a contour plot of the phase is given in Figure 32. The actual phase aberration that was measured interferometrically is given in Figure 33.

P1 = 0.	P11 = .03
P2 = .10	P12 = .02
P3 = .17	P13 = .009
P4 = -.07	P14 = -.048
P5 = -.26	P15 = .0
P6 = -.21	P16 = .22
P7 = .03	P17 = .12
P8 = .006	P18 = -.05
P9 = -.063	P19 = 0.
P10 = .07	P20 = 0.

Figure 3.1 Zernike polynomial coefficients obtained from phase retrieval algorithm - applied to two-focus problem (aberrated case)

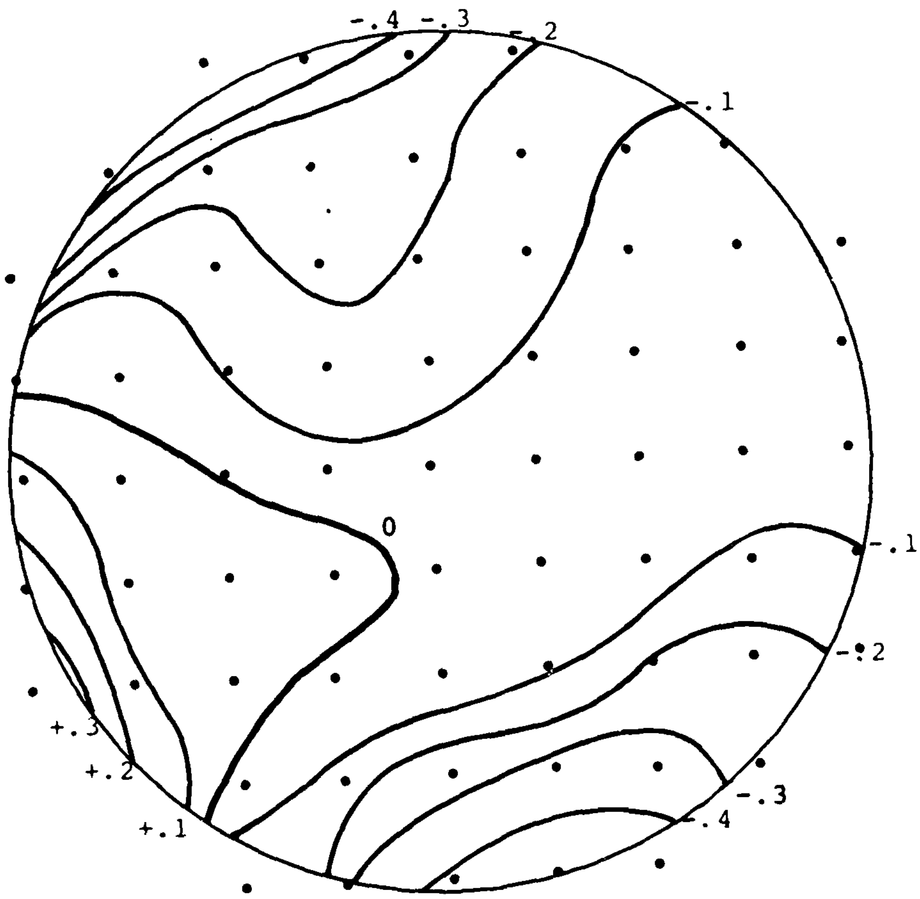

Figure 32. Estimated phase from phase retrieval algorithm applied to aberrated data

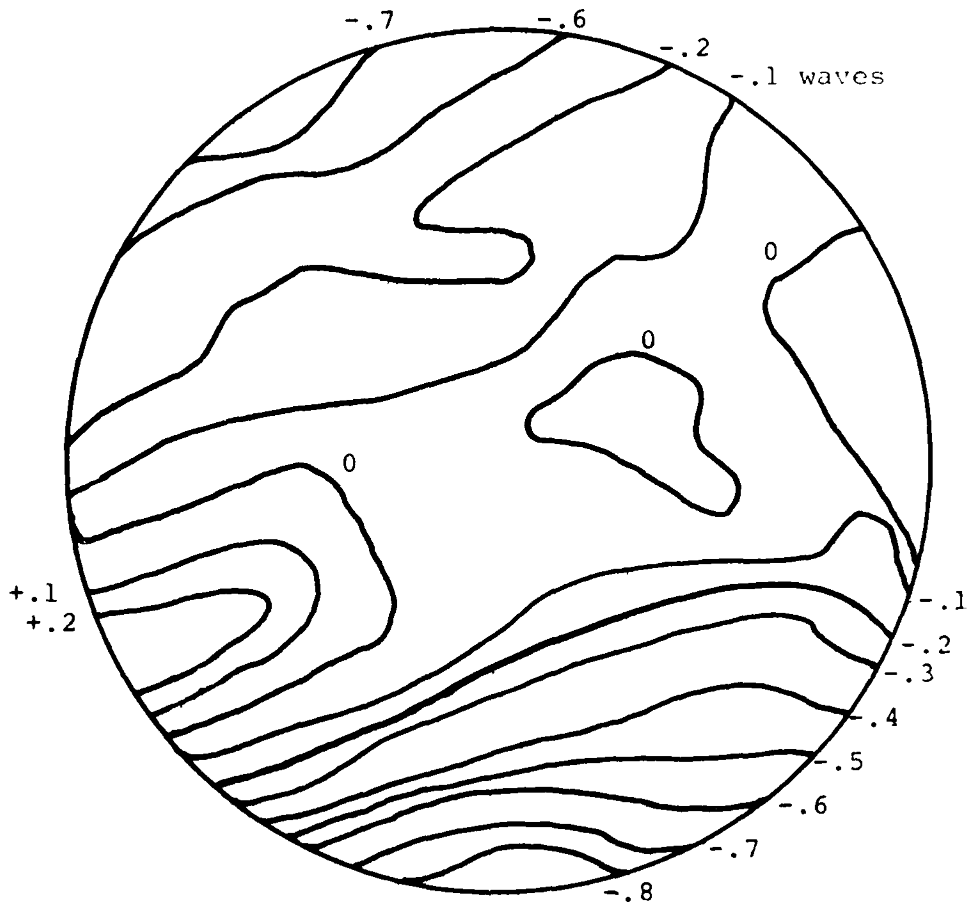

Figure 3.3. Measured phase from interferogram

8 BLIND TEST

To test the phase retrieval algorithm, the customer requested that personnel from Draper Lab give us several noisy, undersampled point spread functions. These were prepared by Dr. V.N. Mahajan and his staff at the Optical Systems Division in Cambridge, MA. We subsequently received three aberrated point spread functions, each "sampled by an 8x8 array of detector elements. The width of the detector elements is $2.13\lambda F$, where λ is the wavelength of the object radiation and F is the focal ratio *(f#) of the optical* system."* The three point spread functions are shown in Figure 34.

-18	-9	-5	-11	33	13	-7	-15
6	1	27	33	30	4	-3	0
-45	-15	2	29	179	12	27	0
14	-2	6	66	352	58	-15	-4
-2	12	1	61	95	58	-11	3
29	-20	3	16	34	13	5	15
-2	-8	26	35	11	-4	-19	-14
-16	-8	-12	-8	-15	-30	-6	-25

(a)

26	-3	5	44	-13	-4	27	-22
-22	-33	4	21	11	5	-9	18
2	13	-11	-29	56	14	6	9
-10	3	10	102	240	29	13	1
-15	-13	41	209	164	5	-8	21
-2	11	16	-6	31	-2	0	16
-9	31	2	-12	20	-3	16	-1
-22	24	-8	-17	-21	-16	-25	10

(b)

-34	-43	14	87	-16	-21	51	108
-30	41	22	-9	27	22	43	-7
-5	53	-81	-32	166	-27	24	-25
53	-63	7	13	375	29	13	40
57	-2	71	15	122	-2	14	69
16	21	-6	-60	56	-41	16	-14
8	-37	12	-2	-14	-94	-91	-40
34	-17	-58	45	-49	-41	-23	-70

(c)

Figure 34. PSF's for the blind test

---

*Letter of June 30, 1981 to R. Gonsalves from V. Mahajan

We exercised the phase retrieval algorithm on the three point spread functions (PSF) as follows. First, we left the sampling interval at 2.13λF#, even though our algorithm assumes the prefix constant to be a integer (we used 2). For each PSF we assumed that the unknown phase could be approximated by 8, by 15, and by 23 terms in a Zernike polynomial expansion. The 8 and 15 term expansions were determined with the all-zero polynomial as a starting point in our search. The 23 term expansion used the 8 term solution as a starting point.

Next we interpolated the PSF's to give us an 8x8 array sampled at 2λF#. The searches described above were repeated.

In Figure 35 we list the Zernike polynomials.

Figure 36 is a summary of the data processing for the 18 cases.

Figures 37 through 82 give the results. For example, Figure 37 shows the input PSF, the estimated PSF, the mean square error between them, and the coefficients of the Zernike polynomials for the estimated phase. Figure 38 shows the estimated phase itself. This first pair of figures is for case 1, sampling interval = 2.13λF#, and 23 Zernike polynomials.

n	Rectangular Coordinates	Polar Coordinates
1	1	1
2	x	$\cos\theta$
3	y	$\sin\theta$
4	$2x^2 + 2y^2 - 1$	$2r^2 - 1$
5	$x^2 - y^2$	$r^2 \cos 2\theta$
6	$2xy$	$r^2 \sin 2\theta$
7	$x(3x^2+3y^2-2)$	$(3r^2-2r)\cos\theta$
8	$y(3x^2+3y^2-2)$	$(3r^2-2r)\sin\theta$
9	$x(x^2-3y^2)$	$r^3 \cos 3\theta$
10	$y(3x^2-y^2)$	$r^3 \sin 3\theta$
11	$6x^4 + 12x^2y^2 + 6y^4 - 6x^2 - 6y^2 + 1$	$6r^4 - 6r^2 + 1$
12	$(x^2-y^2)(4x^2+4y^2-3)$	$(4r^4-3r^2)\cos 2\theta$
13	$2xy(4x^2+4y^2-3)$	$(4r^4-3r^2)\sin 2\theta$
14	$x^4 - 6x^2y^2 + y^4$	$r^4 \cos 4\theta$
15	$4xy(x^2-y^2)$	$r^4 \sin 4\theta$
16	$x(10x^4+20x^2y^2+10y^4-12x^2-12y^2+3)$	$(10r^5-12r^3+3r)\cos\theta$
17	$y(10x^4+20x^2y^2+10y^4-12x^2-12y^2+3)$	$(10r^5-12r^3+3r)\sin\theta$
18	$x(x^2+y^2)(5x^2+5y^2-4)$	$(5r^5-4r^3)\cos 3\theta$
19	$y(x^2+y^2)(5x^2+5y^2-4)$	$(5r^5-4r^3)\sin 3\theta$
20	$x^5 - 10x^3y^2 + 5xy^4$	$r^5 \cos 5\theta$
21	$5x^4y - 10x^2y^3 + y^5$	$r^5 \sin 5\theta$
22	$20x^6 + 60x^4y^2 + 60x^2y^4 + 20y^6 - 30x^4 - 60x^2y^2 - 30y^4 + 12x^2 + 12y^2 - 1$	$20r^6 - 30r^4 + 12r^2 - 1$
23	$70x^8 + 280x^6y^2 + 420x^4y^4 + 280x^2y^6 + 70y^8 - 140x^6 - 420x^4y^2 - 420x^2y^4 - 140y^6 + 90x^4 + 180x^2y^2 + 90y^4 - 20x^2 - 20y^2 + 1$	$70r^8 - 140r^6 + 90r^4 - 20r^2 + 1$

Figure 35. Zernike circle polynomials

Assumed Sampling Interval	Case	Number of Zernike Polynomials	Residual Mean Square Error	RMS Value of the Estimated Phase (in waves)
2.13λF#	1	23 15 8	14669 16113 18750	0.368 0.327 0.419
	2	23 15 8	14792 14977 17158	0.187 0.215 0.197
	3	23 15 8	113471 114310 114005	0.434 0.341 0.431
2.00λF#	1	23 15 8	10980 12927 15518	0.451 0.362 0.486
	2	23 15 8	9870 10553 14042	0.213 0.224 0.231
	3	23 15 8	143020 143689 143503	0.541 0.506 0.536

Figure 36. Data Processing Summary

PHRUN25.LOG;1 24-JUL-1981 16:40:13.60

NUMBER OF ZERNIKE POLYNOMIALS = 23
NUMBER OF ITERATIONS =100
ACTUAL NUMBER OF ITERATIONS = 29

INPUT PSF

-18	-9	-5	-11	33	13	-7	-15
6	1	27	33	30	4	-3	0
-45	-15	2	29	179	12	27	0
14	-2	6	66	352	58	-15	-4
-2	12	1	61	95	58	-11	3
29	-20	3	16	34	13	5	15
-2	-8	26	35	11	-4	-19	-14
-16	-8	-12	-8	-15	-30	-6	-25

ESTIMATED PSF

0	0	1	3	4	0	0	0
0	0	0	9	21	2	0	0
1	1	2	22	169	11	1	1
1	1	2	57	343	49	1	1
0	0	2	50	86	47	2	0
0	0	1	9	12	4	2	0
0	0	1	5	2	0	0	1
0	0	1	2	1	0	0	0

MEAN SQUARE ERROR = 14669.0371

COEFFICIENTS OF THE
ZERNIKE POLYNOMIALS

K	P(K)
1	0.00000
2	-0.51416
3	0.32499
4	0.03853
5	0.37366
6	-0.18525
7	-0.18813
8	-0.05068
9	0.01493
10	0.00606
11	0.04404
12	-0.05517
13	-0.18909
14	-0.06202
15	-0.11456
16	0.06494
17	0.00804
18	-0.08093
19	-0.06974
20	-0.12625
21	-0.13419
22	0.00143
23	-0.02685

Figure 37. Blind test results for case 1, 2.13λF#, 23 polynomials

PHRUN25.LOG;1 24-JUL-1981 16:40:13.60
ESTIMATED PHASE ABERRATION (100 = ONE WAVE)

					92	99	101	101	100	95					
			46	59	64	67	69	71	73	76	78	77			
		24	33	37	39	41	43	46	50	54	60	66	69		
	7	17	19	20	21	23	26	29	33	37	42	48	55	59	
	4	6	6	7	9	11	14	18	21	25	28	31	37	43	
-10	-5	-5	-4	-2	0	3	6	9	13	16	18	18	20	24	27
-20	-19	-18	-15	-11	-6	-3	0	4	8	11	11	9	6	7	10
-37	-36	-33	-27	-19	-13	-7	-2	2	6	9	7	3	-2	-4	-3
-56	-54	-48	-39	-28	-18	-9	-2	3	8	9	7	0	-6	-10	-10
-74	-69	-62	-50	-35	-22	-10	0	6	11	12	8	1	-6	-10	-10
-87	-80	-72	-58	-42	-25	-11	0	9	14	14	10	3	-3	-5	-4
	-82	-75	-63	-46	-29	-13	0	9	13	14	10	5	2	3	
	-72	-67	-59	-46	-31	-17	-4	3	8	9	7	6	8	12	
		-46	-43	-38	-30	-20	-12	-6	-2	0	0	3	8		
			-17	-21	-22	-22	-20	-19	-18	-17	-15	-11			
					-12	-23	-31	-38	-44	-48					

RMS PHASE ACROSS APERTURE = 0.368 (WAVES)

Figure 38. Blind test results for case 1,
2.13λF#, 23 polynomials

PHRUN25.LOG;1 27-JUL-1981 15:16:36.82

NUMBER OF ZERNIKE POLYNOMIALS = 15
NUMBER OF ITERATIONS =100
ACTUAL NUMBER OF ITERATIONS = 31

INPUT PSF

-18	-9	-5	-11	33	13	-7	-15
6	1	27	33	30	4	-3	0
-45	-16	2	29	179	12	27	0
14	-2	6	66	352	58	-15	-4
-2	12	1	61	95	58	-11	3
29	-20	3	16	34	13	5	15
-2	-8	26	35	11	-4	-19	-14
-16	-8	-12	-8	-15	-30	-6	-25

ESTIMATED PSF

0	0	0	1	8	3	0	0
0	0	0	5	22	6	1	1
1	0	2	19	168	10	4	1
0	0	1	63	342	49	5	1
0	1	1	46	91	39	11	1
1	0	0	1	2	4	3	3
0	0	0	0	1	1	0	0
0	0	0	1	3	1	1	0

MEAN SQUARE ERROR = 16113.3584

COEFFICIENTS OF THE
ZERNIKE POLYNOMIALS

K	P(K)
1	0.00000
2	-0.52890
3	0.13925
4	0.05675
5	0.08017
6	0.27042
7	-0.18821
8	0.21869
9	-0.20175
10	0.06567
11	-0.05859
12	-0.13863
13	0.19159
14	-0.07769
15	-0.14917

Figure 39. Blind test results for case 1, 2.13λF#, 15 polynomials

PHRUN25.LOG:1 27-JUL-1981 15:16:36.82

ESTIMATED PHASE ABERRATION (100 = ONE WAVE)

					57	68	80	91	101	108					
			39	45	52	61	69	78	85	91	95	96			
		32	34	38	43	49	55	61	66	70	73	74	74		
	25	25	27	29	33	37	40	44	47	49	51	52	53	53	
	17	18	19	21	23	25	27	28	29	30	31	32	34	36	
8	10	11	13	14	15	15	15	15	14	14	14	15	18	22	30
0	3	6	9	10	10	9	7	5	3	2	2	3	7	14	25
-9	-1	3	6	8	7	5	2	0	-3	-5	-5	-3	1	10	25
-17	-6	1	6	8	7	5	1	-2	-6	-9	-9	-6	0	12	30
-27	-11	0	6	9	9	6	2	-2	-6	-9	-9	-6	2	17	40
-38	-17	-3	5	9	10	8	3	-1	-5	-8	-7	-3	7	26	53
	-28	-10	1	8	9	7	4	0	-4	-7	-5	0	13	35	
	-46	-23	-8	0	4	3	0	-3	-7	-8	-6	1	17	43	
		-46	-26	-15	-9	-8	-10	-13	-16	-16	-12	-1	17		
			-58	-43	-35	-31	-32	-33	-34	-33	-27	-14			
					-77	-71	-69	-68	-68	-64					

RMS PHASE ACROSS APERTURE = 0.327 (WAVES)

Figure 40. Blind test results for case 1, 2.13λF#, 15 polynomials

PHRUN25.LOG;1 28-JUL-1981 16:08:13.69

NUMBER OF ZERNIKE POLYNOMIALS = 8
NUMBER OF ITERATIONS =100
ACTUAL NUMBER OF ITERATIONS = 27

INPUT PSF

-18	-9	-5	-11	33	13	-7	-15
6	1	27	33	30	4	-3	0
-45	-16	2	29	179	12	27	0
14	-2	6	66	352	58	-15	-4
-2	12	1	61	95	58	-11	3
29	-20	3	16	34	13	5	15
-2	-8	26	35	11	-4	-19	-14
-16	-8	-12	-8	-15	-30	-6	-25

ESTIMATED PSF

0	0	1	5	8	1	0	0
0	0	1	19	39	3	1	0
1	1	1	26	159	11	5	1
0	1	6	74	348	64	4	1
0	0	0	31	99	5	0	0
0	0	0	0	2	0	0	0
0	0	0	1	1	0	0	0
0	0	0	2	2	1	0	0

MEAN SQUARE ERROR = 18750.3301

COEFFICIENTS OF THE
ZERNIKE POLYNOMIALS

K	P(K)
1	0.00000
2	-0.65838
3	0.19238
4	0.09076
5	0.45863
6	0.11742
7	-0.22798
8	0.03849

Figure 41. Blind test results for case 1, 2.13λF#, 8 polynomials

PHRUN25.LOG;1 28-JUL-1981 16:08:13.69

ESTIMATED PHASE ABERRATION (100 = ONE WAVE)

					134	132	131	131	132	135					
			102	99	97	96	95	95	96	98	101	106			
		71	69	68	67	66	66	66	67	68	71	75	79		
	43	43	44	44	43	43	43	43	44	45	47	50	54	58	
	19	21	23	24	25	26	26	27	27	28	29	31	34	37	
-5	0	4	7	10	12	13	14	14	15	16	16	17	19	21	23
-23	-15	-9	-4	0	2	4	5	6	7	7	7	8	8	8	9
-38	-28	-20	-13	-8	-4	-1	0	2	2	2	2	1	1	0	0
-50	-38	-28	-20	-13	-8	-4	-1	0	0	0	0	-1	-3	-5	-7
-62	-48	-36	-26	-17	-11	-6	-3	-1	0	0	-1	-3	-6	-9	-12
-73	-57	-42	-31	-21	-13	-7	-3	-1	0	0	-1	-4	-7	-12	-17
	-66	-49	-36	-24	-15	-8	-4	-1	0	0	-1	-4	-9	-14	
	-76	-57	-42	-29	-18	-11	-5	-1	0	0	-2	-6	-11	-17	
		-67	-50	-35	-23	-14	-8	-4	-2	-2	-4	-8	-14		
			-60	-44	-31	-21	-13	-8	-6	-6	-9	-13			
					-42	-30	-22	-16	-14	-14					

RMS PHASE ACROSS APERTURE = 0.419 (WAVES)

Figure 42. Blind test results for case 1, 2.13λF#, 8 polynomials

PHRUN25.LOG;1 28-JUL-1981 12:56:30.36

NUMBER OF ZERNIKE POLYNOMIALS = 23
NUMBER OF ITERATIONS =100
ACTUAL NUMBER OF ITERATIONS = 28

INPUT PSF

26	-3	5	44	-13	-4	27	-22
-22	-33	4	21	11	5	-8	18
2	13	-11	-29	56	14	6	9
-10	3	10	102	240	29	13	1
-15	-13	41	209	164	5	-8	21
-2	11	16	-6	31	-2	0	16
-9	31	2	-12	20	-3	16	-1
-22	24	-8	-17	-21	-16	-25	10

ESTIMATED PSF

0	0	0	1	1	0	0	0
0	0	0	1	4	1	0	0
0	0	0	2	50	10	0	0
1	2	13	97	238	24	0	0
1	3	30	207	161	15	1	1
0	0	2	5	26	3	1	0
0	0	0	1	2	1	1	1
0	0	0	1	1	0	0	0

MEAN SQUARE ERROR = 14792.0439

COEFFICIENTS OF THE
ZERNIKE POLYNOMIALS

K	P(K)
1	0.00000
2	-0.12741
3	-0.15363
4	-0.01173
5	-0.19319
6	-0.04978
7	-0.11550
8	0.25747
9	0.02261
10	0.15956
11	-0.07124
12	0.02961
13	-0.08038
14	-0.05428
15	-0.03489
16	0.06735
17	-0.15433
18	-0.04259
19	-0.00326
20	-0.00861
21	-0.04516
22	-0.00050
23	0.00533

Figure 43. Blind test results for case 2, 2.13λF#, 23 polynomials

PHRUN25.LOG;1 28-JUL-1981 12:56:30.36

ESTIMATED PHASE ABERRATION (100 = ONE WAVE)

					-6	-4	-1	1	5	9					
			0	2	3	2	2	3	6	12	18	20			
		8	12	13	10	6	1	0	1	7	15	23	23		
	17	22	24	22	16	8	0	-5	-6	-2	6	16	22	16	
	28	33	34	30	21	10	0	-9	-14	-12	-4	6	16	15	
32	35	40	41	36	26	13	0	-12	-19	-19	-13	-3	8	11	-2
35	38	43	45	40	30	16	2	-11	-20	-24	-20	-10	1	6	-3
33	37	43	45	41	33	20	5	-8	-19	-24	-21	-13	-3	3	-4
27	31	37	41	40	33	22	8	-4	-15	-20	-19	-12	-3	2	-4
19	21	28	33	34	31	22	11	0	-10	-15	-14	-8	0	3	-3
11	8	15	22	25	25	19	11	2	-5	-8	-7	-2	4	6	-2
	-3	0	7	13	15	13	9	3	-1	-3	-1	3	8	9	
	-10	-13	-7	-1	2	4	3	1	0	0	2	6	10	9	
		-21	-22	-17	-11	-8	-6	-5	-4	-2	0	5	7		
			-29	-30	-27	-23	-20	-17	-15	-11	-7	-4			
					-39	-39	-37	-34	-31	-27					

RMS PHASE ACROSS APERTURE = 0.187 (WAVES)

Figure 44. Blind test results for case 2, 2.13λF#, 23 polynomials

PHRUN25.LOG;1 28-JUL-1981 13:58:32.63

NUMBER OF ZERNIKE POLYNOMIALS = 15
NUMBER OF ITERATIONS =100
ACTUAL NUMBER OF ITERATIONS = 27

INPUT PSF

26	-3	5	44	-13	-4	27	-22
-22	-33	4	21	11	5	-8	18
2	13	-11	-29	56	14	6	9
-10	3	10	102	240	29	13	1
-15	-13	41	209	164	5	-8	21
-2	11	16	-6	31	-2	0	16
-9	31	2	-12	20	-3	16	-1
-22	24	-8	-17	-21	-16	-25	10

ESTIMATED PSF

0	0	0	0	0	3	2	0
0	0	0	0	4	8	2	1
0	0	0	2	44	15	1	0
1	3	9	100	236	23	1	1
0	2	36	207	160	10	1	1
0	0	1	6	17	5	1	0
0	0	0	0	1	2	1	1
0	0	0	0	0	1	1	0

MEAN SQUARE ERROR = 14977.6211

COEFFICIENTS OF THE
ZERNIKE POLYNOMIALS

K	P(K)
1	0.00000
2	-0.13208
3	-0.18848
4	0.16422
5	-0.14907
6	0.13722
7	-0.10132
8	0.17617
9	0.02508
10	0.24696
11	-0.16436
12	0.06881
13	0.13409
14	-0.00229
15	0.00968

Figure 45. Blind test results for case 2, 2.13λF#, 15 polynomials

PHRUN25.LOG;1 28-JUL-1981 13:58:32.63

ESTIMATED PHASE ABERRATION (100 = ONE WAVE)

					29	35	41	49	57	65					
			29	32	34	35	39	44	51	59	67	71			
		38	40	38	35	32	32	35	41	49	58	64	67		
	47	51	48	41	33	27	24	25	29	37	46	54	59	57	
	62	61	53	42	31	22	16	14	17	24	33	43	50	50	
64	72	68	58	43	29	17	9	6	7	13	22	32	40	42	35
73	79	74	61	45	29	15	5	0	0	5	13	23	31	35	29
77	83	77	64	47	30	14	3	-2	-3	0	7	16	24	28	24
74	83	78	66	49	32	16	4	-2	-4	-1	5	13	21	24	19
65	78	77	66	51	35	20	8	1	-1	0	6	13	20	22	16
48	67	70	64	52	38	24	14	7	4	5	10	16	21	22	15
	48	58	57	50	39	29	19	13	11	12	16	21	24	23	
	19	38	44	43	37	30	24	20	19	20	23	27	28	25	
		7	23	29	30	28	26	24	24	26	29	32	31		
			-9	6	14	19	21	24	26	30	33	34			
					-11	0	9	16	22	27					

RMS PHASE ACROSS APERTURE = 0.215 (WAVES)

Figure 46. Blind test results for case 2, 2.13λF#, 15 polynomials

PHRUN25.LOG;1   28-JUL-1981 12:36:51.12

NUMBER OF ZERNIKE POLYNOMIALS = 8
NUMBER OF ITERATIONS =100
ACTUAL NUMBER OF ITERATIONS = 29

INPUT PSF

26	-3	5	44	-13	-4	27	-22
-22	-33	4	21	11	5	-8	18
2	13	-11	-29	56	14	6	9
-10	3	10	102	240	29	13	1
-15	-13	41	209	164	5	-8	21
-2	11	16	-6	31	-2	0	16
-9	31	2	-12	20	-3	16	-1
-22	24	-8	-17	-21	-16	-25	10

ESTIMATED PSF

0	0	0	0	1	1	1	0
0	0	0	1	7	5	2	0
0	0	1	6	59	13	3	1
1	0	2	108	235	27	5	1
0	0	1	209	168	24	5	1
0	0	0	4	9	3	1	0
0	0	0	0	1	0	0	0
0	0	0	0	0	0	0	0

MEAN SQUARE ERROR = 17158.5293

COEFFICIENTS OF THE
ZERNIKE POLYNOMIALS

K	P(K)
1	0.00000
2	-0.20418
3	-0.07825
4	-0.11455
5	-0.24277
6	0.11323
7	-0.09764
8	0.24352

Figure 47. Blind test results for case 2, 2.13λF#, 8 polynomials

PHRUN25.LOG;1 28-JUL-1981 12:36:51.12
ESTIMATED PHASE ABERRATION (100 = ONE WAVE)

					-11	-13	-15	-17	-17	-15					
			-4	-4	-6	-9	-12	-16	-18	-18	-15	-8			
		0	2	2	0	-4	-9	-14	-17	-19	-18	-13	-4		
	0	7	9	8	4	0	-6	-12	-16	-19	-19	-16	-8	4	
	6	12	14	13	9	3	-2	-9	-15	-18	-20	-18	-11	0	
-1	10	16	18	17	13	7	0	-6	-13	-17	-20	-18	-13	-3	13
0	11	18	20	19	15	9	2	-4	-11	-16	-19	-18	-14	-4	10
-3	9	17	20	19	15	10	3	-3	-10	-15	-18	-18	-14	-5	8
-9	4	13	17	17	14	9	3	-3	-10	-15	-18	-18	-14	-5	8
-19	-3	6	11	12	10	6	1	-5	-11	-15	-18	-18	-14	-5	7
-33	-15	-4	2	5	4	1	-3	-8	-13	-17	-19	-19	-14	-6	7
	-32	-18	-10	-5	-5	-6	-9	-13	-17	-20	-22	-20	-15	-6	
	-53	-37	-26	-20	-17	-17	-19	-21	-24	-26	-26	-24	-18	-8	
		-60	-47	-39	-34	-32	-32	-32	-33	-34	-32	-28	-21		
			-73	-62	-55	-50	-48	-47	-45	-44	-41	-35			
					-80	-73	-68	-64	-61	-57					

RMS PHASE ACROSS APERTURE = 0.197 (WAVES)

Figure 48. Blind test results for case 2, 2.13λF#, 8 polynomials

NUMBER OF ZERNIKE POLYNOMIALS = 23
NUMBER OF ITERATIONS =100
ACTUAL NUMBER OF ITERATIONS = 21

INPUT PSF

-34	-43	14	87	-16	-21	51	108
-30	41	22	-9	27	22	43	-7
-5	53	-81	-32	166	-27	24	-25
53	-63	7	13	375	29	13	40
57	-2	71	15	122	-2	14	69
16	21	-6	-60	56	-41	16	-14
8	-37	12	-2	-14	-94	-91	-40
34	-17	-58	45	-49	-41	-23	-70

ESTIMATED PSF

0	0	0	1	0	0	0	0
0	0	0	2	5	1	0	0
0	0	0	1	139	2	1	0
0	0	1	14	348	20	3	0
0	0	1	4	95	2	1	1
0	0	0	1	11	1	0	0
0	0	0	0	1	0	0	0
0	0	0	0	0	0	0	0

MEAN SQUARE ERROR = 113471.9531

COEFFICIENTS OF THE
ZERNIKE POLYNOMIALS

K	P(K)
1	0.00000
2	-0.72504
3	0.33835
4	0.14078
5	0.30064
6	-0.01004
7	0.04718
8	0.02084
9	0.02034
10	0.01474
11	-0.00880
12	0.00405
13	0.01477
14	0.01639
15	0.03228
16	-0.00119
17	0.00482
18	-0.01799
19	-0.03260
20	0.04583
21	-0.01725
22	0.00017
23	-0.00588

Figure 49. Blind test results for case 3, 2.13λF#, 23 polynomials

PHRUN25.LOG;1 28-JUL-1981 15:38:26.96

ESTIMATED PHASE ABERRATION (100 = ONE WAVE)

					108	111	113	116	119	123					
			77	83	86	90	94	98	103	108	113	116			
		48	57	62	67	71	76	81	86	92	97	101	104		
	19	31	39	44	49	54	59	65	70	75	80	85	88	89	
	7	17	24	29	34	39	44	49	54	59	64	68	71	74	
-17	-3	5	11	16	20	25	29	34	39	43	48	51	55	58	61
-23	-11	-4	0	4	8	11	15	20	24	29	33	36	40	43	48
-28	-19	-14	-9	-6	-3	0	3	7	11	16	20	23	26	31	37
-33	-26	-22	-19	-15	-12	-10	-6	-2	1	5	9	12	16	21	28
-38	-33	-30	-27	-24	-21	-18	-14	-10	-6	-2	0	3	7	13	21
-43	-39	-36	-34	-31	-27	-24	-20	-16	-12	-8	-5	-1	2	8	17
	-44	-42	-39	-36	-32	-27	-23	-19	-15	-11	-8	-5	0	6	
	-48	-45	-42	-39	-34	-29	-24	-19	-15	-12	-9	-6	-1	4	
		-47	-43	-38	-33	-27	-22	-17	-13	-10	-7	-5	-1		
			-41	-35	-28	-22	-17	-12	-8	-6	-4	-4			
					-21	-14	-9	-4	-2	-1					

RMS PHASE ACROSS APERTURE = 0.434 (WAVES)

Figure 50. Blind test results for case 3, 2.13λF#, 23 polynomials

PHRUN25.LOG;1 28-JUL-1981 14:12:11.06

NUMBER OF ZERNIKE POLYNOMIALS = 15
NUMBER OF ITERATIONS =100
ACTUAL NUMBER OF ITERATIONS = 26

INPUT PSF

-34	-43	14	87	-16	-21	51	108
-30	41	22	-9	27	22	43	-7
-5	53	-81	-32	166	-27	24	-25
53	-63	7	13	375	29	13	40
57	-2	71	15	122	-2	14	69
16	21	-6	-60	56	-41	16	-14
8	-37	12	-2	-14	-94	-91	-40
34	-17	-58	45	-49	-41	-23	-70

ESTIMATED PSF

0	0	0	1	4	1	0	0
0	0	0	2	14	1	0	0
0	0	0	2	135	2	0	0
0	0	1	11	351	13	1	0
0	1	2	8	99	7	2	1
0	0	0	0	0	0	0	0
0	0	0	0	0	0	0	0
0	0	0	0	1	0	0	0

MEAN SQUARE ERROR = 114310.4766

COEFFICIENTS OF THE
ZERNIKE POLYNOMIALS

K	P(K)
1	0.00000
2	-0.48972
3	0.37731
4	0.04506
5	0.11653
6	-0.00631
7	-0.19206
8	0.00039
9	-0.22465
10	-0.00996
11	-0.03206
12	-0.03229
13	-0.01440
14	-0.06289
15	-0.00741

Figure 51. Blind test results for case 3, 2.13λF#, 15 polynomials

PHRUN25.LOG;1 28-JUL-1981 14:12:11.06

ESTIMATED PHASE ABERRATION (100 = ONE WAVE)

					78	82	87	91	96	100					
			45	51	56	60	65	69	73	78	82	85			
		20	27	32	37	41	46	50	54	58	62	66	69		
	-1	5	11	16	21	25	29	34	38	42	46	50	54	56	
	-13	-6	0	4	8	12	17	21	25	30	34	38	42	44	
-30	-22	-15	-10	-5	0	3	8	12	16	21	26	30	34	36	38
-36	-28	-21	-16	-11	-6	-2	1	6	11	15	20	25	29	32	34
-39	-31	-24	-19	-14	-10	-5	-1	3	8	13	17	22	27	30	32
-40	-32	-26	-20	-16	-11	-7	-2	1	6	12	17	22	26	30	32
-39	-32	-26	-21	-16	-12	-7	-3	1	6	12	17	22	27	31	34
-39	-32	-26	-21	-17	-12	-8	-3	1	6	11	17	22	27	31	34
	-33	-28	-23	-18	-14	-10	-5	0	4	10	15	21	26	30	
	-37	-32	-27	-23	-19	-15	-10	-5	0	4	10	16	21	25	
		-41	-37	-33	-29	-25	-20	-15	-10	-5	0	6	11		
			-52	-49	-45	-42	-37	-33	-28	-22	-17	-11			
					-71	-67	-64	-59	-54	-49					

RMS PHASE ACROSS APERTURE = 0.341 (WAVES)

Figure 62. Blind test results for case 3, 2.13λF#, 15 polynomials

PHRUN25.LOG;1 28-JUL-1981 15:15:08.26

NUMBER OF ZERNIKE POLYNOMIALS = 8
NUMBER OF ITERATIONS =100
ACTUAL NUMBER OF ITERATIONS = 22

INPUT PSF

-34	-43	14	87	-16	-21	51	108
-30	41	22	-9	27	22	43	-7
-5	53	-81	-32	166	-27	24	-25
53	-63	7	13	375	29	13	40
57	-2	71	15	122	-2	14	69
16	21	-6	-60	56	-41	16	-14
8	-37	12	-2	-14	-94	-91	-40
34	-17	-58	45	-49	-41	-23	-70

ESTIMATED PSF

0	0	0	0	1	0	0	0
0	0	0	1	8	1	0	0
0	0	0	1	140	2	1	0
0	0	2	12	350	20	2	0
0	0	0	3	97	3	1	0
0	0	0	1	8	1	0	0
0	0	0	0	1	0	0	0
0	0	0	0	0	0	0	0

MEAN SQUARE ERROR = 114005.8438

COEFFICIENTS OF THE
ZERNIKE POLYNOMIALS

K	P(K)
1	0.00000
2	-0.70795
3	0.35687
4	0.14237
5	0.31047
6	-0.01610
7	0.02125
8	0.01797

Figure 53. Blind test results for case 3, 2.13λF#, 8 polynomials

PHRUN25.LOG;1 28-JUL-1981 15:15:08.26
ESTIMATED PHASE ABERRATION (100 = ONE WAVE)

					103	109	114	119	124	129					
			71	78	83	89	94	99	103	108	112	116			
		47	53	59	65	70	75	79	84	88	92	97	101		
	24	30	36	42	48	52	57	62	66	70	74	78	83	87	
	9	15	21	27	32	36	41	45	50	54	58	62	66	71	
-10	-4	2	7	13	17	22	26	31	35	39	43	47	51	56	61
-22	-15	-10	-4	0	5	9	14	18	22	26	30	34	38	43	48
-32	-26	-20	-15	-10	-5	-1	2	6	10	14	18	23	27	32	37
-40	-34	-29	-24	-19	-14	-10	-6	-2	1	5	9	13	18	22	27
-47	-41	-36	-31	-26	-22	-17	-13	-9	-6	-2	2	6	10	15	20
-52	-46	-41	-36	-31	-27	-23	-19	-15	-11	-7	-3	1	5	10	16
	-49	-44	-39	-35	-30	-26	-22	-18	-14	-10	-6	-2	2	7	
	-50	-45	-40	-36	-32	-28	-24	-20	-16	-11	-7	-2	1	7	
		-44	-40	-35	-31	-27	-23	-19	-15	-10	-6	-1	3		
			-36	-32	-28	-24	-20	-16	-11	-7	-2	2			
					-23	-19	-14	-10	-6	-1					

RMS PHASE ACROSS APERTURE = 0.431 (WAVES)

Figure 54. Blind test results for case 3, 2.13λF#, 8 polynomials

PHRUN25.LOG;1 28-JUL-1981 16:40:58.35

NUMBER OF ZERNIKE POLYNOMIALS = 23
NUMBER OF ITERATIONS =100
ACTUAL NUMBER OF ITERATIONS = 25

INPUT PSF

-2	-2	-6	-5	1	-8	0	-2
0	5	30	38	32	3	2	4
-13	0	-12	41	220	25	15	14
-12	11	-1	87	353	80	-29	5
4	9	4	65	93	63	-6	-2
2	-23	5	14	31	16	4	17
-1	-7	33	35	20	1	-17	-11
-7	-4	-8	0	-19	-31	-8	-28

ESTIMATED PSF

0	1	3	5	1	0	0	0
0	1	5	23	13	5	1	1
2	1	2	37	207	14	6	3
1	3	5	79	345	74	5	1
0	0	7	52	89	49	1	0
0	0	1	6	15	11	0	0
0	0	1	2	4	2	0	0
0	0	1	1	1	0	0	0

MEAN SQUARE ERROR = 10980.7637

COEFFICIENTS OF THE
ZERNIKE POLYNOMIALS

K	P(K)
1	0.00000
2	-0.67001
3	0.36708
4	0.11526
5	0.36444
6	0.04485
7	-0.04228
8	-0.13217
9	0.05469
10	0.12285
11	0.03617
12	0.04297
13	-0.16960
14	-0.07437
15	0.02564
16	0.00318
17	0.04489
18	0.05263
19	-0.12719
20	-0.00918
21	-0.01912
22	0.00500
23	-0.07443

Figure 55. Blind test results for case 1, $2\lambda F\#$, 23 polynomials

PHRUN25.LOG;1 28-JUL-1981 16:40:58.35

ESTIMATED PHASE ABERRATION (100 = ONE WAVE)

					123	120	117	115	113	108					
			109	104	96	91	90	92	95	98	101	98			
		87	80	70	65	65	67	71	74	77	81	86	88		
	60	60	49	44	44	48	53	58	61	62	62	64	70	72	
	40	33	27	27	30	35	41	47	51	52	49	46	47	55	
8	19	13	11	14	18	22	28	34	40	43	40	34	30	34	38
-6	0	-2	-1	2	5	8	13	20	29	34	34	26	19	18	24
-22	-16	-16	-13	-9	-6	-4	0	9	20	28	30	23	13	9	12
-39	-31	-30	-26	-21	-17	-13	-7	2	15	25	28	22	12	6	5
-56	-45	-44	-40	-33	-27	-20	-11	1	14	25	28	23	13	8	2
-74	-56	-56	-54	-46	-37	-26	-13	0	15	25	28	24	18	13	-1
	-65	-64	-64	-58	-48	-34	-18	-2	13	23	28	27	24	17	
	-75	-65	-68	-66	-57	-42	-25	-8	8	20	28	31	29	11	
		-64	-61	-62	-57	-46	-30	-12	4	19	30	35	25		
			-52	-47	-44	-37	-24	-7	9	23	32	24			
					-28	-19	-9	2	13	18					

RMS PHASE ACROSS APERTURE = 0.451 (WAVES)

Figure 56. Blind test results for case 1, 2λF#, 23 polynomials

PHRUN25.LOG;1 24-JUL-1981 16:11:05.26

NUMBER OF ZERNIKE POLYNOMIALS = 15
NUMBER OF ITERATIONS =100
ACTUAL NUMBER OF ITERATIONS = 30

INPUT PSF

-2	-2	-6	-5	1	-8	0	-2
0	5	30	38	32	3	2	4
-13	0	-12	41	220	25	15	14
-12	11	-1	87	353	80	-29	5
4	9	4	65	93	63	-6	-2
2	-23	5	14	31	16	4	17
-1	-7	33	35	20	1	-17	-11
-7	-4	-8	0	-19	-31	-8	-28

ESTIMATED PSF

0	0	0	2	7	3	1	0
1	0	0	12	33	7	2	1
1	1	2	39	204	19	6	2
0	0	2	78	345	69	7	1
0	1	1	53	93	51	14	2
2	1	0	1	1	4	6	4
0	0	0	1	1	1	1	0
0	0	0	1	2	1	1	0

MEAN SQUARE ERROR = 12927.4395

COEFFICIENTS OF THE
ZERNIKE POLYNOMIALS

K	P(K)
1	0.00000
2	-0.57599
3	0.14083
4	0.09045
5	0.21900
6	0.22991
7	-0.17272
8	0.24472
9	-0.21831
10	0.06116
11	-0.04909
12	-0.15268
13	0.16786
14	-0.02360
15	-0.17726

Figure 57. Blind test results for case 1, $2\lambda F\#$, 15 polynomials

PHRUN25.LOG;1 24-JUL-1981 16:11:05.26

ESTIMATED PHASE ABERRATION (100 = ONE WAVE)

					75	90	105	117	127	134					
			44	55	66	78	89	98	104	109	111	110			
		32	38	46	54	63	70	76	80	82	83	82	79		
	22	25	30	35	41	47	51	54	56	57	56	55	54	53	
	15	18	21	25	29	32	34	35	35	34	32	32	32	34	
5	7	10	14	17	19	20	20	19	17	15	13	13	14	19	28
-4	0	5	8	11	12	11	9	7	4	1	0	0	2	10	24
-13	-5	0	5	7	8	6	3	0	-4	-7	-9	-8	-3	6	25
-22	-11	-2	3	6	6	4	1	-3	-8	-12	-13	-12	-5	8	31
-32	-16	-4	2	7	7	5	1	-3	-8	-12	-14	-11	-1	15	42
-44	-23	-8	2	7	9	7	3	-1	-7	-10	-11	-7	4	24	56
	-34	-14	-1	6	9	8	4	0	-5	-8	-8	-2	11	34	
	-51	-26	-9	1	5	6	3	-1	-5	-8	-7	0	16	43	
		-46	-25	-11	-4	-2	-4	-8	-11	-13	-10	-1	17		
			-52	-34	-25	-21	-21	-24	-26	-27	-23	-11			
					-60	-54	-52	-53	-54	-53					

RMS PHASE ACROSS APERTURE = 0.362 (WAVES)

Figure 58. Blind test results for case 1, 2λF#, 15 polynomials

PHRUN25.LOG;1 28-JUL-1981 16:23:00.68

NUMBER OF ZERNIKE POLYNOMIALS = 8
NUMBER OF ITERATIONS =100
ACTUAL NUMBER OF ITERATIONS = 33

INPUT PSF

-2	-2	-6	-5	1	-8	0	-2
0	5	30	38	32	3	2	4
-13	0	-12	41	220	25	15	14
-12	11	-1	87	353	80	-29	5
4	9	4	65	93	63	-6	-2
2	-23	5	14	31	16	4	17
-1	-7	33	35	20	1	-17	-11
-7	-4	-8	0	-19	-31	-8	-28

ESTIMATED PSF

0	1	1	10	4	0	0	0
0	0	1	35	35	1	0	0
1	1	2	34	206	11	5	1
1	2	14	95	347	95	1	0
1	1	2	21	116	26	0	0
0	0	0	0	4	2	0	0
0	0	0	1	1	1	0	0
0	0	1	2	1	1	0	0

MEAN SQUARE ERROR = 15518.1748

COEFFICIENTS OF THE
ZERNIKE POLYNOMIALS

K	P(K)
1	0.00000
2	-0.72672
3	0.36828
4	0.09200
5	0.48953
6	0.28294
7	-0.13445
8	-0.10324

Figure 59. Blind test results for case 1, $2\lambda F\#$, 8 polynomials

PHRUN25.LOG;1 28-JUL-1981 16:23:00.68
ESTIMATED PHASE ABERRATION (100 = ONE WAVE)

					144	140	136	133	131	127					
			114	110	107	105	103	102	101	99	97	93			
		82	78	76	75	75	76	76	76	76	75	72	67		
	52	49	48	48	49	51	53	55	56	57	57	55	51	45	
	22	21	22	24	27	31	34	37	40	42	42	41	38	32	
-2	-2	-1	1	5	9	14	19	24	28	30	32	31	28	23	15
-26	-24	-21	-16	-10	-4	2	8	13	18	22	24	24	21	16	8
-46	-42	-37	-30	-23	-15	-7	0	6	12	16	18	19	16	11	3
-63	-57	-50	-41	-32	-23	-14	-6	1	7	12	15	15	13	8	0
-77	-69	-60	-50	-40	-30	-20	-10	-2	4	9	12	13	11	6	-2
-88	-79	-68	-57	-46	-34	-23	-13	-4	2	8	11	12	10	4	-4
	-87	-75	-63	-50	-38	-26	-15	-5	1	7	11	11	9	3	
	-94	-81	-67	-54	-40	-28	-16	-6	1	7	10	10	7	1	
		-86	-71	-57	-43	-29	-18	-7	0	6	9	9	5		
			-75	-60	-45	-31	-19	-9	-1	4	7	6			
					-48	-34	-22	-12	-3	1					

RMS PHASE ACROSS APERTURE = 0.486 (WAVES)

Figure 60. Blind test results for case 1, $2\lambda F\#$, 8 polynomials

PHRUN25.LOG;1 28-JUL-1981 13:26:43.47

NUMBER OF ZERNIKE POLYNOMIALS = 23
NUMBER OF ITERATIONS =100
ACTUAL NUMBER OF ITERATIONS = 28

INPUT PSF

2	4	-4	-11	-6	-3	-10	1
8	-25	5	9	11	8	-13	19
-3	20	-21	-24	75	20	5	10
-8	8	12	130	251	39	4	12
6	-13	59	219	164	9	-12	20
3	14	14	3	32	0	-6	18
-4	33	-5	-16	25	0	17	4
6	29	-11	-9	-18	-16	-21	3

ESTIMATED PSF

0	0	0	0	2	2	0	0
0	0	0	0	9	6	0	0
0	1	1	3	65	23	1	0
0	1	13	123	245	30	2	0
1	5	46	215	156	15	1	0
3	7	7	7	27	4	1	1
1	1	1	0	4	2	1	1
0	0	0	0	1	1	0	0

MEAN SQUARE ERROR = 9870.0830

COEFFICIENTS OF THE
ZERNIKE POLYNOMIALS

K	P(K)
1	0.00000
2	-0.21956
3	-0.10900
4	0.15145
5	0.07393
6	-0.26152
7	-0.04469
8	0.23940
9	-0.02488
10	0.14144
11	0.04048
12	0.03028
13	-0.07496
14	0.06684
15	0.06582
16	0.07916
17	-0.20647
18	-0.08788
19	-0.00951
20	-0.01193
21	0.07280
22	-0.00148
23	-0.03374

Figure 61. Blind test results for case 2, 2λF#, 23 polynomials

PHRUN25.LOG;1 28-JUL-1981 13:26:43.47
ESTIMATED PHASE ABERRATION (100 = ONE WAVE)

					43	54	64	73	81	84					
			18	26	31	36	41	48	56	65	70	64			
		13	18	20	22	23	24	27	32	40	50	57	50		
	10	15	18	20	20	18	15	13	14	20	29	41	48	36	
	16	18	22	25	24	18	11	5	2	4	11	23	37	41	
19	18	21	27	31	28	20	9	-1	-7	-8	-2	8	23	35	27
24	20	24	32	35	32	21	7	-5	-14	-17	-14	-4	10	26	29
28	21	25	33	37	33	22	7	-7	-18	-22	-21	-14	0	16	24
33	21	23	31	36	33	23	8	-6	-17	-24	-25	-20	-8	7	15
41	21	18	24	30	30	22	10	-3	-14	-22	-25	-22	-13	0	6
54	24	14	16	21	23	19	11	0	-10	-18	-22	-21	-14	-3	-4
	33	12	7	10	13	13	9	1	-6	-13	-17	-16	-10	-5	
	49	17	2	0	3	5	4	1	-3	-7	-9	-7	-4	-8	
		30	6	-3	-4	-1	0	1	1	1	2	4	1		
			18	2	-2	-1	2	7	11	15	17	13			
					4	5	10	17	23	26					

RMS PHASE ACROSS APERTURE = 0.213 (WAVES)

Figure 62. Blind test results for case 2, $2\lambda F\#$, 23 polynomials

PHRUN25.LOG;1 28-JUL-1981 13:44:53.22

NUMBER OF ZERNIKE POLYNOMIALS = 15
NUMBER OF ITERATIONS =100
ACTUAL NUMBER OF ITERATIONS = 31

INPUT PSF

2	4	-4	-11	-6	-3	-10	1
8	-25	5	9	11	8	-13	19
-3	20	-21	-24	75	20	5	10
-8	8	12	130	251	39	4	12
6	-13	59	219	164	9	-12	20
3	14	14	3	32	0	-6	18
-4	33	-5	-16	25	0	17	4
6	29	-11	-9	-18	-16	-21	3

ESTIMATED PSF

0	0	0	0	2	2	1	0
0	0	0	0	10	7	2	1
0	0	0	3	65	12	3	1
0	2	9	126	248	21	2	0
4	15	47	219	166	9	1	1
2	2	3	9	24	5	2	2
0	0	0	0	3	2	2	0
0	0	0	0	1	1	0	0

MEAN SQUARE ERROR = 10553.9707

COEFFICIENTS OF THE
ZERNIKE POLYNOMIALS

K	P(K)
1	0.00000
2	-0.19623
3	-0.13809
4	0.19114
5	0.03964
6	-0.42954
7	-0.01990
8	0.04450
9	-0.12483
10	0.24520
11	0.05519
12	-0.03948
13	-0.16192
14	0.11369
15	0.11729

Figure 63. Blind test results for case 2, $2\lambda F\#$, 15 polynomials

PHRUN25.LOG;1 28-JUL-1981 13:44:53.22
ESTIMATED PHASE ABERRATION (100 = ONE WAVE)

					45	57	66	73	80	87					
			9	21	32	40	46	50	54	59	65	76			
		-1	7	16	23	28	31	33	35	37	41	49	63		
	0	3	8	13	17	19	21	21	21	21	23	28	39	57	
	10	9	10	11	13	14	13	12	11	9	9	12	20	35	
32	21	15	12	11	10	10	8	6	4	1	0	1	7	19	39
47	31	21	15	11	9	7	5	2	0	-3	-5	-5	-2	6	23
61	39	25	16	11	7	5	2	0	-3	-6	-9	-10	-8	-2	11
73	46	29	17	10	6	3	0	-2	-5	-8	-11	-13	-12	-7	2
83	52	31	17	9	4	1	-1	-3	-5	-8	-11	-13	-13	-10	-3
91	56	32	17	7	2	0	-2	-3	-5	-7	-9	-11	-12	-11	-6
	59	32	15	5	0	-2	-3	-3	-4	-5	-6	-8	-9	-9	
	61	32	14	3	-1	-3	-3	-2	-1	-1	-1	-3	-4	-5	
		32	12	2	-2	-3	-1	0	3	4	5	4	3		
			12	2	-1	-1	1	5	10	13	14	15			
					0	2	7	13	19	24					

RMS PHASE ACROSS APERTURE = 0.224 (WAVES)

Figure 64. Blind test results for case 2, 2λF#, 15 polynomials

PHRUN25.LOG;1 28-JUL-1981 12:23:35.56

NUMBER OF ZERNIKE POLYNOMIALS = 8
NUMBER OF ITERATIONS =100
ACTUAL NUMBER OF ITERATIONS = 27

INPUT PSF

2	4	-4	-11	-6	-3	-10	1
8	-25	5	9	11	8	-13	19
-3	20	-21	-24	75	20	5	10
-8	8	12	130	251	39	4	12
6	-13	59	219	164	9	-12	20
3	14	14	3	32	0	-6	18
-4	33	-5	-16	25	0	17	4
6	29	-11	-9	-18	-16	-21	3

ESTIMATED PSF

0	0	0	0	1	2	1	0
0	0	0	1	8	8	3	1
0	0	1	6	77	24	5	1
1	0	1	133	252	32	7	2
1	0	2	221	167	29	7	2
0	0	0	9	16	5	2	1
0	0	0	1	2	1	1	0
0	0	0	0	1	1	1	0

MEAN SQUARE ERROR = 14042.0928

COEFFICIENTS OF THE
ZERNIKE POLYNOMIALS

K	P(K)
1	0.00000
2	-0.26867
3	-0.05244
4	0.19270
5	0.19999
6	-0.14494
7	-0.04886
8	0.26674

Figure 65. Blind test results for case 2, $2\lambda F\#$, 8 polynomials

PHRUN25.LOG;1   28-JUL-1981 12:23:35.56

ESTIMATED PHASE ABERRATION (100 = ONE WAVE)

					68	72	77	82	88	97					
			45	51	55	57	59	61	65	71	80	94			
		32	39	43	44	44	44	44	45	49	55	67	83		
	19	29	34	36	36	34	31	29	29	30	35	43	57	77	
	18	26	30	31	29	25	21	18	15	15	18	24	36	54	
5	17	25	28	27	24	19	14	9	5	3	4	9	19	35	58
5	17	24	26	24	20	15	8	2	-2	-5	-5	-1	6	21	42
5	17	23	24	23	18	12	4	-2	-8	-12	-12	-10	-2	11	31
5	15	22	24	22	17	10	2	-4	-10	-15	-17	-14	-7	4	24
4	15	22	23	21	16	10	2	-4	-11	-16	-18	-16	-9	2	21
2	14	21	23	22	17	11	3	-3	-10	-14	-16	-15	-8	3	22
	13	20	23	22	18	12	6	0	-7	-11	-12	-10	-4	7	
	10	19	23	23	20	15	9	3	-2	-5	-6	-4	3	15	
		17	22	23	22	18	13	8	4	1	1	5	13		
			21	24	24	22	18	15	12	10	12	16			
					26	25	24	22	21	21					

RMS PHASE ACROSS APERTURE = 0.231 (WAVES)

Figure 66. Blind test results for case 2, 2λF#, 8 polynomials

NUMBER OF ZERNIKE POLYNOMIALS = 23
NUMBER OF ITERATIONS =100
ACTUAL NUMBER OF ITERATIONS = 21

INPUT PSF

-5	-6	-18	8	-3	-1	8	-19
-12	71	-8	-24	33	13	37	-19
-19	35	-110	-5	207	-19	13	1
-11	-49	10	29	381	55	-17	68
8	9	70	15	122	7	-5	81
-14	31	-22	-53	56	-36	13	4
-9	-26	16	-17	4	-85	-95	-42
-13	-44	-38	51	-61	-63	-34	-76

ESTIMATED PSF

0	0	0	0	0	0	0	0
0	0	0	1	1	0	0	0
0	0	0	2	77	2	0	0
0	0	0	7	250	9	1	0
0	0	0	1	4	0	0	0
0	0	0	0	0	0	0	0
0	0	0	0	0	0	0	0
0	0	0	0	0	0	0	0

MEAN SQUARE ERROR = 143020.9531

COEFFICIENTS OF THE
ZERNIKE POLYNOMIALS

K	P(K)
1	0.00000
2	-0.96808
3	0.44031
4	0.00094
5	0.00295
6	-0.00611
7	-0.03005
8	-0.00654
9	-0.06176
10	-0.04902
11	-0.00080
12	-0.00158
13	-0.00516
14	-0.00155
15	-0.00162
16	0.03939
17	0.00549
18	0.02958
19	0.00728
20	0.04183
21	0.01596
22	0.00012
23	-0.00040

Figure 67. Blind test results for case 3, 2λF#, 23 polynomials

PHRUN25.LOG;1 28-JUL-1981 14:59:21.27

ESTIMATED PHASE ABERRATION (100 = ONE WAVE)

					80	85	90	95	100	104					
			60	66	72	76	81	86	90	94	99	102			
		40	47	53	58	62	67	72	76	81	85	89	93		
	17	25	31	37	42	47	52	57	61	66	71	75	80	83	
	2	9	16	21	27	32	37	42	47	52	58	62	67	72	
-19	-11	-4	1	7	13	18	24	29	35	40	45	51	56	61	66
-31	-23	-16	-10	-4	1	6	12	18	23	29	35	40	46	52	58
-41	-34	-27	-21	-15	-9	-3	2	7	13	19	25	31	37	43	50
-50	-43	-37	-31	-25	-19	-13	-7	-2	3	9	15	21	27	34	41
-58	-52	-46	-41	-35	-29	-23	-18	-12	-6	0	5	10	17	24	31
-66	-61	-56	-51	-45	-40	-34	-29	-23	-18	-12	-7	-1	5	12	20
	-71	-67	-62	-57	-52	-47	-42	-36	-31	-26	-20	-15	-8	-1	
	-83	-79	-75	-71	-66	-61	-56	-51	-46	-41	-36	-30	-24	-16	
		-92	-88	-84	-80	-76	-71	-66	-61	-57	-51	-46	-39		
			-101	-98	-94	-89	-85	-80	[illegible]	-71	-66	-60			
					-103	-99	-94	-90	-85	-80					

RMS PHASE ACROSS APERTURE = 0.541 (WAVES)

Figure 68. Blind test results for case 3, 2λF#, 23 polynomials

PHRUN25.LOG;1 28-JUL-1981 14:35:45.57

NUMBER OF ZERNIKE POLYNOMIALS = 15
NUMBER OF ITERATIONS =100
ACTUAL NUMBER OF ITERATIONS = 25

INPUT PSF

-5	-6	-18	8	-3	-1	8	-19
-12	71	-8	-24	33	13	37	-19
-19	36	-110	-5	207	-19	13	1
-11	-49	10	29	381	55	-17	68
8	9	70	15	122	7	-5	81
-14	31	-22	-53	56	-36	13	4
-9	-25	16	-17	4	-85	-95	-42
-13	-44	-38	51	-61	-63	-34	-76

ESTIMATED PSF

0	0	0	0	0	0	0	0
0	0	0	0	2	1	0	0
0	0	0	2	77	2	0	0
0	0	1	8	247	6	0	0
0	0	0	1	6	2	0	0
0	0	0	0	0	0	0	0
0	0	0	0	0	0	0	0
0	0	0	0	0	0	0	0

MEAN SQUARE ERROR = 143689.0156

COEFFICIENTS OF THE
ZERNIKE POLYNOMIALS

K	P(K)
1	0.00000
2	-0.94646
3	0.27765
4	0.06029
5	0.12885
6	-0.00213
7	0.01058
8	0.01554
9	-0.02690
10	0.04606
11	-0.02607
12	-0.04588
13	0.00858
14	-0.04661
15	0.01193

Figure 69. Blind test results for case 3, $2\lambda F\#$, 15 polynomials

PHRUN25.LOG;1 28-JUL-1981 14:35:45.57

ESTIMATED PHASE ABERRATION (100 = ONE WAVE)

					94	100	105	110	115	119					
			72	79	84	90	95	99	103	107	111	114			
		55	61	66	71	76	81	85	89	93	96	100	103		
	36	41	47	52	56	61	65	69	73	77	80	83	86	89	
	22	27	32	37	41	45	49	53	56	60	63	66	69	72	
4	9	14	18	22	26	29	33	36	40	43	46	49	52	55	57
-7	-3	0	4	8	11	15	18	21	24	28	31	34	37	39	42
-18	-14	-11	-7	-4	-1	1	4	7	10	14	17	20	23	26	28
-28	-25	-22	-19	-16	-13	-10	-7	-4	-1	1	5	8	11	14	17
-37	-34	-31	-29	-26	-23	-20	-17	-14	-11	-8	-5	-1	1	4	7
-46	-43	-40	-38	-35	-32	-29	-26	-23	-20	-17	-13	-10	-6	-3	0
	-51	-49	-46	-43	-41	-38	-34	-31	-28	-24	-20	-17	-13	-9	
	-60	-58	-55	-52	-49	-46	-42	-39	-35	-31	-27	-23	-18	-14	
		-68	-65	-62	-58	-55	-51	-47	-43	-38	-33	-29	-24		
			-77	-73	-70	-65	-61	-57	-52	-47	-41	-36			
					-84	-80	-75	-69	-64	-58					

RMS PHASE ACROSS APERTURE = 0.506 (WAVES)

Figure 70. Blind test results for case 3, 2λF#, 15 polynomials

NUMBER OF ZERNIKE POLYNOMIALS = 8
NUMBER OF ITERATIONS =100
ACTUAL NUMBER OF ITERATIONS = 18

INPUT PSF

-5	-6	-18	8	-3	-1	8	-19
-12	71	-8	-24	33	13	37	-19
-19	36	-110	-5	207	-19	13	1
-11	-49	10	29	381	55	-17	68
8	9	70	15	122	7	-5	81
-14	31	-22	-53	56	-36	13	4
-9	-26	16	-17	4	-85	-95	-42
-13	-44	-38	51	-61	-63	-34	-76

ESTIMATED PSF

0	0	0	0	0	0	0	0
0	0	0	0	1	0	0	0
0	0	0	3	76	4	0	0
0	0	0	6	251	7	0	0
0	0	0	1	3	1	0	0
0	0	0	0	0	0	0	0
0	0	0	0	0	0	0	0
0	0	0	0	0	0	0	0

MEAN SQUARE ERROR = 143503.1094

COEFFICIENTS OF THE
ZERNIKE POLYNOMIALS

K	P(K)
1	0.00000
2	-0.98760
3	0.37287
4	-0.00100
5	-0.00231
6	-0.00026
7	0.02823
8	0.00475

Figure 71. Blind test results for case 1, 2λF#, 8 polynomials

PHRUN25.LOG;1 28-JUL-1981 14:45:12.10
ESTIMATED PHASE ABERRATION (100 = ONE WAVE)

					77	83	88	92	97	101					
			56	62	67	72	77	82	86	91	95	99			
		40	45	51	56	61	66	71	75	79	84	88	92		
	23	29	34	39	45	50	54	59	63	68	72	76	80	84	
	11	17	22	28	33	37	42	47	51	56	60	64	68	72	
-5	0	5	10	15	20	25	30	34	39	43	47	52	56	61	65
-17	-11	-6	-1	3	7	12	17	21	26	30	35	39	44	48	53
-29	-24	-19	-14	-9	-4	0	4	8	13	17	22	27	31	36	41
-41	-36	-31	-27	-22	-17	-13	-8	-4	0	4	9	14	19	24	29
-53	-48	-44	-39	-35	-30	-26	-21	-17	-12	-7	-3	1	6	11	17
-65	-61	-56	-52	-47	-43	-39	-34	-30	-25	-20	-15	-10	-5	0	5
	-73	-68	-64	-60	-56	-51	-47	-42	-38	-33	-28	-23	-17	-12	
	-84	-80	-76	-72	-68	-64	-59	-55	-50	-45	-40	-34	-29	-23	
		-92	-88	-84	-80	-75	-71	-66	-62	-57	-51	-46	-40		
			-99	-95	-91	-87	-82	-78	-73	-68	-62	-57			
					-102	-98	-93	-88	-83	-78					

RMS PHASE ACROSS APERTURE = 0.536 (WAVES)

Figure 72. Blind test results for case 3, 2λF#, 8 polynomials

Notes Added in Revision

January 27, 1982

The results of our phase estimates, pages 62 to 97, were given to V. Mahajan of Draper Labs on August 14, 1981. Several problems with our data were identified by Draper personnel when they tried to reconcile our phases with their input phases. Our Zernike polynomials are unnormalized (the search does not require normalized polynomials), there is an apparent handedness difference, and our phase array is defined on a 16x16 grid whereas the Draper phase is defined on a 21x21 grid. These differences made it impossible to show that the phase estimation algorithm was working correctly.

In view of these difficulties, we (Draper and EIKONIX personnel) decided to attempt a reconciliation of the differences in software and to have EIKONIX perform another round of testing, this time without a blindfold. Thus we rewrote our software to produce a point spread function based on a 21x21 grid for the phase and to sort out the handedness problem.

We buffered the 21x21 grid (in the spatial frequency domain) with zeroes to form a 64x64 grid. Then we used a 2-D, 64x64 FFT to compute a coherent impulse response, squared the samples, and averaged them with a 6.5x6.5 detector. This produced a 9x9 array from which we selected an 8x8 array to be used as the observed point spread function.

This procedure approximated the way that Draper produced the 8x8 PSF array. The major difference is that they buffer the 21x21 array to 128x128, Fourier transform the array, square the samples, and use a 13x13 detector. Also, the 13x13 detector size is realized by frequency domain multiplication, which requires another pair of 128x128 Fourier transforms. Since we use this procedure so often during our phase estimation search, we could not afford to use the larger (128x128 vs. 64x64) array or calculate the second pair of transforms.

Next, we sorted out the handedness problem. This was done by putting the actual Draper phase into our algorithm described above. It was immediately obvious that an x-y inversion existed and that our y and Draper's y were defined in opposite senses. We modified our software to rectify this problem.

In Figure 73 we show the Draper phase and in Figure 74 we show the Draper PSF and the EIKONIX PSF. The differences in Figure 74 are so slight that we proceeded with confidence into the phase estimation algorithm.

First we performed phase retrieval on the noiseless PSF (the PSF on the left in Figure 74). Since we are no longer blind, we are able to see how well the estimation is done at each step in the search. The results are summarized in Figure 75. Starting at an all-zero phase assumption we find the best 6-parameter phase (an unimportant constant phase, two tilts, and 3 quadratic terms); then, starting at this solution, we find the best 10-parameter phase, etc., to 15 and to 23 parameters.

It interesting to note that the final rms phase difference between the estimated and actual phase is 0.0542 waves. In discussion with Draper personnel, we find that this is approximately the same error that one calculates when a polynomial of this size is fitted directly to the phase itself. Thus, we conclude that phase retrieval on the noiseless PSF was successful. Our estimated phase is shown in Figure 76.

Next we repeated phase retrieval for the first noisy PSF, Figure 34(a). This was derived from the same Draper phase but noise is added to the PSF. We calculated the rms phase difference between actual and estimated by normalizing both phases. We calculated the constant and set of tilts that minimized the rms phase of each, then calculated the difference. The results are summarized in Figures 77 and 78.

Figure 77 shows that the best results are obtained with only 10 parameters. Apparently, for more parameters the algorithm starts to use the extra degrees of freedom to fit the noise. Since the metric (MSE) is availalbe for inspection and since the expected noise variance may be known, this implies that one could continue using more parameters in the search until the expected residual MSE is achieved. There the search would be terminated.

We note that for this noisy PSF the expected MSE is

$$\begin{aligned} \text{MSE} &= (\#\ \text{of PSF samples})\ (\text{noise variance}) \\ &= 64\ (2\%\ \text{of DL-PSF peak})^2 \\ &= 64\ (0.02 * 835)^2 \\ &= 17{,}848 \end{aligned}$$

and the algorithm yields a MSE that drops from 18,277 to 15,494 as the number of parameters is increased from 6 to 10. Thus 10 parameters is a reasonable stopping point.

Finally we repeated the phase retrieval algorithm on the second, noisy PSF. The results are given in Figures 79 and 80.

In summary, the phase retrieval algorithm was reworked so that there is no effective miss-match between the Draper and EIKONIX software. The polynomials are still different but the manner in which a given polynomial-generated phase is converted to a PSF is the same. The algorithm then yielded a phase that leaves a residual of about 0.1 waves between the actual and estimated phases, when the input PSF is undersampled by a factor of 4 in both x and y directions and when there is a 2% noise on the measured, undersampled PSF.

										-12										
						-30	-38	-26	-21	-19	-18	-16	-21	-23						
				-34	-25	-24	-31	-20	-13	-21	-15	-9	-15	-18	-22	-20				
			-23	-24	-11	-11	-14	-6	-5	-4	-3	-4	-10	-12	-17	-22	-19			
		-20	-16	-9	-2	-6	-1	1	6	4	3	0	-4	-8	-12	-17	-21	-33		
		-15	-9	1	1	1	3	4	14	16	13	11	6	2	-10	-21	-31	-39		
	-18	-15	0	8	7	13	11	12	20	23	10	11	16	11	0	-11	-20	-28	-38	
	-10	-2	5	10	11	17	16	14	19	24	22	18	20	15	7	-1	-11	-18	-36	
	-7	4	10	11	13	22	23	17	16	20	26	28	23	16	14	5	-2	-10	-33	
	-7	6	10	14	20	30	27	19	17	18	20	28	23	17	22	12	1	-6	-30	
-3	1	8	13	14	25	34	24	22	19	8	10	21	28	22	22	18	9	7	-12	-22
	3	5	14	14	23	31	30	23	18	4	8	16	25	24	21	16	13	6	-6	
	-6	-1	12	13	14	22	30	23	15	11	8	13	21	21	16	12	10	-1	-10	
	-2	1	11	10	11	13	20	17	12	12	15	16	18	18	17	14	12	3	-3	
	-4	-1	4	3	3	9	8	12	11	10	10	9	17	16	16	15	19	13	2	
		-11	-7	-2	-2	1	1	3	4	4	5	5	10	9	10	15	18	20		
		-22	-18	-14	-10	-6	-4	0	-1	-3	-2	1	3	7	9	13	12	15		
			-29	-25	-27	-20	-15	-8	-13	-17	-21	-12	-8	0	3	2	1			
				-33	-32	-38	-26	-16	-17	-35	-33	-28	-20	-18	-15	-13				
						-50	-45	-37	-37	-57	-47	-37	-32	-31						
										-65										

Figure 73. Input Phase from Draper Labs

0	1	1	1	5	2	2	1
1	2	2	3	24	7	2	2
0	2	2	4	164	28	4	2
1	3	5	51	372	31	4	2
1	2	10	53	110	33	4	2
1	1	2	2	7	5	2	2
1	1	1	2	1	1	1	1
0	0	1	0	1	1	1	0

(a)

0	1	1	1	5	2	2	1
1	1	2	3	25	8	3	2
0	2	2	4	162	28	4	2
1	3	5	51	372	32	4	2
1	2	10	53	111	33	4	2
1	1	2	2	7	5	2	2
1	1	1	2	1	1	2	1
0	0	1	0	1	1	1	0

(b)

Figure 74. (a) Noiseless PSF from Draper Labs
(b) EIKONIX generated PSF

# of Parameters	MSE Between PSF's	Residual RMS Phase
6	2023	0.0795
10	839	0.0573
15	130	0.0566
23	76	0.0542

Figure 75. Phase Retrieval Summary for the Noiseless PSF

										-35										
						-37	-30	-25	-22	-21	-22	-24	-29	-36						
				-39	-29	-22	-16	-12	-10	-9	-10	-13	-17	-24	-32	-43				
			-35	-24	-16	-9	-5	-2	0	0	-1	-4	-8	-14	-21	-31	-43			
		-32	-21	-11	-5	0	3	5	6	6	5	3	0	-5	-12	-21	-32	-45		
		-19	-9	-1	3	8	10	12	13	12	11	9	5	1	-4	-12	-22	-34		
	-21	-9	0	6	10	14	16	17	17	17	15	13	10	6	1	-5	-13	-24	-38	
	-12	-1	6	12	16	18	20	21	21	20	19	17	14	11	6	0	-6	-16	-28	
	-5	3	11	16	19	22	23	23	23	22	21	20	17	14	10	5	0	-9	-20	
	-1	7	14	18	21	23	24	25	25	24	23	21	19	17	14	9	3	-3	-13	
-11	0	8	15	19	22	24	25	25	25	24	24	22	21	19	16	12	7	1	-7	-18
	0	7	14	18	21	23	24	24	24	24	23	22	21	20	17	14	10	4	-3	
	-4	4	11	15	19	21	22	22	23	22	22	21	21	19	18	15	11	6	0	
	-10	0	6	11	14	17	18	19	19	20	20	19	19	18	17	14	11	7	0	
	-19	-9	-1	4	8	11	13	14	15	15	16	16	16	15	14	12	9	5	0	
		-20	-11	-5	0	2	5	7	8	9	10	11	11	11	10	8	6	2		
		-35	-25	-17	-12	-7	-4	-1	0	1	3	3	4	4	4	2	0	-3		
			-42	-33	-26	-21	-16	-13	-10	-8	-7	-5	-4	-4	-4	-5	-8			
				-52	-44	-37	-32	-28	-25	-22	-20	-18	-17	-16	-16	-17				
						-58	-52	-46	-42	-39	-36	-34	-32	-31						
										-60										

Figure 76. Phase Retrieval Estimate for the Noiseless PSF (compare to Figure 73)

INPUT PSF							
-18	-9	-5	-11	33	13	-7	-15
6	1	27	33	30	4	-3	0
-45	-16	2	29	179	12	27	0
14	-2	6	66	352	58	-15	-4
-2	12	1	61	95	58	-11	3
29	-20	3	16	34	13	5	15
-2	-8	26	35	11	-4	-19	-14
-16	-8	-12	-8	-15	-30	-6	-25

(a)

ESTIMATED PSF							
0	0	1	4	4	1	1	0
0	1	1	13	24	1	0	0
0	1	1	24	171	2	1	0
1	1	4	60	340	52	3	1
1	2	4	53	86	46	1	0
0	0	1	13	17	6	0	0
0	0	1	2	3	1	0	0
0	0	1	1	1	0	0	0

MEAN SQUARE ERROR = 14377.8516

(b)

# of Parameters	MSE Between PSF's	Residual RMS Phase
6	18277	0.0930
10	15494	0.0890
15	14731	0.1030
23	14377	0.1065

(c)

Figure 77. (a) First noisy PSF
(b) Estimated PSF
(c) Phase Retrieval Summary

										-45										
						-36	-35	-32	-31	-31	-32	-35	-39	-43						
				-33	-33	-29	-24	-19	-15	-14	-15	-18	-23	-29	-34	-37				
			-31	-31	-26	-19	-11	-4	0	1	1	-2	-7	-14	-21	-27	-29			
		-26	-29	-26	-18	-9	0	7	12	15	15	12	6	0	-9	-16	-21	-21		
		-26	-25	-19	-10	0	9	16	21	24	24	22	17	10	2	-6	-13	-16		
	-17	-22	-20	-12	-3	6	15	22	26	29	30	28	24	18	10	2	-5	-10	-9	
	-14	-18	-14	-6	2	11	18	24	28	30	31	30	28	23	16	8	0	-4	-5	
	-10	-12	-8	-1	6	13	19	23	26	29	30	30	28	25	20	13	5	0	-1	
	-4	-6	-3	2	8	14	18	21	24	26	27	28	27	25	21	15	9	3	1	
12	1	-1	0	5	10	14	17	19	21	22	23	24	25	24	21	16	10	5	3	6
	7	3	4	8	11	14	16	17	18	19	20	21	22	21	19	15	10	6	4	
	12	7	7	9	12	14	15	15	16	16	17	18	19	18	16	13	8	5	3	
	16	11	9	10	12	13	14	14	14	14	14	15	15	14	12	9	5	2	1	
	19	13	10	10	10	11	11	11	11	11	10	10	10	9	6	3	0	-2	-3	
		13	9	8	7	8	7	7	6	6	5	4	3	1	-1	-4	-7	-10		
		11	6	3	2	2	1	1	0	0	-2	-3	-5	-8	-11	-15	-18	-20		
			0	-2	-4	-5	-6	-8	-9	-11	-13	-15	-18	-21	-24	-28	-31			
				-12	-15	-17	-18	-20	-22	-25	-27	-30	-34	-37	-41	-45				
						-31	-34	-36	-39	-42	-45	-49	-53	-57						
										-64										

Figure 78. Phase Retrieval Estimate for the First Noisy PSF (compare to Figure 73)

INPUT PSF

26	-3	5	44	-13	-4	27	-22
-22	-33	4	21	11	5	-8	18
2	13	-11	-29	56	14	6	9
-10	3	10	102	240	29	13	1
-15	-13	41	209	164	5	-8	21
-2	11	16	-6	31	-2	0	16
-9	31	2	-12	20	-3	16	-1
-22	24	-8	-17	-21	-16	-25	10

(a)

ESTIMATED PSF

0	0	0	0	1	1	0	0
0	1	0	1	4	3	1	0
0	1	1	2	53	17	2	1
0	1	12	101	235	26	3	1
1	2	40	207	161	8	1	0
1	1	1	4	30	4	1	0
0	1	0	0	2	1	1	0
0	0	0	0	1	1	0	0

MEAN SQUARE ERROR = 14524.2539

(b)

# of Parameters	MSE Between PSF's	Residual RMS Phase
6	18,655	0.1312
10	16,486	0.1039
15	14,913	0.0944
23	14,524	0.1062

(c)

Figure 79. (a) Input PSF
(b) Estimated Phase
(c) Phase Retrieval Summary

										-22										
						-36	-32	-27	-21	-14	-9	-5	-3	-4						
				-25	-27	-26	-22	-17	-12	-7	-3	-1	-1	-3	-8	-14				
			-14	-17	-18	-15	-11	-7	-2	1	3	3	1	-2	-8	-15	-24			
		-4	-8	-10	-9	-5	-1	2	6	9	10	8	5	0	-7	-16	-25	-34		
		-2	-4	-3	0	3	8	12	15	16	16	13	9	2	-6	-16	-26	-34		
	-1	-1	0	3	7	11	16	19	21	22	21	18	12	5	-4	-15	-25	-34	-41	
	-3	0	3	8	13	18	22	25	27	27	25	21	15	7	-2	-13	-24	-34	-40	
	-6	0	5	11	17	22	26	29	30	29	27	23	18	9	0	-11	-22	-32	-38	
	-9	-1	5	12	19	24	28	31	32	31	29	25	19	11	2	-8	-19	-29	-35	
-25	-13	-4	4	12	19	25	29	31	32	32	30	26	21	13	4	-5	-16	-25	-31	-33
	-19	-8	1	9	17	23	27	30	31	31	30	26	22	15	6	-2	-12	-21	-27	
	-24	-13	-3	5	13	19	24	27	29	30	29	26	22	16	8	0	-9	-16	-21	
	-31	-19	-9	0	7	14	19	23	25	27	27	25	22	17	10	2	-5	-11	-16	
	-38	-26	-16	-8	0	6	12	16	20	22	23	23	20	16	11	5	-1	-6	-11	
		-33	-25	-17	-9	-2	3	8	13	16	18	19	18	15	12	7	2	-2		
		-41	-33	-26	-20	-13	-7	-1	3	8	11	13	14	14	12	9	5	1		
			-43	-36	-31	-25	-19	-12	-6	-1	3	7	10	11	11	10	7			
				-47	-42	-37	-31	-25	-18	-11	-5	0	4	7	9	9				
						-50	-44	-38	-30	-23	-15	-8	-2	2						
										-36										

Figure 80. Phase Retrieval Estimate for the Second Noisy PSF (Compare to Figure 73)

DISTRIBUTION LIST

Capt Doris Hamill RADC/OCSE	5	
RADC/TSLD GRIFFISS AFB NY 13441	1	2
RADC/DAP GRIFFISS AFB NY 13441	2	3
ADMINISTRATOR DEF TECH INF CTR ATTN: DTIC-DDA CAMERON STA BG 5 ALEXANDRIA VA 22314	12	5
Eikonix Corp Attn: Dr. Robert Gonsalves 23 Crosby Dr. Bedford, MA 01730	5	3
Aerospace Corporation Attn: Mr. Steve Burrin Advanced Systems Technology Division 2400 E. El Segundo Blvd. Bldg 125/1054 El Segundo, CA 90245	1	4
The Aerospace Corp. Attn: Dr. Silvertooth P.O. Box 92957 El Segundo, CA 90009	1	5
Air Force Wright Aeronautical Laboratory FIEC ATTN: Mr. Joseph Johnson Wright Patterson AFB, OH 45433	1	6
Airesearch Manufacturing Co. of California Attn: Mr. Oscar Buchmann 2525 West 190th Street Torrance, CA 90509	1	7

Analytic Decisions Incorporated Attn: Mr. Richard Mollicone 5336 West Rosecrans Avenue Suite 203 Lawndale, CA 22209	1	8
Analytic Decisions, Incorporated Attn: Mr. Gary Glaser 1401 Wilson Blvd Arlington, VA 22209	1	9
Center for Analysis Attn: Mr. Jim Justice 13 Corporate Plaza NNewport Beach, CA 92660	1	10
The Charles Stark Draper Laboratory, Inc. Attn: Dr. Keto Soosaar 555 Technology Square Cambridge, MA 02139	1	11
Charles Starke Draper Labs Attn: Dr. V. Mahajan 555 Technology Square MS-85 Cambridge, MA 02139	1	12
DARPA/STO Attn: Maj E. Deitz 1400 Wilson Blvd Arlington, VA 22209	1	13
DARPA/STO Attn: Lt. Col A. Herzberg 1400 Wilson Blvd Arlington, VA 22209	1	14
DARPA/DEO Attn: Col R. Prater 1400 Wilson Blvd Arlington, VA 22209	1	15
DARPA/MIS 1400 Wilson Blvd Arlington, VA 22209	1	16

Eastman Kodak Co. Attn: Richard Price KA- Lincoln Plant 901 Elmgrove Rd. Rochester, N.Y. 14650	1	17
General Research Corporation Attn: Mr. G.R. Curry P.O. Box 3587 Santa Barbara, CA 93105	1	18
General Research Corporation Attn: Mr. Thomas Zakrzewski 7655 Old Springhouse Road McLean, VA 22101	1	19
Hughes Aircraft Company Attn: Mr. Ken Beale Centinela & Teale Streets Culver City, CA 90230	1	20
Hughes Aircraft Company Attn: Fritz Benning MS 6/E 126 Centinela & Teal Sts Culver City, CA 90230	1	21
Institute of Defense Analyses Attn: Dr. Hans Wolfhard 400 Army Navy Drive Arlington, VA 22202	1	22
Itek Corporation Attn: Mr. Edward Galat 10 Maguire Road Lexington, MA 02173	1	23
Kaman Sciences Corporation Attn: Dr. Walter E. Ware 1500 Garden of Gods Road P.O. Box 7463 Colorado Springs, CO 80933	1	24
Lockheed Missiles & Space Company Attn: Mr. Paul Williamson 3251 Hanover Street Palo Alto, CA 94304	1	25

Naval Electronic Systems Command PME-106-4 Attn: Mr. Charles Good National Center I Washington, D.C. 20360	1	26
Naval Research Laboratory EOTPO Attn: Dr. John McCallum 4555 Overlook Ave, SW Washington, D.C. 20375	1	27
Naval Sea Systems Command Attn: Dr. S. Siannigar PMS-405 NC1 Room 11N08 Washington, D.C. 20742	1	28
NASA Ames Research Center MS244-7 Moffett Field, CA 94035	1	29
OPTICAL SCIENCES CO Attn: Dr. D. Fried P.O. Box 446 Placentia, CA 92670	1	30
Perkin-Elmer Corp Attn: Mr. H. Levinstein 100 Wooster Heights Rd. Danbury, CT 06810	1	31
Photon Research Associates Attn: Mr. Jim Myer P.O. Box 1318 La Jolla, CA 92038	1	32
Riverside Research Attn: HALO Library, Mr. Bob Passut 1701 N. Fort Myer Drive Arlington, VA 22209	1	33
Rockwell International Attn: Russell Loftman (Space Systems Group) 12214 Lakewood Blvd. Downey, CA 90241 (Mail Code - SL 56)	1	34

Science Applications, Inc. Attn: Mr. Richard Ryan 3 Preston Court Bedford, MA 01730	1	35
Sensor Systems Group Attn: Joseph S. Titus 181 West Street Waltham, Mass 02154	1	36
TRW Attn: Mr. Len Pincus Bldg. R-5 Room 2031 Redondo Beach, CA 90278	1	37
University of Arizona Attn: Robert Shannon % Charles Peyton Administration Bldg. Tucson, AZ 85721	1	38
U.S. Army/DARCOM Attn: Mr. Bernie Chasnov AMC Bldg 5001 Eisenhower Ave Alexandria, VA 22333	1	39
U.S. Army Missile Command Attn: DRSMI-RAS/Mr. Fred Haak Redstone Arsenal, AL	1	40
Space Division Attn: Maj T. Fern SD/YLV, P. O. 92960 Worldway Postal Center Los Angeles, CA 90009	1	41
RGB Associates, Inc. Attn: Dr. Richard Barakat P.O. Box 8 Wayland, MA 01778	1	42

ERIM
Attn: Dr. Stan Robinson
P.O. Box 8618
Ann Arbor, MI 48107

Itek Corp.
Attn: John Watson
Optical Systems Division
10 Maguire Rd.
Lexington, MA 02173

Hughes Aircraft Co.
Attn: Brent Ellerbrooke
Centenela & Teal Streets
Culver City, CA 90230

MISSION
of
Rome Air Development Center

RADC plans and executes research, development, test and selected acquisition programs in support of Command, Control Communications and Intelligence (C^3I) activities. Technical and engineering support within areas of technical competence is provided to ESD Program Offices (POs) and other ESD elements. The principal technical mission areas are communications, electromagnetic guidance and control, surveillance of ground and aerospace objects, intelligence data collection and handling, information system technology, ionospheric propagation, solid state sciences, microwave physics and electronic reliability, maintainability and compatibility.